DECLARATION

Name: Antigoni Kopsida

Email: antigkop@gmail.com

Title of the Msc Dissertation: Analysis of a masonry viaduct of Parc Güell in Barcelona by funicular modeling

Supervisor: Professor Pere Roca

Year: 2011

I hereby declare that all information in this document has been obtained and presented in accordance with academic rules and ethical conduct. I also declare that, as required by these rules and conduct, I have fully cited and referenced all material and results that are not original to this work.

I hereby declare that the MSc Consortium responsible for the Advanced Masters in Structural Analysis of Monuments and Historical Constructions is allowed to store and make available electronically the present MSc Dissertation.

University: Universitat Politecnica de Catalunya

Date: 29/07/2011

Signature: _____

ACKNOWLEDGEMENTS

First of all I would like to thank my supervisor of the thesis professor Pere Roca for his precious advice during the dissertation. It has been an honor working with him for all the things I learned from him all these months. Also my participation in this Master would not be possible without the economic support of the European Union which I would like to thank for awarding me the Erasmus Mundus scholarship category B. This dissertation would never be created without the generous help of the Departament d'Arquitectura i Projectes Urbans, Sector d'Urbanisme of the Ajuntament de Barcelona and the architects M.Luisa Aguado and Anna Ribas Seix that offered to help me by providing me previous structural studies on the viaducts of Parc Güell and the architectural drawings of the viaducts. I would like also to thank professor of The Pennsylvania State University Thomas Boothby who as a visiting professor in UPC gave me important advice in the graphic statics method. Also I would like to underline how important was the help of the phd candidate Yohei Endo for being always available to reply my questions regarding GID program and also thank all the professors, phd candidates and workers of UPC for their welcome attitude all these months. Moreover I want to thank the associate professor Charis Gantes and professor George Gazetas from the School of Civil Engineering of National Technical University of Athens for supporting my application to the master program and express my appreciation to them for all the precious knowledge I earned from them as a student at the National Technical University of Athens. Also I cannot forget two important friends that I made from this master program my apartment mate at Padova Ana Nicusan and my apartment mate of Barcelona Iris Koltsida and thank them for sharing with them all these months the beautiful and also the difficult moments. Last but not least I would like to thank my beloved family for always supporting me. Their support means always a lot to me. Thank you dad, mama and Christina for always believing on me.

ABSTRACT

Park Güell is one of the most visited and characteristic monuments in the city of Barcelona designed by the modernist architect Antoni Gaudi. Park Güell was designed as a real estate project but due to economic reasons the project failed and opened as a public park in 1922. The main purpose of the thesis is the analysis of the stability of the lower viaduct of the three main viaducts of the Park Güell that can be found at the south-east side of the park.

Since the lower viaduct is a masonry structure it is important the presentation of all the methods used historically for the analysis of the stability of historic masonry structures. Among them the method of graphic statics and the method of funicular analysis are applied for the calculation of the thrust line of the structure in order to investigate its stability.

The general information regarding the historic and artistic significance of Park Güell is important in order to understand the significance of the whole structure where the viaduct is contained. Also reporting the architectural arrangement of the viaduct, its structural characteristics and its materials is necessary for a deeper understanding of the function of the structure before its stability analysis. Also a previous structural study by BIS architects offers conclusions on the structural capacity of the viaduct.

The three-dimensional model of the structure in AutoCAD 3D allows the better understanding of the geometry of the structure and uses for the application of the graphic statics method. The graphic statics method is applied in two dimensions and is taking into account all the loads applied on the structure in order to investigate its stability. The results of the graphic statics method is the thrust line of the viaduct that must fit inside the limits of the geometry of the structure in order to consider that the structure is stable according to safe theorem.

The application of the funicular analysis with the MASONRISK application of program GID for a characteristic part of the viaduct is another method for the investigation of the stability of the viaduct. The objective of the method is to create a catenary net that its deformed shape due to its loading is contained within the limits of the structure in order to prove that the structure is stable according to safe theorem. The solution obtained is a three dimensional catenary network.

Finally some general conclusions regarding the two methods are made presenting their advantages and disadvantages for the analysis of the stability of historic masonry structures and also some recommendations for the improvement of the methods.

RESUMEN

Park Guell es uno de los monumentos más visitados y característicos de la ciudad de Barcelona. Este parque fue diseñado por el arquitecto modernista Antoni Gaudi. Park Guell fue diseñado originalmente como un proyecto de finca raíz, pero por problemas económicos el proyecto no tuvo éxito y termino siendo abierto como parque público en 1922. El propósito principal de esta tesis es el de analizar la estabilidad del más bajo de los tres viaductos localizados en la parte sur-oriental de Park Guell.

Dado que el viaducto bajo consideración está construido en mampostería, es importante hacer una revisión bibliográfica de los métodos utilizados históricamente para evaluar la estabilidad de estructuras con esta tipología. Dos de estos métodos, el de estática grafica y el de análisis funicular, son utilizados en este estudio para determinar la línea de empuje y así evaluar la estabilidad de la estructura.

Para lograr entender el significado del viaducto estudiado dentro del contexto general del parque, es importante conocer la información acerca del valor histórico y artístico de Park Guell. Asimismo, es fundamental entender el valor funcional de la estructura antes de investigar la estabilidad de la misma. Para esto, se debe conocer su diseño arquitectónico, las características estructurales y los materiales que la componen. Un estudio previo llevado a cabo por la firma arquitectónica BIS, da conclusiones acerca de la capacidad estructural del viaducto.

La realización de un modelo tridimensional de la estructura en AutoCAD 3D permite un mejor entendimiento de la geometría y puede ser utilizado para la aplicación del método de estática grafica. Para evaluar la estabilidad de la estructura, el método de estática grafica es aplicado bidimensionalmente teniendo en cuenta todas las cargas existentes. Como resultado de la aplicación de este método, la línea de empuje es determinada. De acuerdo con el teorema de seguridad, la línea de empuje debe estar dentro de los límites geométricos de la estructura para que su estabilidad sea verificada.

El método del análisis funicular fue utilizado también para investigar una porción característica del viaducto estudiado. La aplicación MASONRISK del programa GID fue utilizada para este fin. El objetivo de este método es crear una malla catenaria deformada debido a las cargas actuantes que está dentro de los límites geométricos de la estructura. De esta forma, la estabilidad del sistema es verificada de acuerdo con el teorema de la seguridad. La solución obtenida es una malla catenaria tridimensional.

Finalmente, se presentan conclusiones generales acerca de la aplicación de los dos métodos utilizados, haciendo énfasis en las ventajas and desventajas de cada uno con respecto al análisis de estabilidad de estructuras históricas de mampostería. Adicionalmente, se hacen recomendaciones para el mejoramiento de los métodos de análisis utilizados en este estudio.

ΠΕΡΙΛΗΨΗ

«Ανάλυση της θολωτής κατασκευής από πέτρα του πάρκου Γκουέλ της Βαρκελώνης με αναπαράσταση της κατασκευής από καλωδιωτό μοντέλο»

Το πάρκο Güell είναι ένα από τα πιο επισκέψιμα και χαρακτηριστικά μνημεία της Βαρκελώνης το οποίο σχεδιάστηκε από τον μοντερνιστή αρχιτέκτονα Αντονί Γκαουντί. Το πάρκο Güell σχεδιάστηκε ως συγκρότημα κατοικιών προς πώληση αλλά για οικονομικούς λόγους το εγχείρημα απέτυχε και άνοιξε ως δημόσιο πάρκο το 1922. Ο κύριος σκοπός της εργασίας είναι η ανάλυση της σταθερότητας της χαμηλότερης σε διάταξη θολωτης κατασκευής από τις τρεις θολωτές κατασκευές του πάρκου Güell που βρίσκονται στη νοτιοανατολική πλευρά του του πάρκου.

Εφόσον η χαμηλότερη σε διάταξη θολωτή κατασκευή είναι κατασκευή από πέτρα είναι σημαντική η παρουσίαση όλων των μεθόδων που χρησιμοποιήθηκαν ιστορικά για τη στατική ανάλυση των ιστορικών κατασκευών από πέτρα. Ανάμεσά τους η μέθοδος γραφικής στατικής ανάλυσης και ανάλυσης με προσωμοίωση με καλώδιωτό μοντέλο εφαρμόζονται για τον υπολογισμό της γραμμής θλίψης της κατασκευής με σκοπό να διερευνηθεί η ευστάθειά της.

Οι γενικές πληροφορίες σε σχέση με την καλλιτεχνική και ιστορική αξία του πάρκου Güell είναι σημαντικές ώστε να γίνει κατανοητή η σημασία όλης της κατασκευής στην οποία η θολωτή κατασκευή περιέχεται. Επίσης η παρουσίαση της αρχιτεκτονικής διάταξη της κατασκευής, τα στατικά χαρακτηριστικά της και τα υλικά της είναι σημαντικά για τη βαθύτερη κατανόηση της λειτουργίας της κατασκευής πριν τη στατική ανάλυση της ευστάθειας της. Επίσης η προηγούμενη μελέτη της εταιρίας BIS architects προσφέρει σημαντικά συμπεράσματα για τη στατική συμπεριφορά της θολωτής κατασκευής.

Η κατασκευή του τρισδιάστατου μοντέλου της κατασκευής στο AutoCAD 3D επιτρέπει τη καλύτερη κατανόηση της γεωμετρίας της κατασκευής και χρησιμοποιείται επίσης για την εφαρμογή της γραφικής στατικής μεθόδου. Η γραφική στατική μέθοδος εφαρμόζεται στις δύο διαστάσεις και λαμβάνει υπόψη όλα τα φορτία που εφαρμόζονται στη κατασκευή με σκοπό να αναλύσει τη ευστάθεια της. Το αποτελέσμα της γραφικής στατικής μεθόδου είναι η γραμμή θλίψης της θολωτής κατασκευής η οποία πρεπεί να περιέχεται μέσα στα ορια της γεωμετρίας της κατασκευής με σκοπό να θεωρηθεί ότι η κατασκευή είναι ευσταθής σύμφωνα με το θεώρημα του κατωτάτου ορίου.

Η εφαρμογή της μεθόδου προσομοίωσης της κατασκευής με καλώδια με την εφαρμογή MASONRISK του προγράμματος GID για ένα χαρακτηριστικό μέρος της κατασκευής είναι μία άλλη μέθοδος διερεύνησης της ευστάθειας της κατασκευής. Ο σκοπός της μεθόδου είναι να δημιουργήσει ένα καλωδιωτο δίκτυο του οποίου το παραμορφωμένο σχήμα λόγω της φόρτισης του να περιέχεται στα όρια της κατασκευής με σκοπό τηςν απόδειξη της ευστάθειας της κατασκευής σύμφωνα με το θεώρημα κατωτάτου ορίου. Η λύση που προκύπτει είναι ένα τρισδιάστατο καλωδιωτό μοντέλο.

Τέλος εξάγονται μερικά γενικά συμπεράσμτα σχετικά με τος δύο μεθόδους παρουσιάζοντας τα πλεονεκτήματα και τα μειονεκτήματα τους για της ανάλυση της ευστάθεις των ιστορικών κατασκευών από πέτρα και γίνονται κάποιες προτάσεις σχετικα με τη βελτίωση των μεθόδων.

TABLE OF CONTENTS

LIST OF FIGURES

LIST OF TABLES

1. INTRODUCTION AND OBJECTIVES

1.1 Introduction

The monuments play always a very important role in the architecture of a city. There is no doubt that they add cultural, architectural and historic value to any city that contains them. Park Güell is one of the most visited and characteristic monuments in the city of Barcelona. It is a monument designed by one of the most famous architects of the 19th century and maybe the most representative of modernism the Catalan Antoni Gaudi.

During my visit at Barcelona in October of 2009 I had the chance to visit park Güell and walk through the various structures that Gaudi designed. All the structures through the park are masterpieces of architecture however the structures that most captured my interest where the stone viaducts-porticoes. The main purpose of their construction was to facilitate the transportation through the site and through its different levels. However the unique characteristic of them is despite the fact that the structures have a simple function this of the transportation through the site, are each one of them a piece of art, representing different styles of architecture. Also the material of their construction which is stone taken originally from the site gives a rustic and original sense as if there were part of the nature, and not built architectural works.

The thesis is focusing in the study of the lower viaduct of the main three viaducts of Park Güell. The main difficulty of the study was the luck of original structural drawings or any officially measured and verified structural drawing available. With the kind contribution of the Ajuntament of Barcelona it was possible an access to some architectural drawings that could be used as a base for the investigation of the stability of the lower viaduct. However the non uniform character of Gaudi‘s structure and the different geometry of each structural in combination with the various architectural details element is making the modeling of the structure a complicated task. For this reason many simplifications in the geometry have been adopted to make possible the study of the viaduct.

1.2 Objective

The main purpose of the thesis is the analysis of the lower viaduct of the three main viaducts of the Park Güell that can be found at the south-east side of Park Güell. The analysis of the stability is aiming at finding an appropriate thrust line that is contained within the limits of the structure so according to the safe theorem the structure is stable. The process of finding the thrust line of the structure has been based in two different methods. The first is the method of graphic statics and the second is the method of funicular analysis with the use of program GID. The specific objectives of the thesis are the following:

1. The review of the methods of analysis of the masonry structures with emphasis at the methods of limit analysis and funicular modeling

2. The presentation of the historical and architectural information related to Park Güell and the lower viaduct in particular.
3. The description of the architectural and structural function of the viaduct and its material. The description is also based on structural drawings from previous studies and recent photos. Also the presentation of the results from previous study made by BIS architects regarding the stability of the viaduct and its structural elements through the Finite Element Analysis method.
4. The three-dimensional modeling of the structure in AutoCAD 3D and the calculation of the volumes of the different structural and architectural elements. The application of the graphic statics method is taking into account the loads of the structure in order to prove the stability or not of the structure. The graphic statics method is applied in a characteristic part of the structure due to the symmetry conditions
5. The application of the funicular analysis with the program GID for a characteristic part of the viaduct. The objective is to find a deformed catenary net that is contained within the limits of the geometry of the structure.
6. General conclusions about the stability of the structure and comparison of the two methods used for the investigation of its stability. Conclusions regarding the use of the funicular analysis method with the program GID and its advantages in order to be established as a method of finding a potential thrust included within the structure for future studies on historic masonry structure.

2. STATE OF ART

2.1 Analysis of masonry historic structures

A big part of world's architectural heritage consists of historic buildings in masonry. In addition to their historical and cultural values, such monuments often have important economical values. As an example, the earthquake of 2009 at L' Aquila had as a result damages at the historic buildings and churches and considerable number of human losses. As a result, the town and region lost income from the tourism while many churches are closed for restoration.

The analysis of masonry structures is an issue that has been always studied from the scientists from time of the ancient civilizations until today. In the ancient times the engineers were basing their calculations in empirical rules and the solution was found often after a trial and error process. The ancient constructions treatises are the first proofs of engineering research on the masonry structures. The gothic geometrical rules and the empirical rules before the scientific revolution were giving more information on the design of the structural members and the behavior of the masonry structure. By the middle of 17th century scientists and designers experienced the need for rational principles or methods stemming from scientific theories. In 1675 Hooke provided the solution for the equilibrium of an arch by means of an anagram included in the book "A description of Helioscopes and some other Instruments", which was only deciphered after his death in 1703. The solution was: "Ut pendet continuum flexile, sic stabit contiguum rigidum inversum" which means as hangs the flexible line, so but inverted will stand the rigid arch. David Gregory wrote a treatise on the catenary curve in 1690. In 1698 stated that only the inverted catenary is the correct shape for an arch. Arches shaped differently are stable if it is possible to fit a catenary within their thickness. In fact, the catenary is worth to describe the equilibrium of an arch with uniform depth subject to dead load. Other arch shapes, depth variations and load conditions require different curves the so-called anti-funicular shapes. The curve thus determined is called "equilibrium line".

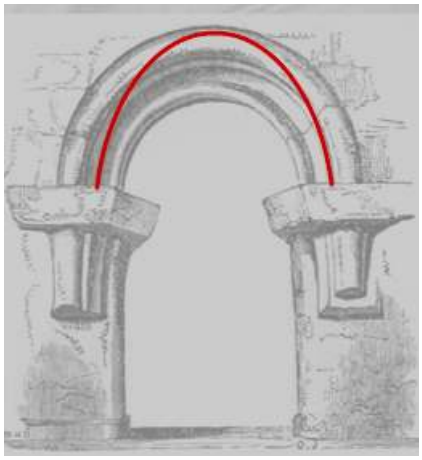

Figure 2.1 Equilibrium line of an arch

Late on several researchers contributed to a graphically oriented procedure stemming from the catenary principle including La Hire at 18_{th} century and Rankine at 19_{th} century. Accurate formulations were provided

during the 19_{th} century by Gerstner (Germany), Méry (France) and Moseley (England), the latter on 1833 being the most scientific and comprehensive one. The arch is first decomposed in a series of real or fictitious voussoirs separated by a series of planes (the planes do not need to be parallel). The thrust line is defined as the geometrical locus of the points of application of the sectional forces (the resulting forces over each plane between voussoirs) across the arch. An arch is stable if it is possible to find thrust line contained between its boundaries.

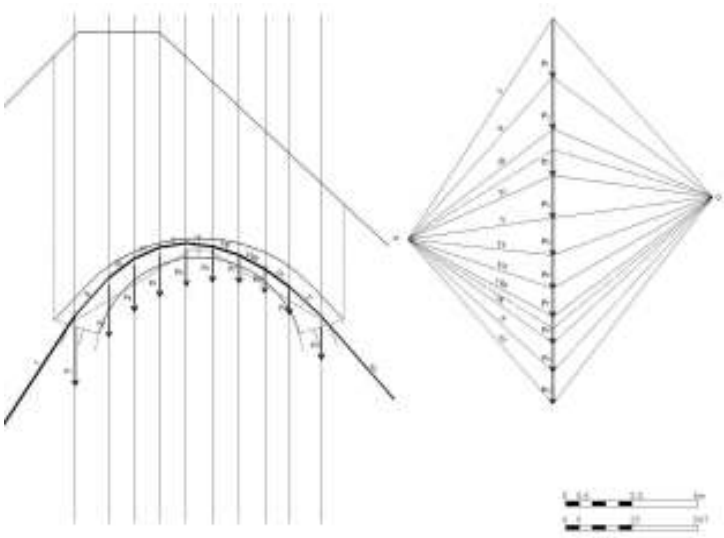

Figure 2.2 The graphic statics method for the definition of the thrust line for a masonry arch

Charles-Agustin Coulomb (1736-1806) proposed in 1773 the first general and accurate theory on the stability of masonry arches. The basic assumptions are:

(1) Sliding between voussoirs is unlikely due to the existence of frictional forces
(2) Collapse will be caused by the rotation between parts due to the appearance of a number of hinges.

The modern formulation of Limit Analysis is attributed at Heyman (1966). Under these conditions**,** the limit theorems of limit analysis, based on plasticity theory, are applicable to masonry structures according to Kooharian (1953) and Praguer (1959). Failure will be caused due to the generation of a mechanism.

Though many historic masonry structures have survived for centuries, there is always a need for new tools to analyze the stability and the safety of such structures. The use of applications applying the funicular analysis method is more appropriate for a three-dimensional equilibrium approach. Regarding the analysis of masonry historic structures is always important to have in mind that the basic static equilibrium is the most important principle, even if is often neglected.

2.2 Limit Analysis

The main hypotheses of the Limit Analysis according to Heyman are:

1. Masonry has null tensile stress
2. The compression strength of the material is infinite
3. Sliding between stone blocks is impossible

There are three main theorems that represent the concept of the limit analysis, the safe or lower bound theorem, the upper bound theorem and the uniqueness theorem. According to the safe or lower bound theorem the structure is safe, meaning that the collapse will not occur, if a statically admissible state of equilibrium can be found. This occurs when a thrust line can be determined, in equilibrium with the external loads, which falls within the boundaries of the structure. The load applied is a lower bound of the actual ultimate load, the one causing the failure.

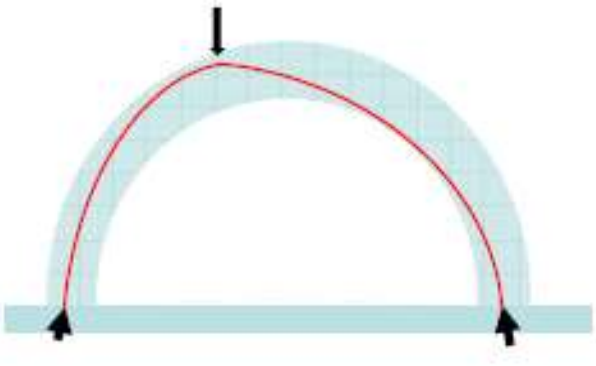

Figure 2.3 According to the safe theorem the thrust line falls within the boundaries of the structure so the arch is safe

According to the upper bound theorem if a kinematically admissible mechanism can be found, for which the work developed by external forces is positive or zero, then the arch will collapse. In other works, if a mechanism is assumed by arbitrarily placing a sufficient number of hinges, the load which results from equating the work of the external forces to zero is an upper-bound of the actual ultimate load.

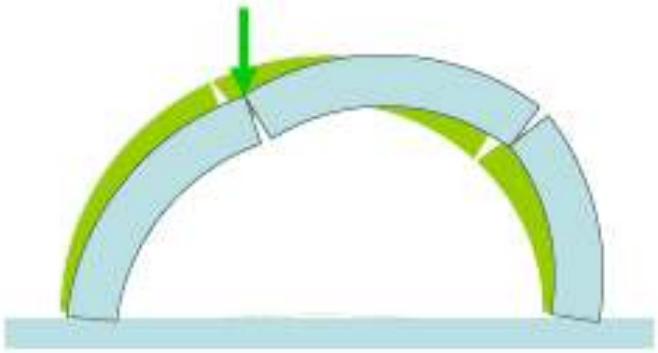

Figure 2.4 Collapse mechanism of an arch according to the upper bound theorem

According to the uniqueness theorem a limit condition will be reached which means that the structure will be about to collapse if a both statically and kinematically admissible collapsing mechanism can be found. In other words, the collapsing configuration will be reached if a thrust line can be found causing as many plastic hinges as needed to develop a mechanism. Plastic hinges are caused by the thrust line becoming tangent to the boundaries. When this occurs, the load is the true ultimate load, the mechanism is the true ultimate mechanism, and the thrust line is the only possible one.

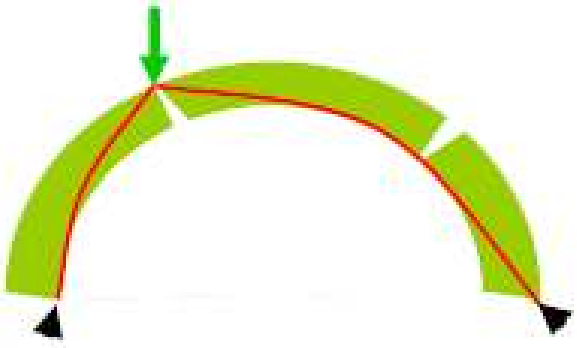

Figure 2.5 The collapse mechanism for the arch is the one corresponding to the formation of four hinges

Limit analysis depicts realistically the collapse and capacity of masonry arches. It constitutes a very reliable and powerful tool and should be used to assess masonry. Limit analysis can be easily applied to arches and skeletal structures. However, its application to 3D structures as domes and vaults is more complex.

Thrust lines are used to illustrate possible collapse modes and to allow users to clearly visualize the forces within the masonry. For most historic structures there are infinite possible load paths. Graphic statics is a powerful method for equilibrium analysis for use in structural engineering.

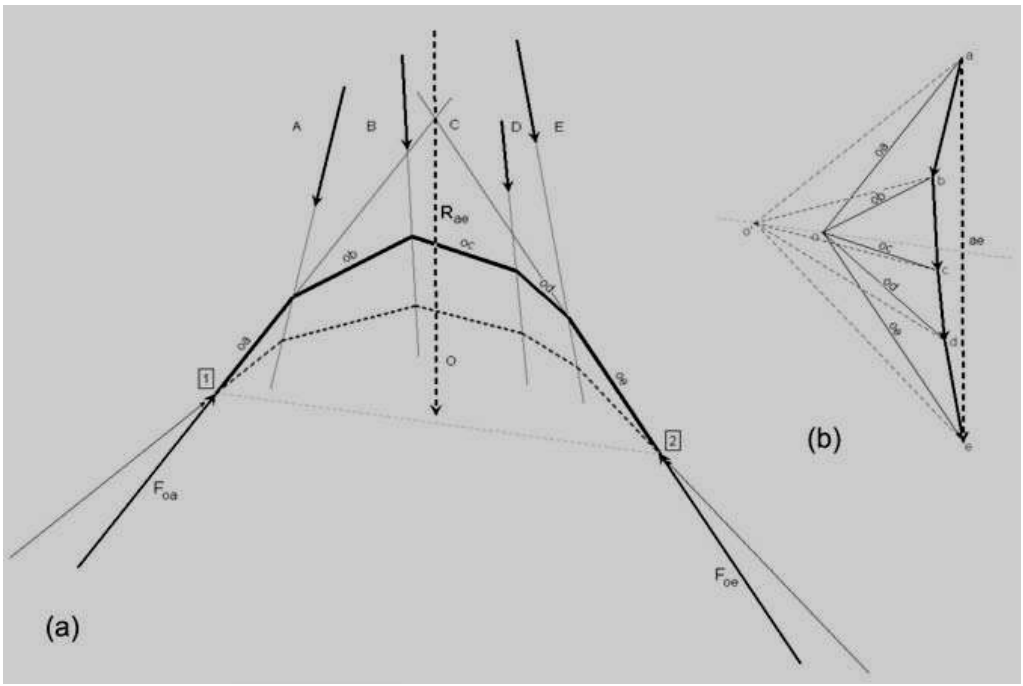

Figure 2.6 Graphic statics is a method that allows the construction of funicular shapes (only tension or compression) for a certain set of loads (a) using Bow's Notation and (b) a force polygon that gives the magnitude of the forces of the segments in the funicular polygon (After Zalewski and Allen, 1998)

Medieval vault builders explored three-dimensional equilibrium, creating complex forms carefully balanced in compression. The structural properties of these sophisticated forms are still poorly understood because of a lack of appropriate analysis methods, methods relating to stability and form. Famous engineers, such as

Robert Maillart, Gustave Eiffel, and Antoni Gaudí used the method of graphic statics to create some of their greatest works.

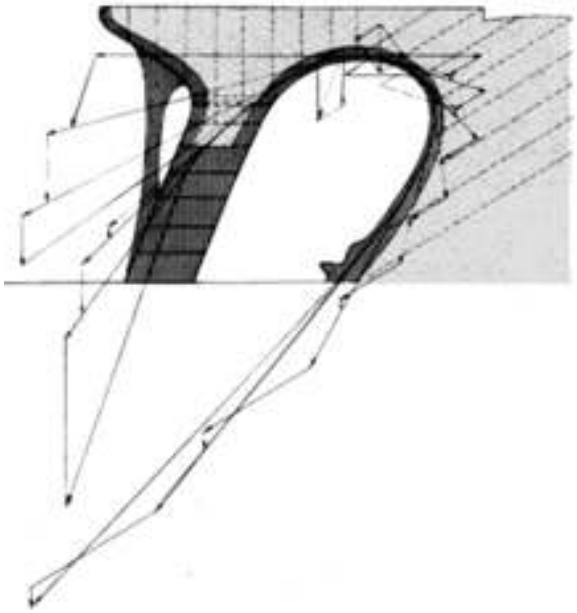

Figure 2.7 Joan Rubio‘s graphical design for the columns and retaining wall of the Park Güell [Rubio 1913]

For the analysis of the masonry historic structures it is important to understand the behavior of masonry structures. In most cases, masonry structures fail due to instability rather than a lack of material strength according to Heyman (1995). Stresses in masonry structures are typically only a fraction of the crushing capacity of the stone. Therefore, rigid block models with the same proportions as the structures are good models to understand their stability. The stability problems can be scaled so an equilibrium approach is most appropriate to understand the structural behavior of masonry constructions. The master builders of the Middle Ages were able to use geometrical rules, developed through centuries of trial and error, to build structural elements by scaling up the same proportions for new larger elements according to Huerta (2004). In those days, there was no knowledge of material properties or allowable stresses. Yet, many of these architectural marvels are still standing in a state of equilibrium.

Structures in unreinforced masonry work in compression, and the tensile capacity of the stone and mortar can be considered as negligible. These considerations then demand new approach in order to understand how these structures work and why they are able to stand for centuries. Linear elastic analysis using finite element methods is mainly concerned with stresses, and is not appropriate for historic structures in masonry. A stability or equilibrium approach will be most valuable, and limit analysis provides a theoretical framework. Although we will never know how exactly the masonry vault is standing, this is not necessary. The safe theorem guarantees that as long as we can demonstrate one way that the structure could stand, i.e. could be in equilibrium with the external forces, then it is safe. This approach initially neglects sliding, which can be checked afterwards to ensure that sufficient friction exists.

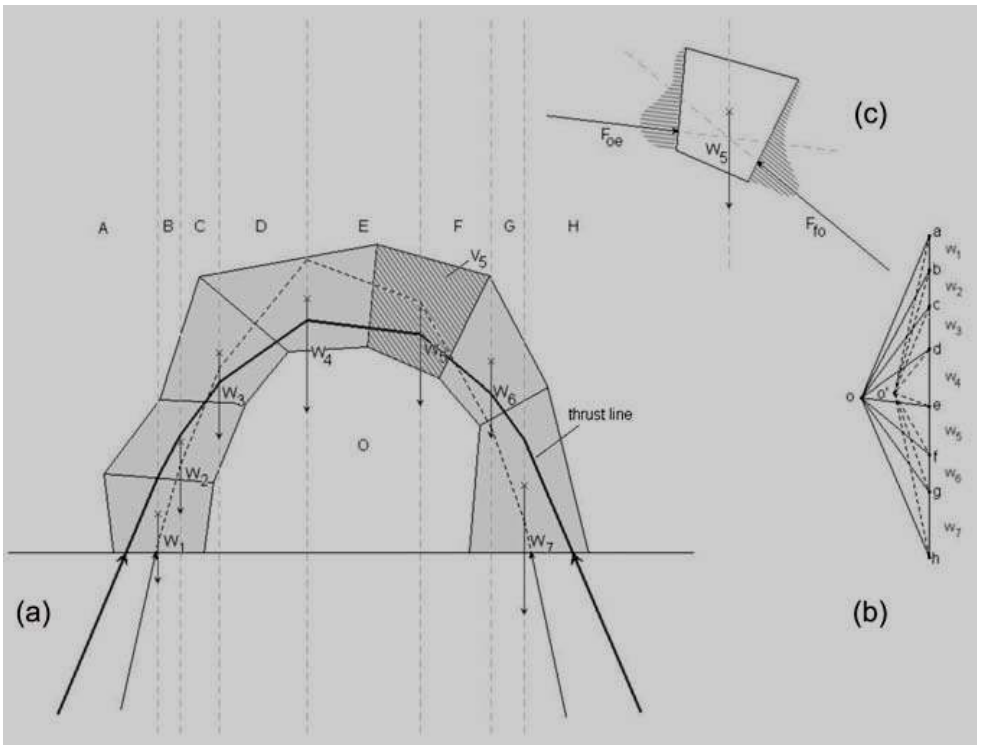

Figure 2.8 The actions of the different blocks are treated as lumped masses applied at their center of gravity (a) The magnitudes of the forces are proportional to their weight and transferred to the force polygon (b) Two possible thrust lines (funicular solutions) are shown in graph (a) and (c) shows the equilibrium of a single "voussoir"

Thrust-line analysis is a particularly powerful method for understanding and exploring the range of lower-bound equilibrium solutions of compression only systems, such as masonry structures. It represents the relative stability of these structures by showing the paths of the resultant compressive forces throughout the structure and, for two-dimensional problems, suggests possible collapse mechanisms (Ochsendorf 2002, Block et al. 2006b).

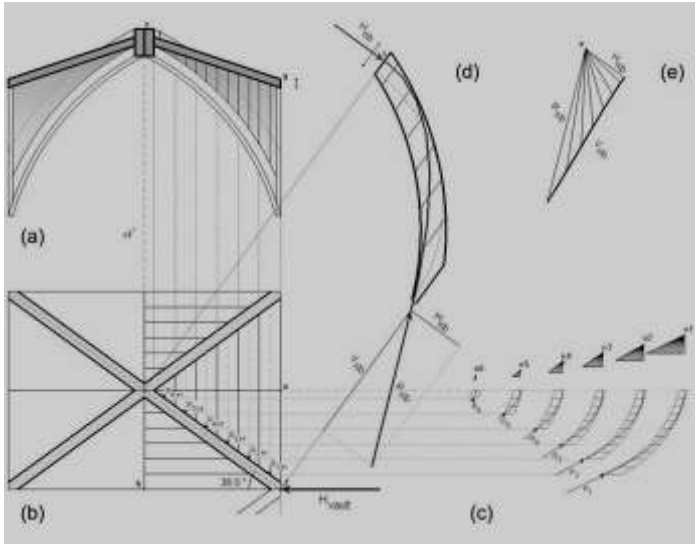

Figure 2.9 A pseudo-3D analysis of a gothic rib vault using graphic statics (Wolfe 1921). The web of the vault is cut into strips which are analyzed as 2D arches. The main ribs bring the forces from those arches down to the supports

However, it is primarily a two-dimensional technique and is therefore most appropriate for the analysis of arches, flying buttresses or any structure which can be reduced to a sectional analysis. Graphic statics can be used to compute thrust lines. The main advantage of using graphical analysis is that the funicular polygon visually represents the forces in the system. In order to analyze three-dimensional structures using the graphic statics method, the analyst typically must slice the structure, reducing it to a combination of two-dimensional problems. In this way, structural behavior is reduced to a combination of arch actions.

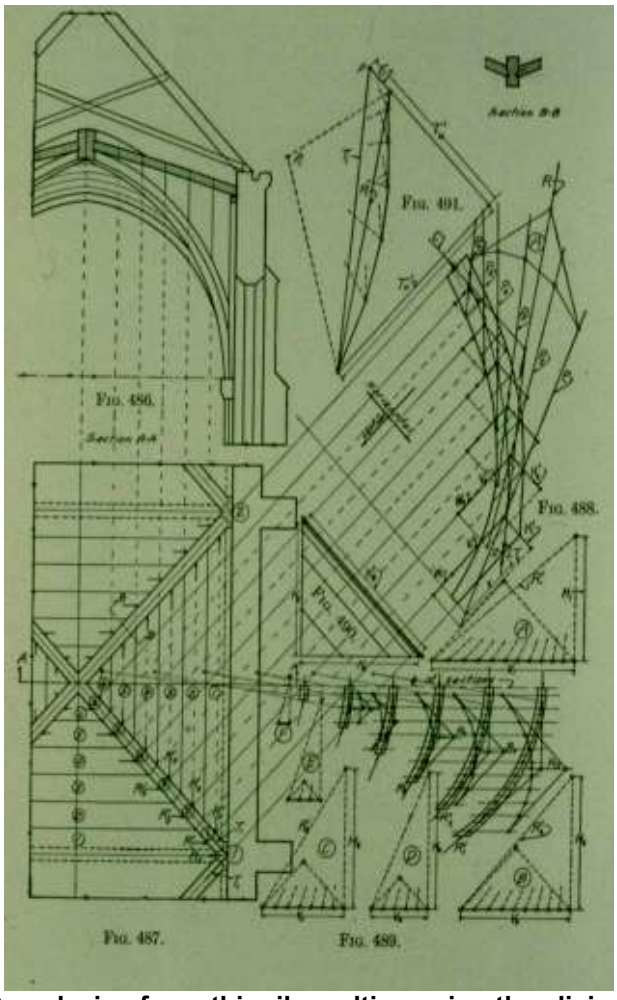

Figure 2.10A pseudo-3D analysis of a gothic rib vaulting using the slicing technique and graphic statics by Wolfe (1921)

2.3 Funicular Modeling

Historically, the catenary analogy was one of the first methods envisaged to assess the stability of masonry buildings. In 1675, Hooke published, in an anagram, the relationship between the shape of a catenary and the shape of the equilibrium line that gives an arch its stability (Heyman, 1989). In 1698, Gregory independently formulated the principle of 'antifunicularity'. He also established the analogy between the tensile forces of the funicular model and the reaction at arch springings, but it was not until 1717 that Stirling proved, by geometric methods, that there is a clear relationship between the stability of a masonry arch and the profile described by a catenary. Poleni in 1748 used Hooke's (1675) hanging chain idea for the analysis of the cracked dome of St Peter's in Rome: "As hangs the flexible line, so but inverted will stand the rigid

arch". He assessed the stability of the dome by hanging a string loaded with weights proportional to segments of a radial slice of the dome.

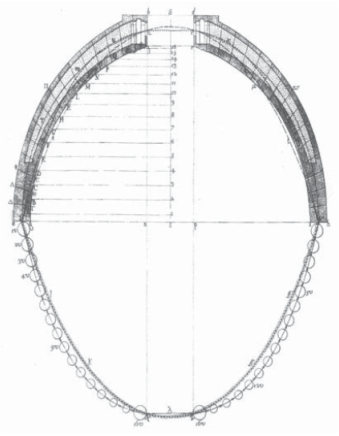

Figure 2.11 Poleni illustrated that the line of thrust is a funicular polygon that may be envisioned as an inverted string loaded with weights for the dome of St. Peter, Rome from Heyman (1996)

It is possible that Wren may have applied the principle described by Hooke to design the dome of St Paul's Cathedral in London. Perronet also applied the anti-funicular principle to find the shape of the arch of Neuilly Bridge, and it is probable that Rondolet also used it in assessing the dome of the Church of Sainte-Genevieve in Paris. Hubsch applied the method to design the vaults and buttresses in Bulach Church and Rottenburg Cathedral in Wurttemberg. Heinzerling formalized the use of the anti-funicular method in his work published in 1869 (Andreu, 2006). The procedure of finding a suitable catenary model of the structure is very challenging and time consuming for a three-dimensional network. It becomes quite difficult to relate the hanging shape to the geometry of the vault.

Figure 2.12 Gaudi 's hanging hanging model for the crypt of the chapel of the Colonia Güell 1898-1919 compared with a model of the geometry of the structure (museum of Sagrada Familia at Barcelona, Spain)

Also, not every network topology works and much iteration is necessary in order to be found a hanging model that fits within the section especially for geometries more complicated than a groin vault. The main problem with three-dimensional equilibrium analysis for masonry vaults is that they are highly indeterminate structures. Antoni Gaudi's physical form-finding process for the church of the Colonia Güell can be used to explain this. The hanging model of the crypt was realized by a highly skilled team from 1898 to 1908. Making the physical hanging model was time consuming. First, before starting to construct a hanging string model, Gaudi had to decide on a suitable force pattern topology that would represent the structural action of the vaults. Then, after choosing the structural logic, it is still challenging to control or even predict the final shape, since the equilibrium of each string influences the equilibrium of the entire network. It is a tedious, iterative process of adjusting and refining.

Figure 2.13 Detail of Gaudi's hanging model hanging model for the crypt of the chapel of the Colonia Güell 1898-1919 (museum of Sagrada Familia at Barcelona, Spain)

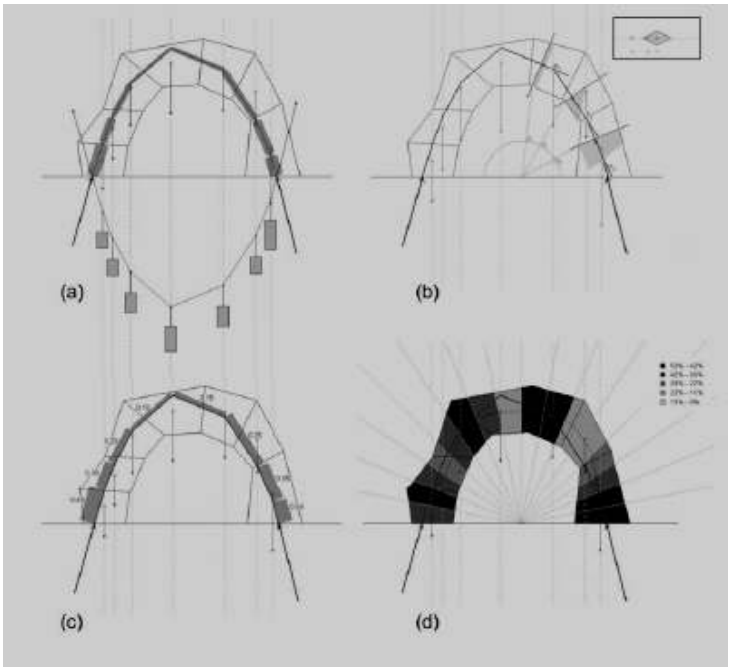

Figure 2.14 Different possible representations for the thrust line: (a) rigid bars, proportional to the forces in every ray combined with the equivalent hanging chain model (b) meaning of resultant on different sections throughout the structure (c) flags indicating the force in each ray and (d) a color code, indicating how far the actual thrust line differs from its most optimal position, the centerline of the structure Block (2003)

Yet the catenary representation is not always understandable, since its meaning is not univocal over its path. Along this line for example, the magnitude of the resultant forces change as it can be seen in Figure 2.14 or the resultants represent very different loading condition in every section as is shown in Figure 2.14b. Some investigations should be done to try to represent in clear ways the ambiguities of the thrust line. Some first attempts to address this are shown in Figure 2.14a-d according to Block (2003). New form-finding programs which explore hanging models in the virtual world, based on dynamic relaxation, such as Kilian's CADenary tool have to deal with the same issues (Kilian and Ochsendorf 2005).

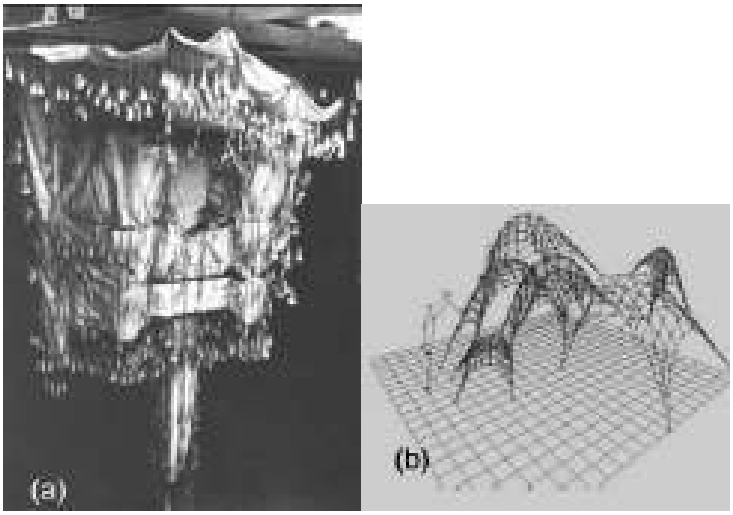

Figure 2.15 (a) Gaudi's hanging weights model to find the form of his Colonia Güell and (b) Kilian's particle spring applet, a virtual hanging chain model

The problem of controlling a virtual hanging strings network has been elegantly and efficiently implemented within a similar optimization framework by Andreu et al. (2007). The analysis of masonry structures by funicular networks Andreu et al (2010) is a method that facilitates the equilibrium exploration through 3D catenary models. This method is computational method for the assessment of skeletal or spatial and curved masonry structures based on the simulation of anti-funicular states of equilibrium by means of cable nets. According to the method, the cables represent the inverted shape of the equilibrium lines (or load paths) experienced by the structural members. In the case of 2D curved structures such as domes and vaults, the cable nets represent, in an approximate way, the distribution of the compression stress fields in equilibrium. The method permits an assessment of stability and determination of the ultimate capacity by application of the static theorem of limit analysis according to Andreu et al (2010). The cable element utilized in the model has been already presented by Andreu et al. (2006, 2007), together with its validation by comparison with available experimental and numerical results.

The concept of anti-funicular equilibrium is used from a computational or virtual perspective. The virtual structure is constructed inverted (upside down) and loaded according to the loading conditions of the structure. After the loading of the structure the initial cable net is deforming. In case that the deformed net is contained in the interior of the structure with the catenary net hanging from the supports then the deformed model of hanging cables simulates a possible state of equilibrium. By inverting the model is possible the

definition of a set of connected equilibrium lines that describes the equilibrium attained by the structure in compression according to Andreu et al (2010).

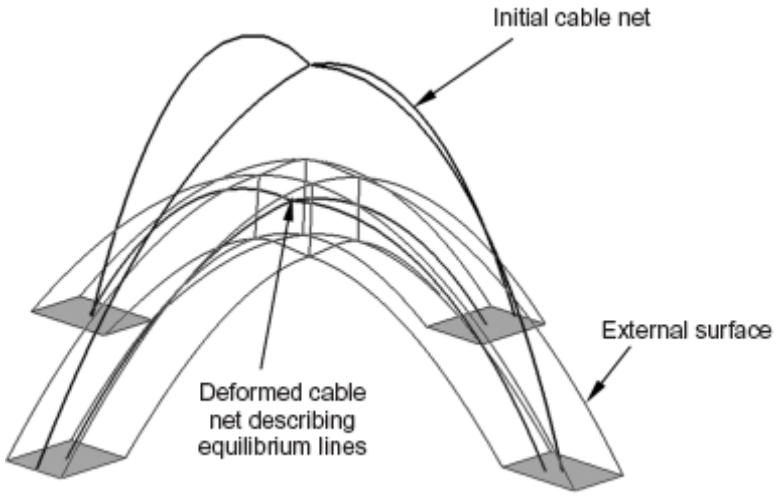

Figure 2.16 Combined modeling of equilibrium lines and external resisting surfaces (inverted representation) according to Andreu et al (2010)

In the case of skeletal structures, plastic theorems can be applied to a cable net representation that comprises linear components as it is shown in Figure 2.17a. In the case of a 2D curved structure such as a dome or general shell structure, O'Dwyer's (1999) approach is used to decompose the structure into a set of multiple arches as it is shown in Figure 2.17b. Every catenary describing an individual linear member must be modeled by a series of cable elements. Thus, the equilibrium lines of the entire structure will be modeled by means of a set of catenary elements connected to a certain number of nodes. In order to assess the safety of masonry construction, the modeling of the external surfaces of the structure is also necessary. For that purpose, the external surface of the structure is simulated by means of a discrete mesh of surface elements.

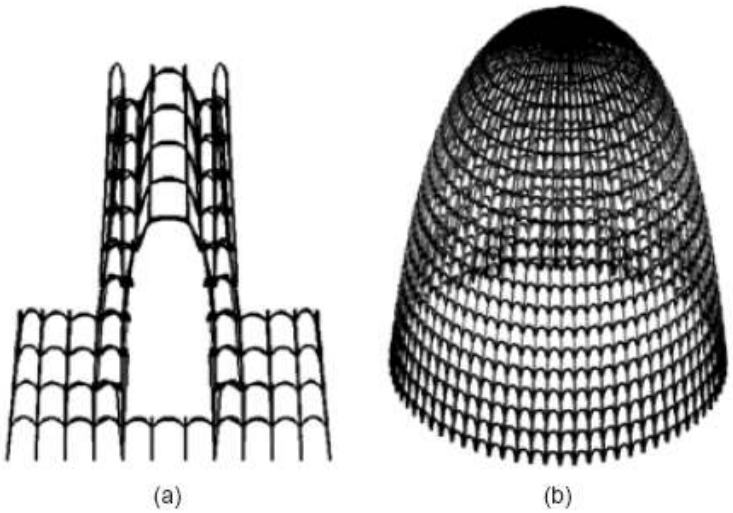

Figure 2.17 (a) Modeling of a skeletal structure and (b) a spatial 2D curved structure by means of a net of cables (inverted representation) according to Andreu et al (2010)

The finite compression strength of masonry can be taken into account by considering a reduced external surface. For that purpose, a plastic distribution of compression stresses is adopted to account for the ultimate state. The stresses are assumed uniform and equal to the compression strength (f_c) in an area centred at the point of application of the thrust as it is shown in the following Figure. The resulting reduced surface must be recalculated for each different value of the thrust (N) acting on the section. Thus far, this possibility has only been utilized in 2D problems for which determination of the maximum eccentricity becomes immediately clear. Determination of reduced strength surfaces for 3D problems requires further development according to Andreu et al (2010).

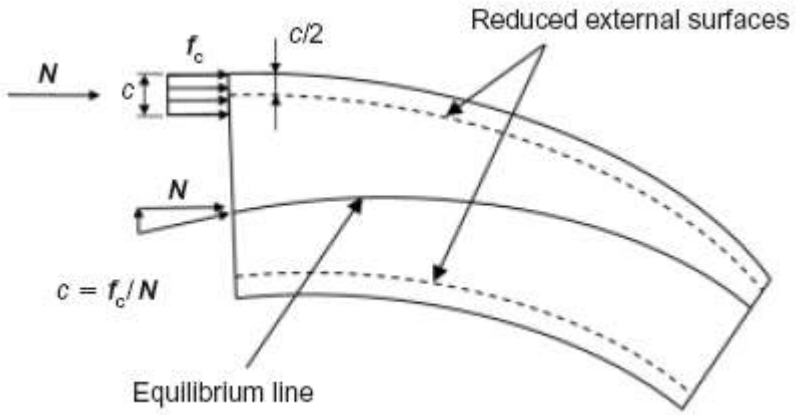

Figure 2.18 Reduced strength surface to account for finite compression strength according to Andreu et al (2010)

A catenary element is defined as the curve adopted by a cable with negligible flexural stiffness, suspended from its ends and submitted to gravity's effect. If a segment of the cable is cut, a set of forces appear at the end nodes which are in equilibrium with the weight of the piece as it is shown in the following Figure.

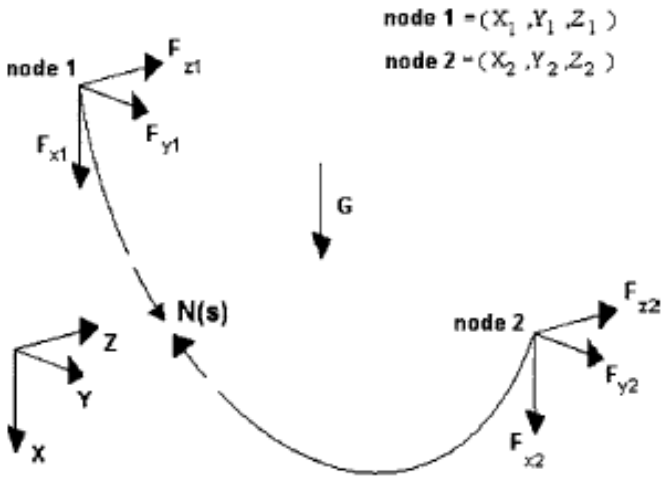

Figure 2.19 Catenary Element

For the catenary element, considering a cable with infinite axial stiffness, the equation that relates the coordinates of the nodes with the forces is known according to Irvine (1992).

$$X_2 = X_1 + \frac{1}{p_0}(\sqrt{Fy_2^2 + Fz_2^2 + (P + Fx_2)^2} - \sqrt{Fy_2^2 + Fz_2^2 + Fx_2^2})$$

$$Y_2 = Y_1 + \frac{Fy_2}{p_0}\left(\arcsin H\left(\frac{P + Fx_2}{\sqrt{Fy_2^2 + Fz_2^2}}\right) - \arcsin H\left(\frac{Fx_2}{\sqrt{Fy_2^2 + Fz_2^2}}\right)\right) \quad (1)$$

$$Z_2 = Z_1 + \frac{Fz_2}{p_0}\left(\arcsin H\left(\frac{P + Fx_2}{\sqrt{Fy_2^2 + Fz_2^2}}\right) - \arcsin H\left(\frac{Fx_2}{\sqrt{Fy_2^2 + Fz_2^2}}\right)\right)$$

Figure 2.20 The equations that relates the coordinates of the nodes with the forces is known (Irvine 1992)

The method has been applied to the lateral towers of the facade of Barcelona Cathedral, Spain. Application of the method requires, as a preliminary step, full definition of the strength surfaces and the initial undeformed cable model as it is shown in the following Figure. The cable model includes 132 elements. The variables chosen for the optimization problem are the length of all cable elements and the coordinates x, y (contained in the horizontal plane) of the end nodes at the base. As shown in Figure 2.21(d) and 2.21(e) the solution obtained is totally contained within the strength surfaces, meaning that the structure can safely resist the entire dead load even if the steel rings were not considered.

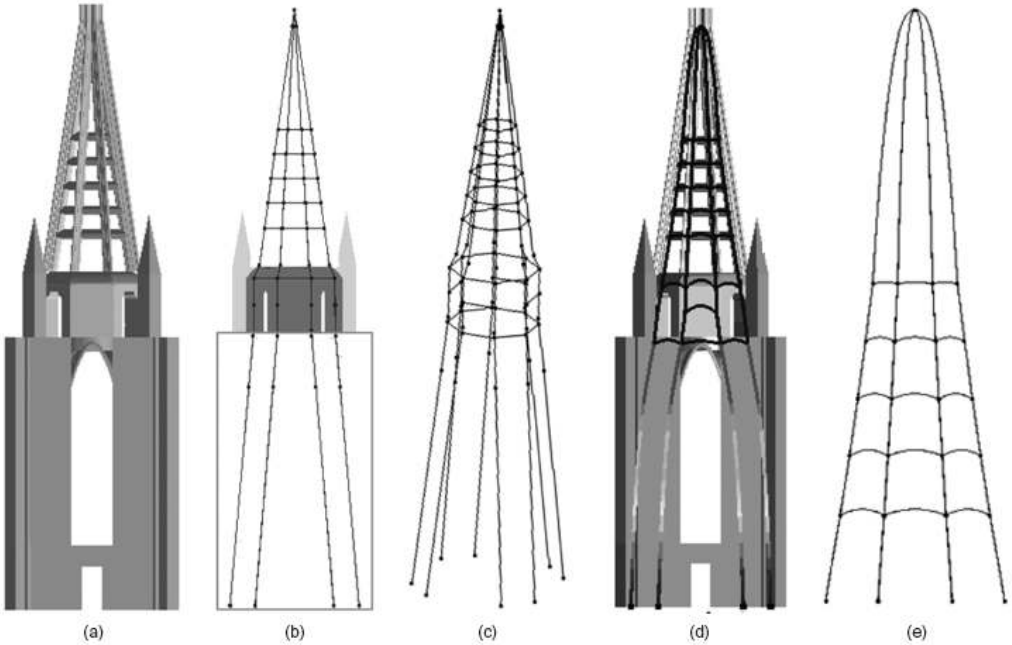

Figure 2.21 (a) Modelling of the external surfaces, (b) and (c) initial funicular model in a reversed presentation (d) deformed funicular model (e) detail of the model

In general it is very hard to control and predict how the final shape of the compression network will look like if local changes are being made or a string model is being assembled and hung under gravity. This is true for both physical and virtual string models as for graphical methods. In order to analyze a three-dimensional indeterminate system these unknowns need to be understood and controlled.

3. DESCRIPTION OF STRUCTURE

3.1 Name, location and description of the whole structure

The site of Park Güell is located on a hillside at the edge of the Collserola mountain range. The main entrance of the park faces southeast onto a narrow street, Carrer d' Olot. In the main entrance there are two colorful gate lodges, which signify the access to the park and also a high wall that surrounds the park at Carrer d' Olot.

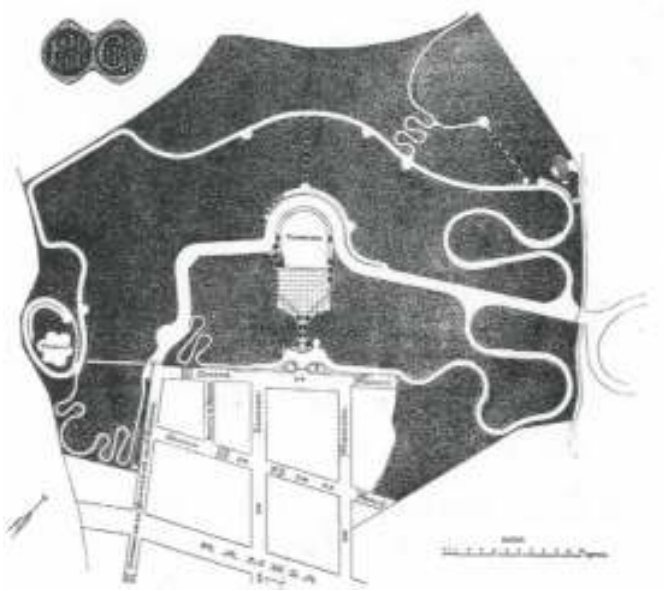

Figure 3.1 General Plan of the park published at "El Park Güell. Memoria descriptiva" of the Annuario of the Association of Architects of Catalonia, 1903

Figure 3.2 General aerial view (Martínez Lapeña and Torres "Park Güell")

The entrance area contains an open space that leads to a staircase which is supported by retaining walls. The double staircase rises in three levels. A grotto-fountain, a serpent's head, and a dragon-lizard straddling and a long ceramic basin dominate the center of the staircase (Kent and Prindle 1993).

Figure 3.3 The wall of the main entrance of Park Güell at Carrer D' Olot (Kent and Prindle "Park Güell")

Excavations cut into the retaining walls provide service areas: a storage area to the left that now is as a cafe, and an enclosure to the right for carriages. Three circulation paths begin from the entrance area. The first to the right is a road five meters wide and follows the inside of the front wall northeast, then winds up the rough terrain to the slopes where sixty villas were originally planned as a part of a residential colony.

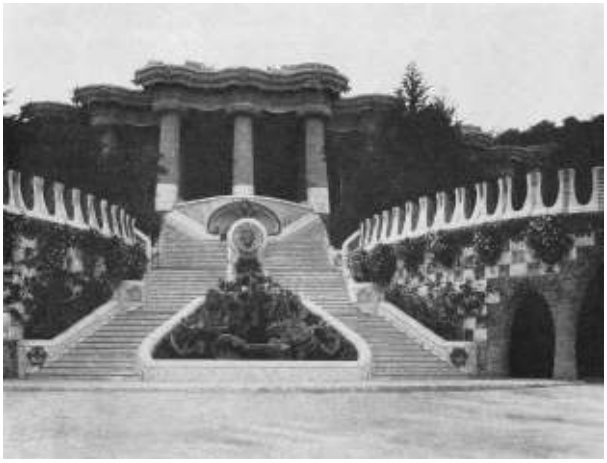

Figure 3.4 The staircase and the Hall Market. View from the main entrance of Park Güell photo from "Antonio Gaudi," by George R. Collins

Another gate at the end of Carrer d' Olot opens onto this road as it begins to curve, crossing the first of three curving portico-bridges in its serpentine ascent (Kent and Prindle 1993). The second to the left is a walkway which runs between the wall and the front of the Güell mansion, then approaches the park's steepest slope, a hill negotiated by a spiral portico and winding paths. An extension of this walkway leads to the highest

point on the site, marked by a large stone Calvary. The third a straight ahead, the monumental staircase rises to the level of the market hall, where to the left is the Baldiri Rexach school-an eighteenth-century mansion and once the home of Eusebi Güell and to the right an open field now planted in formal beds. Beyond the field and farther up the slope lies the original Gaudi house, now a museum, which stands in a copse of pine trees. Staircases beside the market hall and walkways around it both provide access to a third level, where a large plaza (86 x 40 meters) extends back into the hillside, but also out over the roof of the market hall.

The principal artery of the park is an avenue ten meters wide, entering the park to the northeast from the Avinguda del Carmel. Traversing the park above and behind the theater, the avenue is marked by massive stone "trees" suggestive of palms and set like half-columns into the hillside retaining wall. Matched by live Canary Island palms on the other side of the avenue, these stone structures convert the avenue into a shaded terrace overlooking the theater and its bench. The broad avenue exits at the southwest gate of the park, on Sant Josep de la Muntanya.

Access to the upper reaches of the park is provided by the serpentine road, which joins with the broad avenue briefly as it approaches the Avinguda del Carmel entrance, then turns to continue its ascent over the middle and upper bridges of the park. This road would have allowed carriages to reach properties in the upper areas, and is marked by occasional carriage turn-arounds. Higher up, the road begins a long traverse of the hillside, through a nature area past the Trias house, along the broken ridge line at the top of the hill, and on to the southeast where it joins the footpaths approaching the Calvary and summit. The principal features of the park, -the theater-plaza, entrance, and portico-bridges are seen from this point. The summit also looks over Barcelona below and affords views of Mount Tibidabo to the northwest. Ascent and descent from the park summit can also be made by footpaths and short cuts between the park avenues and roads (Kent and Prindle 1993).

Perhaps the most bizarre constructions in Park Güell are its grotto-like bridges or viaducts, permitting the roads on the right side of the site to ascend over the steep topography.

Figure 3.5 Left: View of the lower viaduct Right: Bearing structure of the lower viaduct

Figure 3.6 Left: View of the middle viaduct Right: Bearing structure of the middle viaduct

Avoiding what would otherwise be tight, switchback curves, each of the three columnated bridges carries the road out from the mountain-side to make wider the looping curves by which it makes its serpentine ascent of the site. While each viaduct has its own unique character, all are variously faced with unfinished stone. These structures refuse to be simply functional.

Figure 3.7 Left: View of the upper viaduct Right: Bearing structure of the upper viaduct

3.2 Historical note

The origins of the Park Güell date back to 1899, when Eusebi Güell, a wealthy Catalan businessman member of an influential bourgeois family of Barcelona, bought the land occupying the park by Marquis of Mariano. The park is located in the upper area of Barcelona, at Hill of the Caramel, formerly called “Muntanya Pelada” which means the "Bald Mountain". Later, Count Güell commissioned the architect Antoni Gaudi i Cornet for the urbanization project of the park, which was built between 1900 and 1914. Antoni Gaudi together with Count Güell was aiming at convert the slope of the hill in a residential area. Both wanted to construct a garden city that was similar to those constructed in England where they would provide a high standard urbanization with approximately 60 residences. Despite the work of Gaudi and Güell, the project

became a commercial failure, due to the region, that was at that time little urbanized and was also far from the city center. Only there were sold two plots of land, one of them the current House-Museum Gaudi, where the architect lived from 1906 to 1925, and Casa Trias, property of the lawyer Martí Trias i Domènech. In the year 1914 the works had to stop due to World War I. In the year 1918, after the death of Count Güell the heirs decided to sell the land to the City Council of Barcelona in order to become a public park. Finally, Park Güell opened as a public part in 1922.

3.3 Historical and artistic significance

Gaudi adopted the style of flowing lines and organic forms that produced the floral tracery of the Art Nouveau. But that movement, beginning in arts and crafts, went beyond the decorative use at walls and windows. Park Güell maybe is the project that includes in the largest scale applications of organic forms at architectural structures. For example the viaducts and the gate houses were informed by principles of organicism.

The park except from being an exceptional art nouveau example also is very good representation of the culture of Barcelona in 1900. Moreover is a result of the creative imagination of two men, Eusebi Güell and Antoni Gaudi (1852-1926). Together Güell and Gaudi experienced the transformation of Barcelona into a modern industrial city. Together for fourteen years, from 1900 to 1914, they actually brought all their previous experiments in reality at Park Güell. Along with the chapel crypt at the Colonia Güell, the park is their greatest achievement and a powerful expression of the cultural aspirations of the industrial order Barcelona of the end of 19_{th} century.

The collaboration of culture and industry was a phenomenon characteristic of the age. When the park begun in 1900 Barcelona's industrialists, already the most powerful in Spain, were looking to expand both the economic and cultural influence. Recovering from the loss of colonial markets and cheap resources after the war of 1898, Güell and his peers were facing the challenges of the new era. Park Güell, originally was designed as a real estate project, and was designed to meet those new economic and cultural challenges. Without the colonial markets abroad the textile industry was in crisis so the interest into other type of business appealed to be an attractive and necessary alternative. By the turn of the century Güell himself had moved into other areas, producing cement in a new enterprise and beginning his venture in real estate at park Güell.

Park Güell was to be the ideal destination for Barcelona's new elite, a mountain-side enclave built on the rugged terrain. The park was to be a residential housing project on 15 hectares pulled together from Güell' s purchase of two parcels of undeveloped land. The first and largest was bought in 1899, while the second, at the top of the mountain, was added during construction in 1902. Rising some 60 meters over rocky terrain from 150 to 210 meters above sea level, Muntanya Pelada ("Bald Mountain") was a very steep land to develop a building project than the expanding city bellow. The topography, together with Güell' s triangular plots and the prohibition against clearing the sites of existing trees, make mandatory for the architect a more rustic landscape. The topography was so irregular that from the very beginning it was decided to design the garden villa plots in consort with the natural terrain. Roads and paths of four different widths and building

plots for sixty villas were to be adapted to the contours of the park site. Residents of the park were to have their own chapel, a weekly village market, theater, and public plaza, as well as a protected reserve of fresh water on the site. A high wall would protect the structures and regulate the access. The common buildings and public areas were intended to connect the families together in a residential community.

The inspirations for the park seem to have come from diverse sources. On the one hand the park is an indigenous, Catalan answer to the ideal associated with the English landscape tradition in combination with a contemporary garden city. It is also important, constant references to local geography and Catalan craftsmanship, as well as the insistent use of indigenous vegetation in the landscape. This was a way to point the regional pride which shapes even the most cosmopolitan features of Barcelona's urban landscape. Among the keys of the qualities of life in Park Güell was the tendency to retreat from the newly great city below. Park Güell was to serve as a haven, a private world made possible by the industrial and commercial power of Güell, and made necessary because of the changes in the life of Catalonia. The potential buyers which would need an alternative of the modern and constantly changing life below would find in Park Güell a residential solution. A second key to Park Güell is the recognition of Güell and Gaudi's obsession with integrating the past and the present. Numerous inventions in the park give evidence of the attempts of Gaudi and Güell to include the modern technologies in archaic shapes and the numerous colors of folk art. The dressing with bright ceramic tiles or rustic stone is characteristic of the Catalan tradition. Still, the tradition did not serve only as ornament. Traditional craft also made possible structural configurations to be implemented in the contemporary architecture and engineering, as in the park's gate lodges with their fluid parabolas and hyperbolic paraboloids constructed with traditional Catalan tile vaulting. A third key to understanding the park is Gaudi's integration of sacred impulses in the design. This modern residential garden is involved with the Catalan tradition of shrines and pilgrimages, traditions associated particularly with the monastic heritage of nearby Montserrat, the sacred mountain whose "Black Virgin" had become the patron saint of Catalonia in 1881. In this way Gaudi was synthesizing real estate development with religious tradition.

The great parks and landscape gardens had traditionally reached some of their most romantic heights in artificial ruins or grottoes evoking a mythic past, a spirit of the place often associated with classical gods or more historical figures commemorated in funerary monuments. The Gaudi-Güell response to the tradition may be seen here in the grotto-like porticoes and the bridges they support overhead. Gaudi’s designs create spaces variously reminiscent of mountain shrines, Christian catacombs, grottoes, or cloisters, features which commemorate not gods or heroes, but the genius loci which are found in the sacred Catalan land itself (Kent and Prindle 1993). Here, the park residents could found reminders of the ancient heritage of their land. These bridges are hallmark features of the park. They also account for the character of the higher reaches of the park, thematically as well as aesthetically.

Each one of the Gaudi's bridges represents a different historical style, but what impresses most visitors is the beauty of stone forms that seem rooted in the land itself, originating before or outside of history. Dali saw it in the slumping stone forest of massive jardinieres surmounting the upper bridge, and in one of his better known comments on Gaudi gave the surrealist response: "The open spaces between the artificial trees give me a sense of unforgettable anguish" (Salvador Dali 1942). Most observers find that the archaic effects of

the stonework remind them variously of grottoes, caves, stalactites, architectural ruins, and of course, the rugged landscape.

The program of the portico-bridges would have made possible within the domestic use of the garden city a small-scale version of the pilgrimage-excursions then popular with Catalans. Gaudi had visited such pilgrimage sites in the 1880s, both with a Catalan excursionist society and with the Association of Architects of Catalonia. The garden traditions of the English landscape also meet here with the more popular nineteenth-century enthusiasm for the religious grotto, an enthusiasm reinforced in Catalonia by ideology and tradition.

Substituting his archaic portico-bridges for the more traditional Gothic ruins Gaudi chose to evoke the kind of geological and devotional sites of the Catalan landscape in his drawings. The Catalan fixation on the grotto as an emblem of sanctity was already established. These bridges are hallmark features of the park. They also account for the character of the higher reaches of the park, thematically as well as aesthetically (Kent and Prindle 1993). Gaudi's bridges hint at historical styles, but what strikes most visitors is the beauty of stone forms from the centuries of Moorish occupation. Also the inspiration for the porticoes can be also find in the shrines of Montserrat, the cavernous religious mountain, with sacred caves and labyrinthine paths. The program of the portico- bridges can best be understood as a combination of the two traditions of garden and grotto.

In Gaudi’s bridges the likeness to sacred grottoes and ancient buildings is emphasized by the rough, and archaic stonework applied to the columns. Contemporary with the gate lodges and park entrance, the portico-bridges belong to the critical period from 1901-1903 when Gaudi began to produce the radical innovations grounded in his philosophy of organic form. With their rustic surfaces and their structurally experimental design, the grotto-bridges combine great technical ingenuity with a highly aesthetically appearance.

The spiral ramp, the columns and vaulting of the viaducts, shows that Gaudi was far from just imitating the Gothic architecture in the 1880s. Forms which Gaudi used as revival of medieval forms like rib-work and the fan vaulting of the viaducts were being refashioned in unique organic forms which he saw himself taking directly from the "book of nature." "The column is like the shaft; the trunk of a tree," Gaudi told the young Joan Burgos; "the roof is like the mountain with its ridge and slopes. The vault is the cave of parabolic section. The more resistant terraces of the mountain cliff form lintels and corbels where the weaker strata have eroded away"(Kent and Prindle 1993). In the observation of the nature Gaudi found the structural designs which would correspond to the equilibrium and diversity of nature. The gate houses on the Carrer d' Olot were the first were Gaudi attempted the application of the "book of nature" into forms usable in contemporary life. If the result in work like the portico-bridges of the park impresses today as a radical naturalism, for Gaudi the experience of nature was shaped and mediated at every point by his experience of his culture. For Gaudi, organic form inevitably went beyond aesthetics. Gaudi's organic engineering of the viaducts is an ideological, as much as an artistic, statement. Engineering, a "rational science" had grown up with the use of industrial iron and the materialistic science of frame structures. To Gaudi the architect

distinguished himself from the structural engineer by endowing his creation with a spiritual and a human purpose that moved beyond the mechanics of construction.

In the year of 1969, the Park Güell was nominated Artistic Historical Monument and in 1984 UNESCO included it as a "World Heritage Place of Works of Antonio Gaudi".

3.4 Architectural arrangement of the lower viaduct, structure and materials

There are three main viaducts that facilitate the transition through the Park Güell. All the viaducts were projected with an important width to permit the passage for carriages and some porticoed roads to allow the passage of pedestrians. The plan view of the three viaducts can be seen in Figure 3.8. The viaduct that has the south position in the plan view of the viaducts is the lower viaduct. The viaduct that is at the north position of the three viaducts is called the upper viaduct while the viaduct between the lower and the upper viaduct is called the middle viaduct. Gaudi designed each viaduct with a different structural solution, the lower viaduct with a Gothic style, the middle viaduct with Baroque style and the upper viaduct with Romanesque style. The three different architectural styles of the viaducts can be seen in Figure 3.9. However in this Chapter the emphasis is given in the description of the geometry and the structural system of the lower viaduct. The stability of the lower viaduct will be analyzed in the following Chapter.

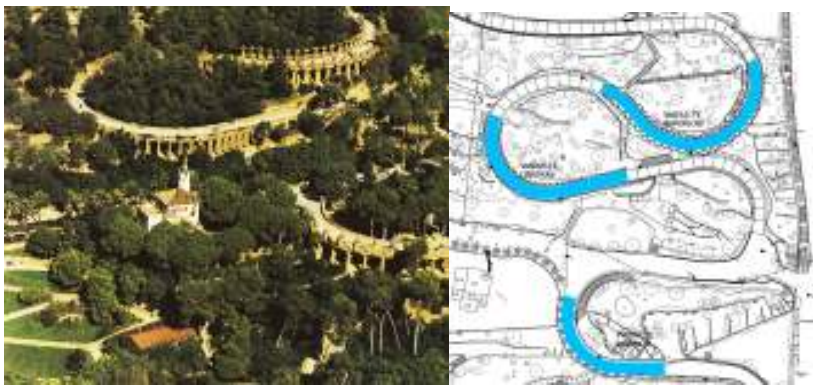

Figure 3.8 Left: General view of the three viaducts Right: Plan view of the viaducts according to previous study of BIS architects

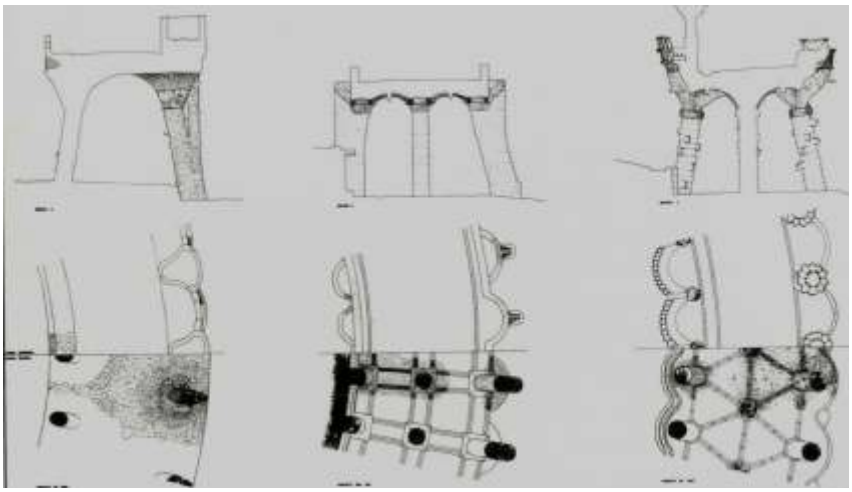

Figure 3.9 Elevations, horizontal sections and isometric drawings of the three viaducts Left: the lower viaduct Middle: The middle viaduct Right: The upper viaduct (Kent and Prindle 1993)

The first of the viaducts, the named also as lower viaduct is located at the bottom of the layout shown in Figure 3.8. The lower bridge curves up to the principal avenue at Gaudi's house in a fairly steep grade. It has a wide of 6.50 m and a length of approximately 50 m as shown in Figure 3.11

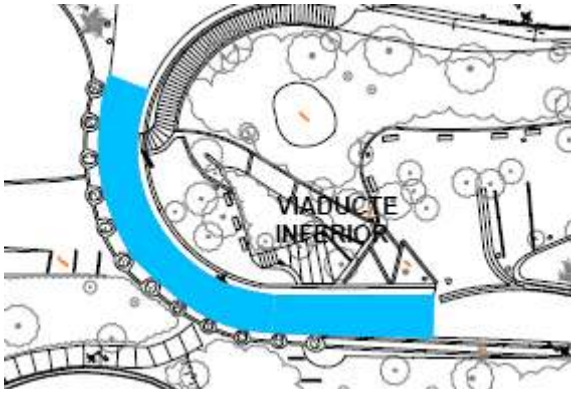

Figure 3.10 Plan view of inferior viaduct (BIS architects)

The arrangement of the columns of the structure form a curve as it can be seen in the plan view of Figure 3.11.

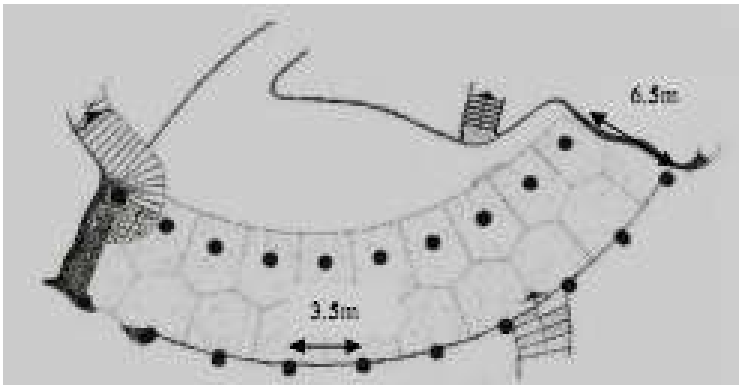

Figure 3.11 Architectural arrangement of the lower viaduct

The general views of the structure both from the north and the east side can be seen in the Figure 3.12.

Figure 3.12 Left: General view from the north side of the lower viaduct Right: General view from the south side

The vertical bearing structure is columns of 80cm in diameter with a maximum height of 6.00m. The columns are made of masonry and are covered with stone as a cladding over the original structure. A section of the structure can be seen in Figure 3.13. The geometry of the columns is described in Figure 3.14.

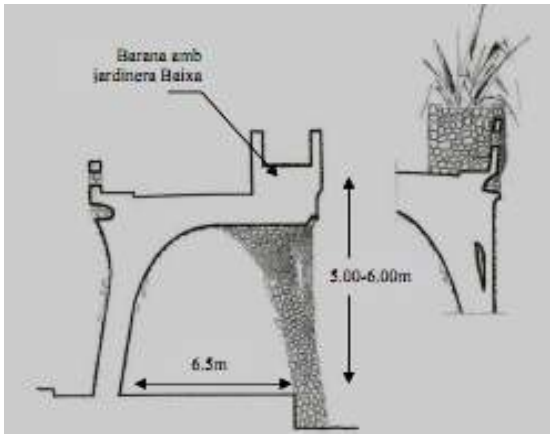

Figure 3.13 Section of the lower viaduct and detail of the jardiniere of the deck of the bridge

Figure 3.14 Detail of the columns in elevation. Photo taken from the north side of the structure

Gaudi's columns combine logic with aesthetic effect as, canted slightly inward. The inclination of the columns apart from impressing aesthetically has also a structural meaning.

Figure 3.15 Stem-like columns in the north side of the bridge of the lower viaduct

This is facilitating the columns to bear the thrust line of the structure within the limits of the columns geometry. The union of the columns is done with a capital that has a mushroom form that terminates in a pentagon. Arising stem-like from these canted columns in the outside curve of the bridge in the north side of the structure there are smaller columns, which support the bridge's overhanging balustrade. The diameter of these auxiliary columns is 50cm. With the main columns of the two sides alternating rather than opposing each other, the rising incline of the bridge yields a complex, rhythmic effect as the visitor walks beneath the curving portico (Kent and Prindle 1993). Elongated stones attached to the brick and tile sub-structure of the columns also enhance the effect as they rise to give an irregular but dynamic effect of fan vaulting. The load transmition to the columns is through the capitals that have a mushroom form as it can be seen in Figure 3.17. The horizontal bearing structure is a stone vault without nerves. The vault is covered with uniform pieces of stone. The finished top of the vault was made with concrete, which appears as a layer over the initial finish with stone. The columns together with the vault assemble the geometry of a parabola.

Figure 3.16 The main columns of the north and south side of the lower viaduct are alterating rather than opposing each other

Figure 3.17 The fan vaulting of the lower viaduct. The transmition of the load is done through the capitals that have a mushroom shape.

On the roadbed overhead, the metamorphosis continues as the portico below becomes the bridge above. The bridge, in turn, supports a series of benches which function also as protective railings. Set into these benches are jardinieres which contain agave plants that emphasize on the relationship between organic and architectural forms. The provocative relationship of grotto and bridge is an experiment varied rather than replicated in the nearby bridges.

Figure 3.18 Left: View of the deck of the bridge Right: Detail of the bench at the south side of the deck of the bridge at its current state with forbidden access due its instability problems

Figure 3.19 Left: View of the jardiniere Right: View of the benches and the jardiniere from the south side of the lower viaduct

On the north side of the deck of the bridge there is a railing made of masonry as shown in the Figure 3.20. The railing is given an asymmetrical form.

Figure 3.20 Railing at the north side of the deck of the bridge of the lower viaduct

3.5 Previous study on the structural capacity of the lower viaduct

The Department of Environment of the City Council (Departament de Medi Ambient de l'Ajuntament de Barcelona) and its representative its Manager Mr. Jorge Campillo Gamez requested during September 2010, the professional Services of Martí Cabestany Puértolas, architect, and David Garcia Carreras, architect and technical director of consultants BIS architects, architecture company specializing in structural design and rehabilitation of buildings, to work on a structural diagnosis of the viaducts of Park Güell, located on mountain of Carmel, at the street Carrer d' Olot of Barcelona.

The purpose of this report is was to locate and identify the various structural lesions, and as a diagnosis what is the structural capacity of the viaducts. The study evaluates the security level that the structure has for the actual use are and is designed to have, concluding the security if the security is admissible or not for safety of the users. It is recommended that all the interventions and recommendations mentioned in the diagnosis, are formalized in an Executive Project Consolidation and structural reinforcement (Projecte Executiu de Consolidació i Reforç Estructural).Since the diagnosis about the current state of the building, the Finite Element analysis is considering the existing geometry and the current state of loading. The verifications were performed with different computation programs depending on the geometry and material of each element.

The elements of the lower viaduct that were analyzed were:

1. The bearing structure
2. The railing with benches
3. The jardinieres
4. The low railing

This study was a compilation of the most significant data from these analyses.

For the definition of the bearing capacity of the material that forms the structure of viaducts (vaults and pillars) have been used values obtained in other similar works and have been conducted with the formulation proposed by the CTE-F in Annex C (although it is designed for ceramics):

It has been considered limestone with a resistance to compression of 60 N/mm^2 and a mortar M-2 (2 N/mm^2). From Annex C of the DB-SE-F the characteristic compressive strength of masonry it is obtained:

$F_k = K \cdot fb^{0.65} \cdot f_m{}^{0.25}. = 0.6 \cdot 60^{0.65} \cdot 2^{0.25}$

Calculating with the values obtained by the material characteristics the compression strength is 102.Kg/cm2. As for tension, is considered a 10% of compression strength 102.1 $kg/cm^2 \cdot 10\% = 10.2\ kg/cm^2$.

Taking a reduction coefficient of 2.5 it is:

Resistance to compression: 102.1 kg/cm^2 reduced to 40 kg/cm^2

Resistance to traction: 10.2 kg/cm^2 reduced to 4 kg/cm^2

It was also recommended carrying out a laboratory test to know the real characteristics of the material that the viaduct is made of.

The detail of all states of loading that might occur due to different parts of the building is according to the values proposed by current regulations, the Technical Building Code of Spain (codi tecnic de l'edificacio). These load states were used in the calculation of the viaducts and the various elements that compose it. There have been many different hypotheses as loading condition and have been generated several possible combinations with the corresponding application of the coefficients that increment the loads.

1. Dead loads

The dead loads were determined based on the dimensions and densities of the materials comprising them. The densities of the materials considered are:

Reinforced concrete: 2.50 t/m^3

Solid bricks: 1.80 t/m^3

Stone: 2.20 t/m^3

Filling of stone and mortar: 2.20 t/m^3

2. Overloading

TRAFFIC LOAD AVERAGE

Loading of Use: 1000 kg/m^2

PADESTRIANS

Load of use: 500 kg/m^2

Vertical loads on handrails: 200 kg/m

Horizontal loads at handrails: 160 kg/m

3. Wind action

The values used for calculating wind were the following:

Wind velocity: v=29 m/s

Dynamic pressure of the wind: q_b = 0.52 kN/m^2

Coefficient of exposure: c_e = 2.0

The Park Güell viaducts were analyzed with the current regulations, the Technical Code of Building of Spain, taking into account the loads foreseen with the circulation of average traffic load. It will be necessary to determine if the structural element complies or doesn't comply with the current regulations. Therefore, a check is made with the values of maximum stress of design (E_d) to compare with the values of the reduced elastic limit of the element's material strength (R_d). From this study we can determine if we deal with a tension that can *meet* the regulations, if the value $E_d \leq R_d$ or *cannot meet* $E_d > R_d$.

When the result of the verifications is to *meet*, we can say that the structure exceeds the safety factors set by the regulations. That means that the admissible stress of the element (R_d) with coefficients of reduction (γ_M) is higher than the tension which is subject according to the calculation (E_d) with the respective coefficients (γ_G, γ_Q). Moreover, this statement considers that the element is in an acceptable state of conservation.

If the condition is *cannot meet*, it means the item does not meet the analysis safety factors set by standards. Then a second verification is performed with the characteristics values of tension (E_k) and compared with the characteristic values of elastic limit of strength of the material (R_k). If the result is admissible, there must be action on the item until it complies with the condition that means it must be strengthened to achieve the security level set in the regulations. In this case, it is necessary to take immediate safety measures so there is not any risk for the security.

If this second comparison result is not acceptable, the item is subject to a tension higher than it can support and therefore must be performed some security action immediately (reinforcements, restrictions of use, etc.)

To analyze the structure of the viaduct a finite element model was carried out with the program Robot. It was modeled using shell elements, to simulate the layer of stone that is the bearing layer, entering the filling as dead weights and skipping the collaboration it may have with the structure. in the reality the behavior of the viaduct is considered to be a bit better than the model. These elements are of 40 cm thickness. In the reality there must be configuration of the thickness of the vault in order for the model of the viaduct to be accurate. The Finite Element model can be seen in Figure 3.21

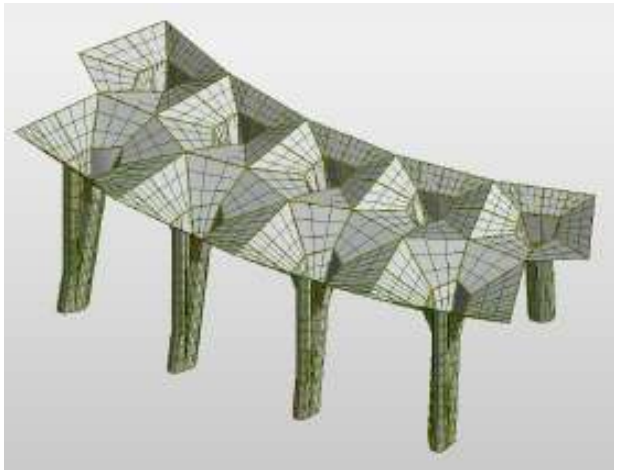

Figure 3.21 Finite Element model of the viaduct

From this analysis there were the following conclusions and recommendations:

4. Bearing structure

The bearing structure of the viaduct meets the condition.

5. Railing with benches

The rail of viaduct does *not meet* the condition and is the condition is not admissible. According to the results obtained in the numerical verification, the railing of the viaduct has a higher stress than those that can support. Therefore, it must be strengthened or limit the access urgently.

6. Deck jardiniere

That jardiniere *meets* the condition. According to the results obtained in the numerical verification, the jardiniere has lower tensions that it can support. Therefore it doesn't need to be strengthened.

7. Low railing

The low rail of viaduct does not meet the condition and is the condition is not admissible.

According to the results obtained in the numerical verification, the low railing presents tensions higher than it can support, with coefficients proposed by the standards, but it has a sufficient supplement of safety for the failure in a matter of urgency. Therefore, we must strengthen but do not need to take urgent action.

After the completion of the analysis the following conclusions have been made. Park Güell is a unique architectural work of the modernist architect Antoni Gaudi i Cornet, with a very important heritage value that requires a specific and accurate treatment. Therefore it was recommend keeping the restriction of access to the railings, planters and benches above the viaduct and make limited the access to the railings and benches under the viaduct, to perform an operation of such consolidation.

Therefore, we recommend keeping limited access to the railings and benches of the viaduct, for performing an operation of consolidation.

Furthermore, the coating of stone of the viaduct and the different elements of this study were excluded because of its maintenance actions, which are already carried out periodically.

As a final conclusion of this structural diagnosis of viaduct of Park Güell in Barcelona, was recommend the implementation and execution, as soon as possible, a basic and executive project of structural consolidation of unstable elements to ensure an appropriate degree of security.

4. GRAPHIC STATICS

4.1 Introduction

The graphic statics method has been applied to the lower viaduct for the calculation of the thrust line of the structure. The purpose of the calculation of the thrust line is the investigation of the stability of viaduct. According to the safe theorem if there is a thrust line that fits in the limits of the structure then the structure is stable.

The architectural information of the lower viaduct is given in Figure 4.1. In gray color is represented the masonry while in brown color is represented the layer of concrete at the deck of the bridge.

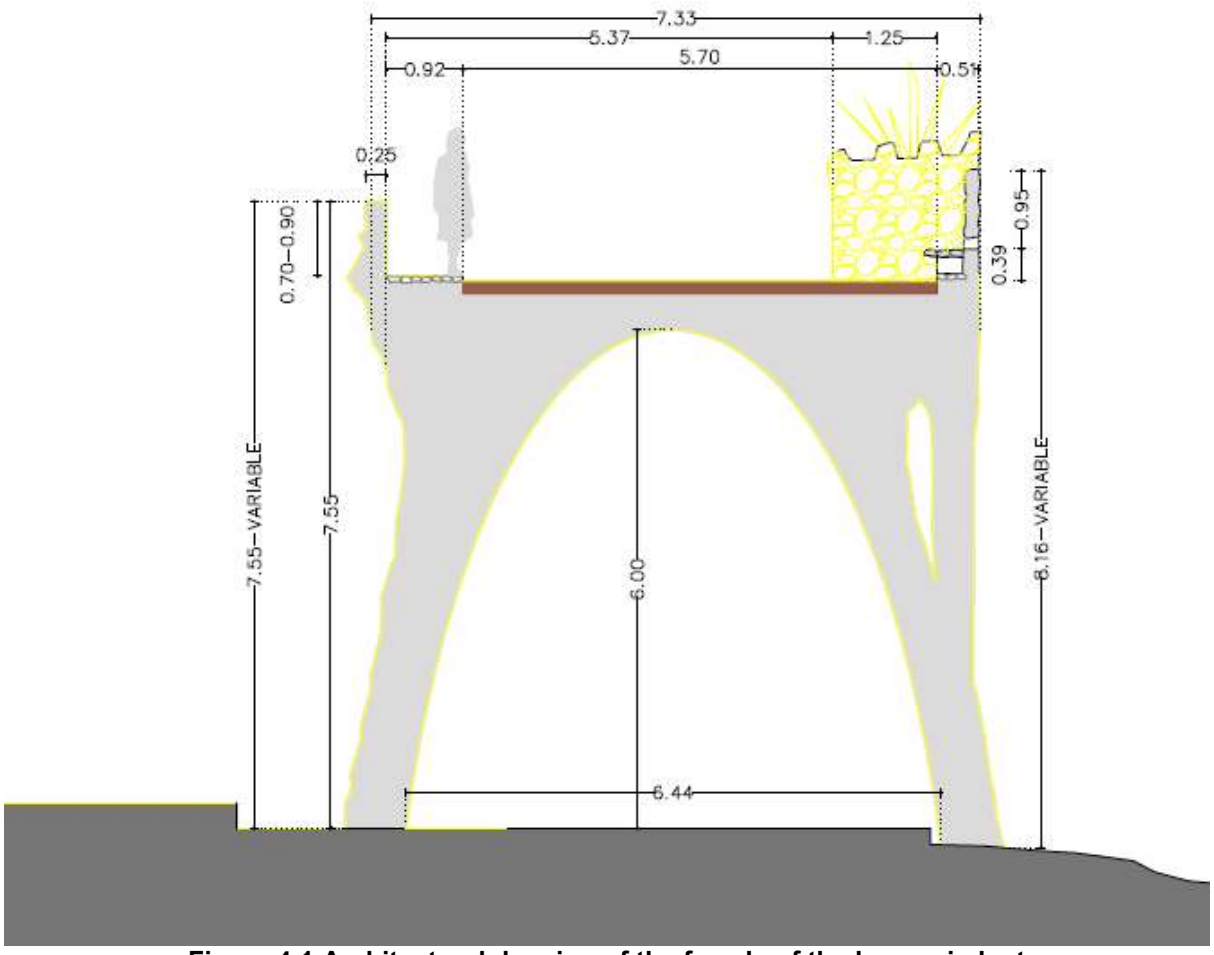

Figure 4.1 Architectural drawing of the facade of the lower viaduct

For the calculation of the thrust line it was necessary the creation of a 3D model in AutoCAD 3D. The creation of the model was based on the architectural information of Figure 4.1, the architectural configuration of chapter 3.4 and photos taken during the in-site inspections. Due to the symmetry of the structure there has been modeled only a part of a structure that is repeated along the structure. A view of the model can be seen in Figure 4.2. The columns are represented with yellow color while the masonry vault is represented with green color. Also the concrete of the deck is represented with gray color. The railing of the north side of the deck is in green color and the jardiniere and the bench of the south side of the deck is in yellow color.

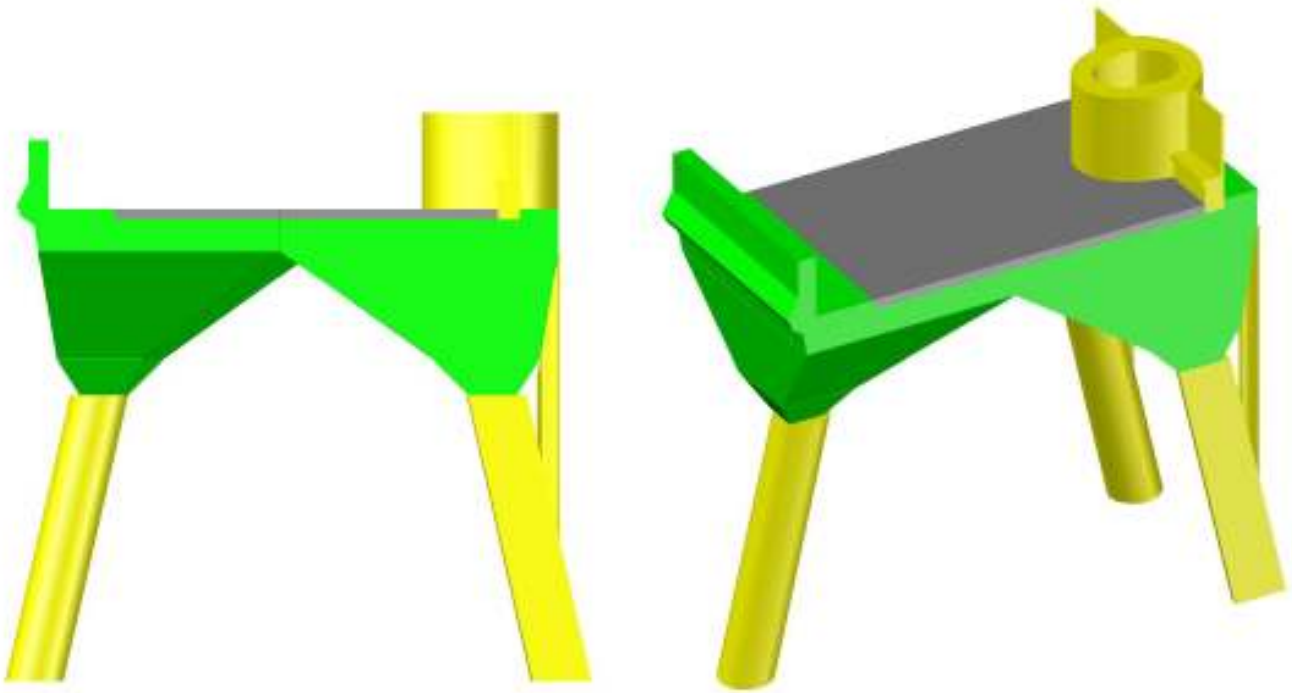

Figure 4.2 Left: View of the 3D model of the lower viaduct of Park Güell Right: 3D view of the model

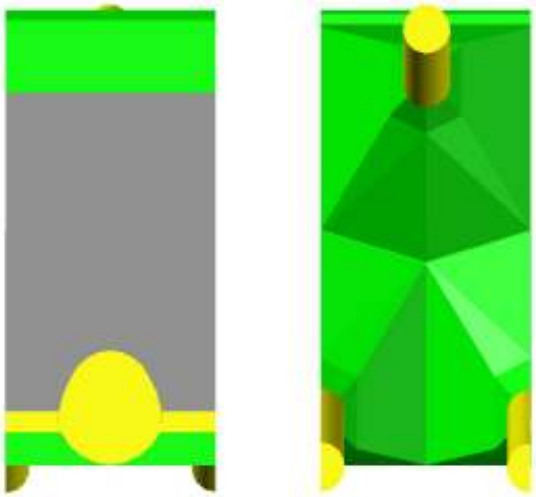

Figure 4.3 Plan view of the 3D model

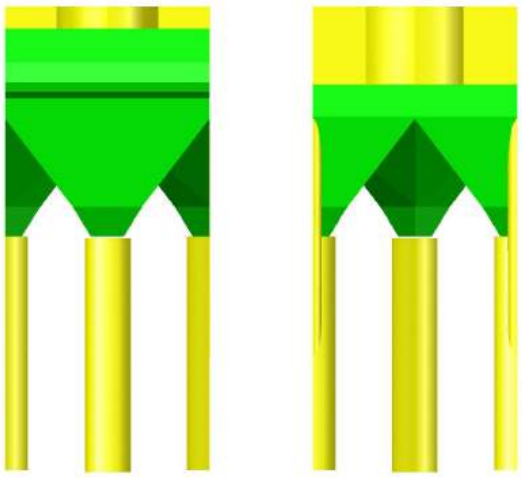

Figure 4.4 North and south view of the 3D model

The plan view of the viaduct and the can be seen in Figure 4.3 while the north and the side view can be seen in Figure 4.4.

4.2 Thrust line calculation

The calculation of the thrust is divided in 2 parts. In the first part the calculation of the thrust line is regarding the model shown in Figure 4.5. This part of the south side of the structure is repeating through the structure. For this reason the thrust line can be calculated in this element.

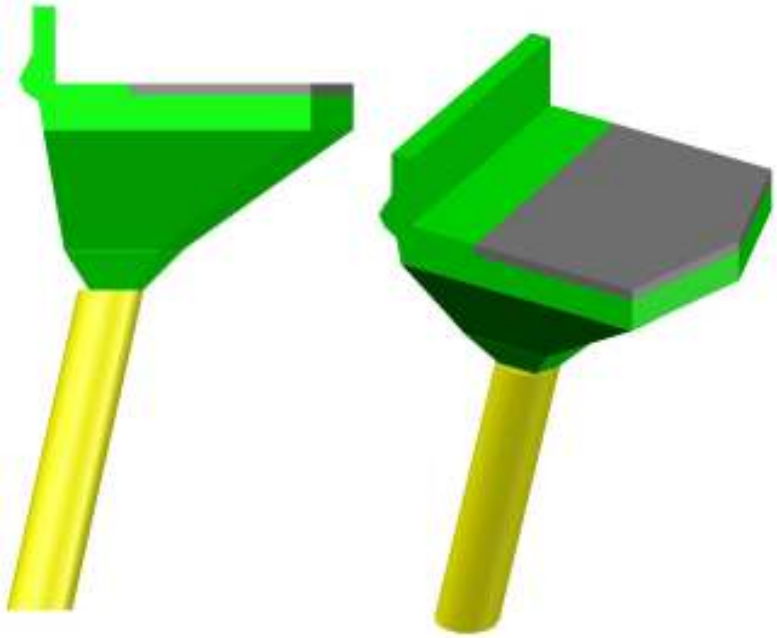

Figure 4.5 View of the characteristic part of the north side of the lower viaduct of Park Güell Right: 3D view of the model

For the calculation of the thrust line the vault is divided in 15 voussoirs. The voussoirs of the part of the structure made of masonry are represented in Figure 4.6 in green and blue color while the concrete voussoirs of the deck of the bridge are represented in Figure 4.6 with grey and blue color. The column is also divided into 8 voussoirs as it can be seen in Figure 4.6. The numbering of the voussoirs of the vault and the column can be seen in Figure 4.7.

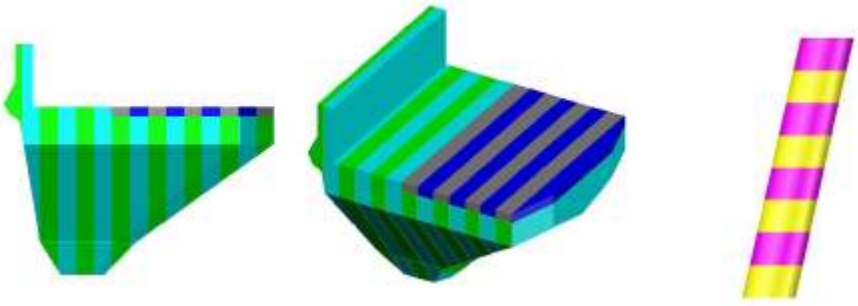

Figure 4.6 Discretization of the model into voussoirs for the mass calculation

The position of the center of the mass for the voussoirs of the vault and the column is obtained with AutoCAD 3D and it can be can be seen at Figure 4.7. The center of the mass differs according to the

material of the voussoir. The coordinates of the center of the mass are necessary because they are the points of application of the self weight of the material either masonry or concrete. Also, the center of the upper surfaces of the voussoirs can be seen in figure 4.7. The center the upper surface is the point of application of the traffic load of the structure.

The coordinates of the center of the mass of each voussoir made of masonry can be seen at Table 4.2 while the coordinates of the center of the mass for the concrete voussoirs can be seen in Table 4.3. The coordinates of the center of the upper surface are presented n Table 4.4.

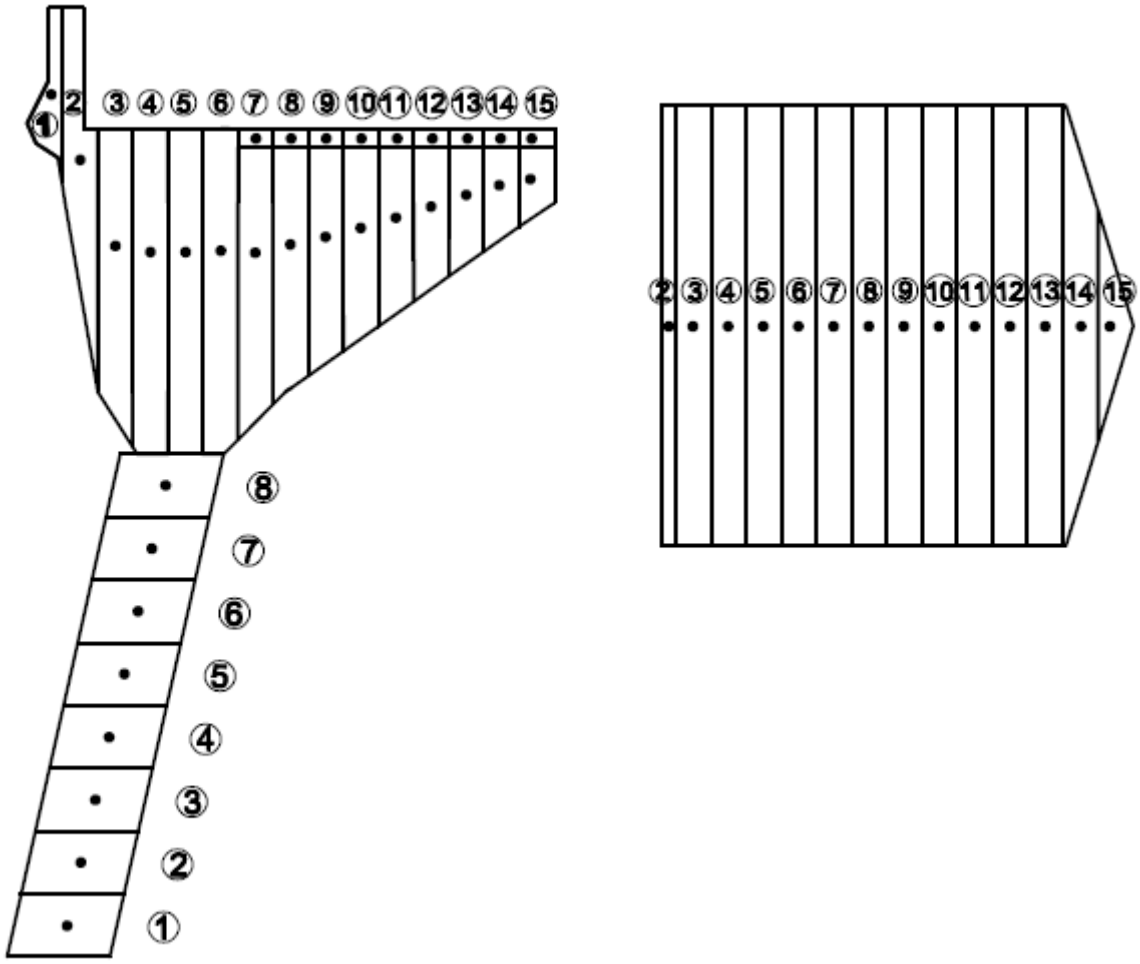

Figure 4.7 Left: Centers of mass of the different voussoirs. Right: Centers of mass of the upper surfaces of the voussoirs at the deck of the bridge

The loads acting on the structure are divided in two categories. The first category is the dead load which is the self weight of the structure. There are three different type of materials in the structure for which the self weight is calculated; the masonry of the vault and the jardiniere, the concrete of the upper layer of the deck and the soil that is used as a filling in the jardiniere for the south side of the structure. The second category of load is the live loads which include the traffic load acting on all the area of the deck. All the loads are according to the loads proposed by the previous structural study about the structural capacity of the lower viaduct made by BIS architects Table 4.1 is presenting the price of the loads acting on the structure.

Table 4.1 Dead and live loads acting on the viaduct

Dead loads			Live load
concrete kg/m^3	masonry kg/m^3	soil kg/m^3	traffic kg/m^2
2300	2200	2000	1000

The pedestrians load proposed by the study of BIS architects is 500 kg/m^3 so it is safer to consider the traffic load as the main live load for the stability evaluation. For the calculation of the self weight loads acting on the structure the volumes of the masonry and concrete voussoirs are given in the Table 4.2 and Table 4.3 accordingly. The self weight acting on the center of the mass of the masonry and concrete voussoirs is calculated with Excel and is also presented in Table 4.2 and Table 4.3. The load is scaled in order to be graphically represented and designed in AutoCAD. For this reason a scaling of 0.02 has been used. The length of the lines representing the size of the vectors of the self weight forces are given in table 4.3 and Table 4.3.

Table 4.2 Self weight and center of the mass of the masonry voussoirs of the vault

Self Weight					
Masonry					
No unit vault	Volume m^3	Load kN	AutoCAD m	Centroid X m	Centroid Y m
1	0.64	14.12	0.28	-15.45	1.86
2	1.67	36.76	0.74	-15.22	1.34
3	1.62	35.63	0.71	-14.94	0.66
4	1.68	36.97	0.74	-14.66	0.61
5	1.68	36.99	0.74	-14.38	0.61
6	1.67	36.64	0.73	-14.10	0.62
7	1.44	31.74	0.63	-13.83	0.60
8	1.36	29.93	0.60	-13.55	0.67
9	1.27	28.00	0.56	-13.27	0.73
10	1.16	25.61	0.51	-12.99	0.80
11	1.03	22.76	0.46	-12.71	0.88
12	0.88	19.45	0.39	-12.43	0.97
13	0.71	15.68	0.31	-12.15	1.06
14	0.45	9.86	0.20	-11.89	1.14
15	0.13	2.80	0.06	-11.64	1.19

Table 4.3 Self weight and center of the mass of the concrete voussoirs of the vault

Self Weight					
Concrete					
No unit arch	Volume m^3	Load kN	AutoCAD m	Centroid X m	Centroid Y m
1	-	-	-	-	-
2	-	-	-	-	-
3	-	-	-	-	-
4	-	-	-	-	-
5	-	-	-	-	-
6	-	-	-	-	-
7	0.15	3.38	0.07	-13.82	1.51
8	0.15	3.38	0.07	-13.54	1.51
9	0.15	3.38	0.07	-13.27	1.51
10	0.15	3.38	0.07	-12.99	1.51
11	0.15	3.38	0.07	-12.71	1.51
12	0.15	3.38	0.07	-12.43	1.51
13	0.15	3.38	0.07	-12.15	1.51
14	0.12	2.65	0.05	-11.88	1.51
15	0.04	0.89	0.02	-11.63	1.51

The traffic load applied at the surface of the deck of the bridge is calculated for the upper surface of each of the voussoirs and is considered to be applied at the center of the upper surface. The prices of the surface of the upper areas of the voussoirs and the traffic load can be seen in Table 4.4.

Table 4.4 Traffic load and center of the upper surface of the voussoirs of the vault

Traffic load					
Stone and concrete					
No unit arch	Area m^2	Load kN	AutoCAD m	Centroid X	Centroid Y
1	-	-	-	-	-
2	0.37	3.75	0.07	-10.54	5.41
3	0.98	9.78	0.20	-10.35	5.41
4	0.98	9.78	0.20	-10.07	5.41
5	0.98	9.78	0.20	-9.79	5.41
6	0.98	9.78	0.20	-9.51	5.41
7	0.98	9.78	0.20	-9.23	5.41
8	0.98	9.78	0.20	-8.95	5.41
9	0.98	9.78	0.20	-8.67	5.41
10	0.98	9.78	0.20	-8.39	5.41
11	0.98	9.78	0.20	-8.11	5.41
12	0.98	9.78	0.20	-7.83	5.41
13	0.98	9.78	0.20	-7.55	5.41
14	0.77	7.67	0.15	-7.27	5.41
15	0.26	2.56	0.05	-7.04	5.41

The self weight of the masonry column for the different voussoirs and the point of its application can be seen in Table 4.5.

Table 4.5 Self weight and center of the mass of the voussoirs of the column

Self Weight					
Masonry					
No unit vault	Volume m^3	Load kN	AutoCAD m	Centroid X m	Centroid Y m
1	0.26	5.67	0.11	-15.32	0.25
2	0.26	5.67	0.11	-15.21	0.75
3	0.26	5.67	0.11	-15.10	1.25
4	0.26	5.67	0.11	-14.99	1.75
5	0.26	5.67	0.11	-14.87	2.25
6	0.26	5.67	0.11	-14.76	2.75
7	0.26	5.67	0.11	-14.65	3.25
8	0.26	5.67	0.11	-14.54	3.75

The graphic representation of the loads is shown in Figure 4.8. A detail of all the different loads acting on the structure can be seen in Figure 4.9. The vectors acting on the same vertical direction are added as it can be seen on the right of the Figure 4.8. The force polygon for the calculation of the resultant force of all the loads acting on the structure can be seen in 4.10. The resultant force is 534.5 KN. The position of the resultant force is very important for the estimation of the thrust line. The funicular polygon is created in order to be graphically calculated the position of the resultant force. In all the drawings that follow the analogy between the lengths of the lines in meters that are representing the force vectors and the size of the force in kN is graphically represented with a scale graph that can be seen at the lower part of the drawing.

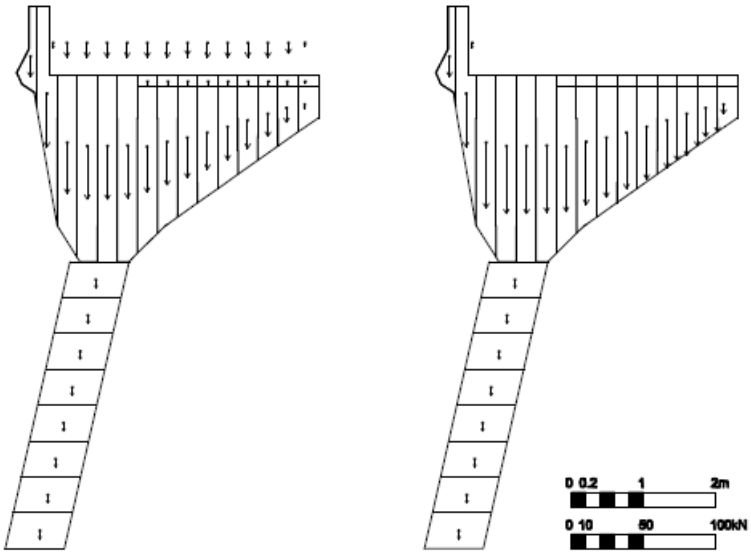

Figure 4.8 Left: Self weight and traffic loads applied to the voussoirs Right: Resultant loads acting at the voussoirs

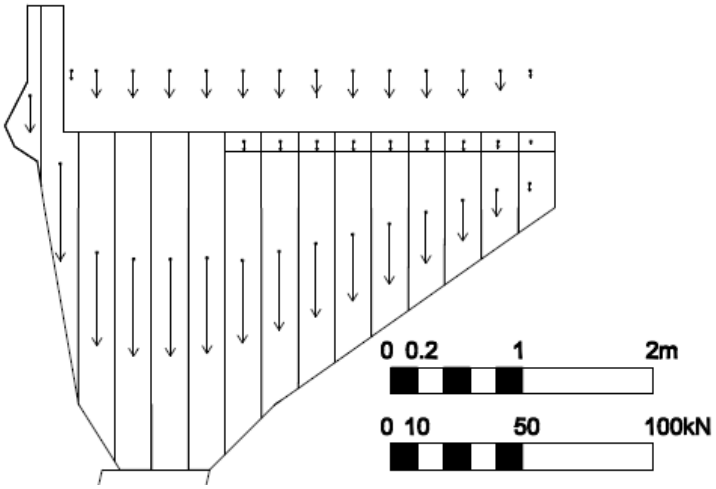

Figure 4.9 Detail of the loads acting on the voussoirs

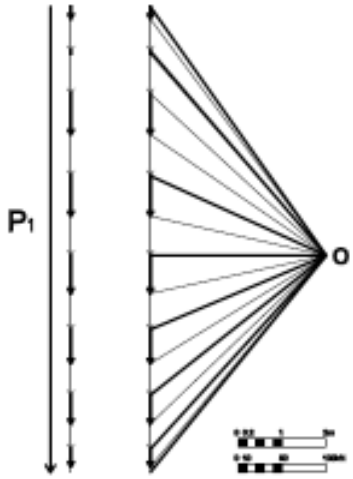

Figure 4.10 Force polygon for the calculation of the resultant force of the loads acting on the vault

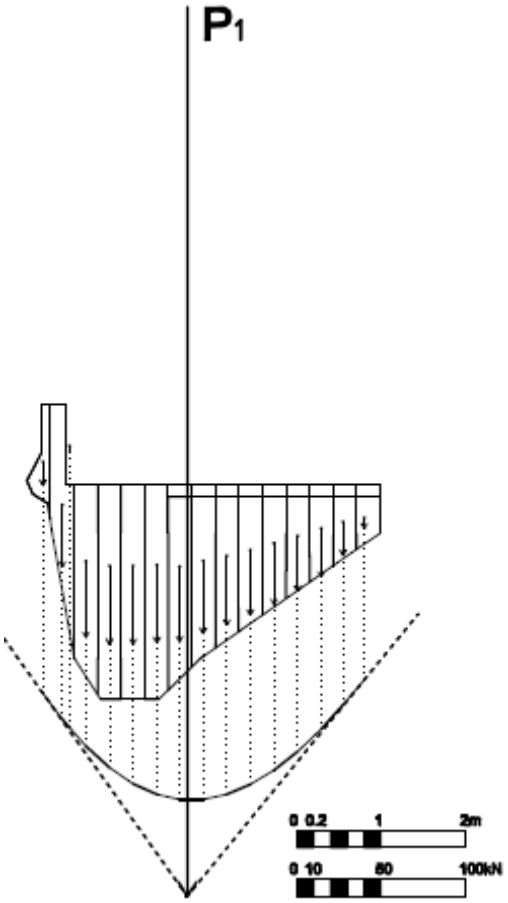

Figure 4.11 Funicular polygon for the calculation of the position of the resultant force

The funicular polygon is shown in Figure 4.11. For the calculation of the thrust line is necessary an estimation of the horizontal thrust applied at the vault. The result presented is taken after many previous trials on the position of the thrust line.

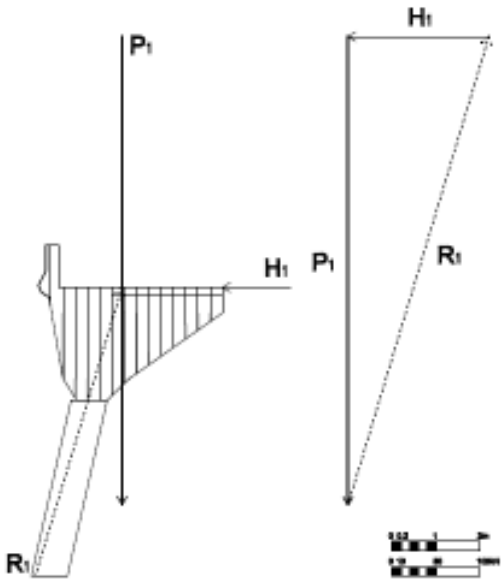

Figure 4.12 Left: Forces acting on the structure Right: Force polygon for the calculation of the size of the forces

The position at the top of the section of the vault is the ideal position for the horizontal thrust. Also the direction of the reaction at the column of the structure which is represented as R_1 is graphically calculated. The vector of the reaction must pass through the intersection of the vectors H_1 and P_1 representing the horizontal thrust and the resultant of the vertical loads on the vault as it can be seen in Figure 4.12. The inclination of the line of the vector R_1 has been chosen similar to the inclination of the column as it can be seen in Figure 4.12. The force polygon on the right of Figure 4.12 has as a result the definition of the size of the vectors of the horizontal thrust H1 and the reaction at the pillar R1. The force polygon that is used at the calculation of the thrust line of the vault can be seen in Figure 4.13.

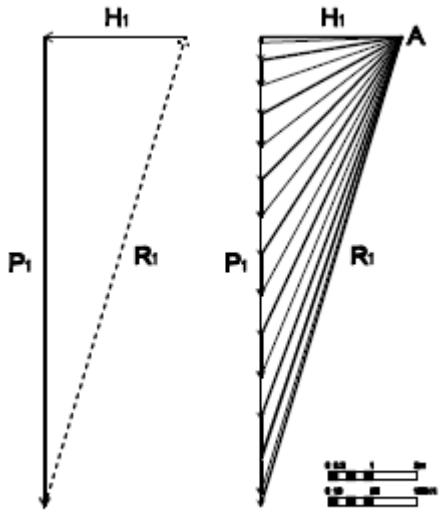

Figure 4.13 Force polygon for the calculation of the thrust line

The thrust line of the vault can be seen in Figure 4.14. The thrust line is in the limits of the structure so the vault is safe according to the safe theorem.

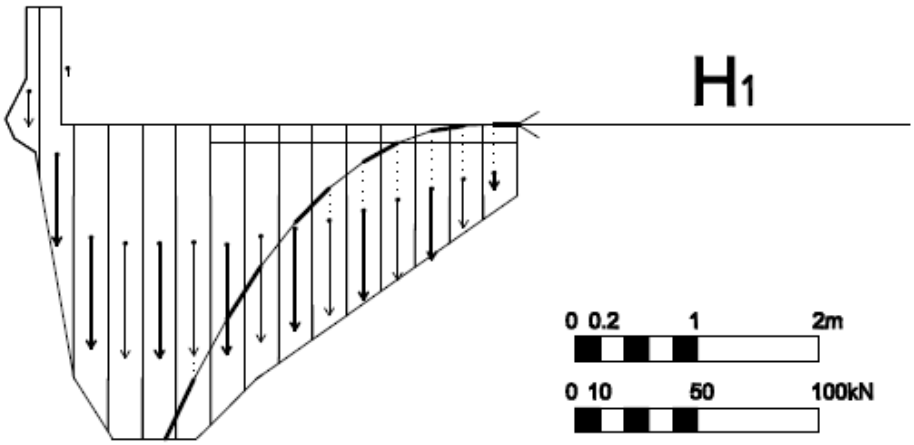

Figure 4.14 Thrust line of the vault. According to the safe theorem the vault is stable since the thrust line is contained within the limits of the vault geometry

However in order to conclude if the structure is stable or not the column must be taken into account too. Before the calculation of the thrust line in the column, it is important to find the sum of the forces that were not included in the thrust line of the vault and these are the forces of voussoirs 1, 2, 3, 4 and 5 as it is shown in Figure 4.15. The resultant force of the five forces as well as the force polygon for calculation of the position of the resultant force can be seen in Figure 4.16. The funicular polygon for finding the exact position of the resultant force V1 can be seen in Figure 4.17.

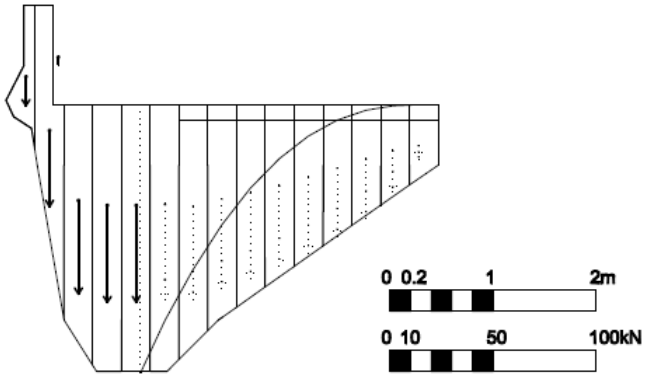

Figure 4.15 Forces which are not included in the thrust line

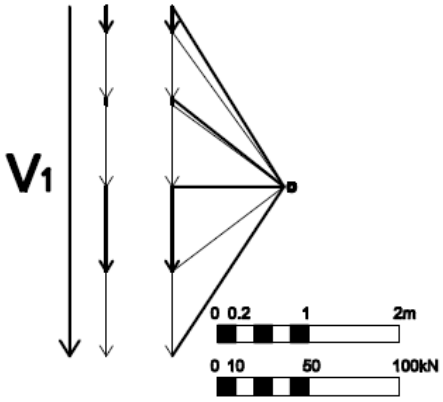

Figure 4.16 Force polygon for the calculation of the resultant force

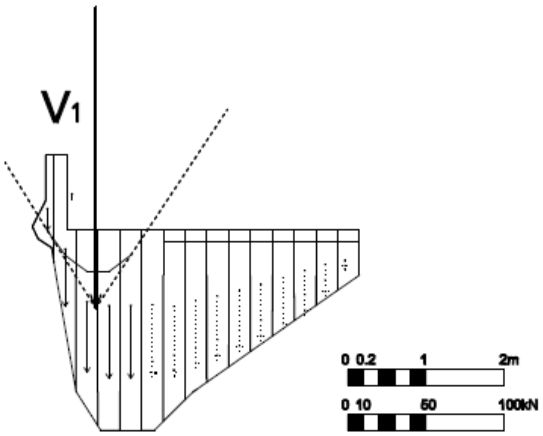

Figure 4.17 Funicular polygon for the calculation of the position of the resultant force

The forces applied at the structure can be seen on Figure 4.18. The forces applied at the column of the structure can be seen on the right of Figure 4.18.

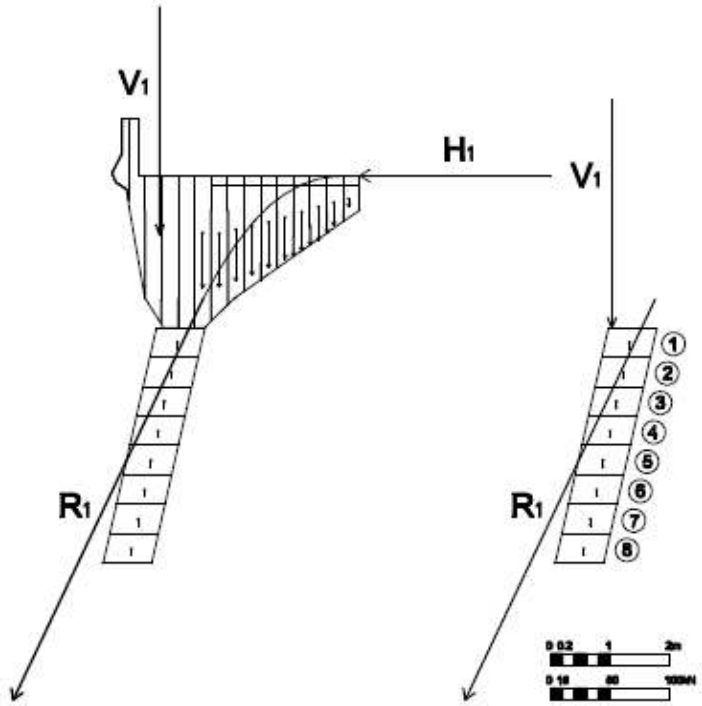

Figure 4.18 Left: Forces acting on the structure Right: Forces acting on the column of the structure

The synthesis of the vectors of the reaction R1 and the forces of the voussoirs of the pillars is shown in the following Figures.

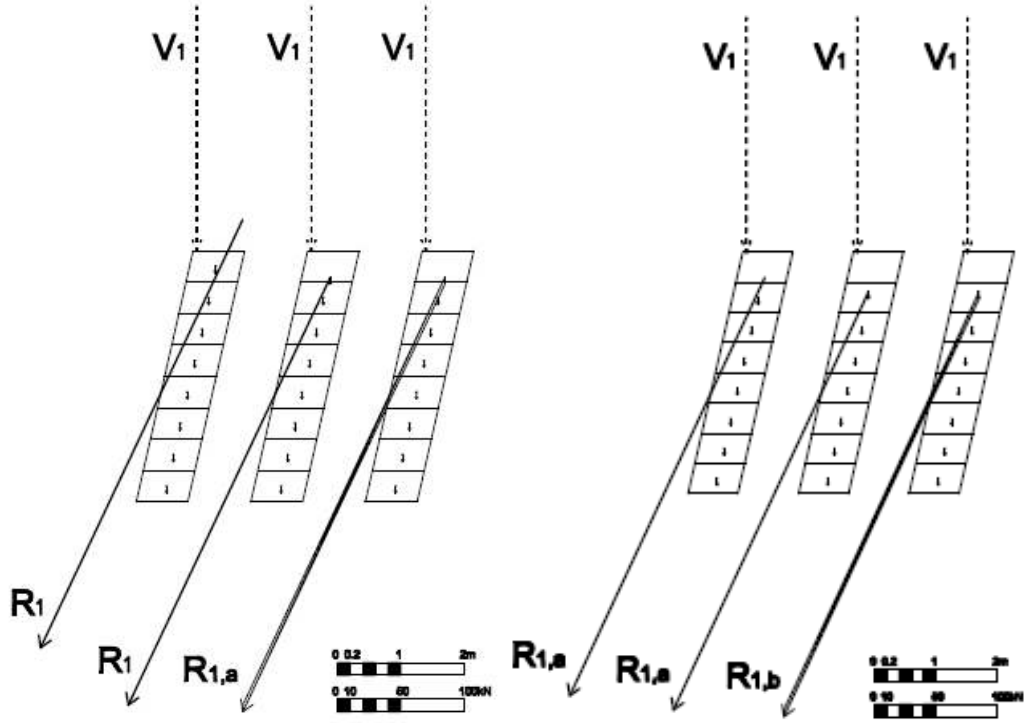

Figure 4.19 Sum of the vector of the resultant force of the thrust line and the force of voussoir 8 on the left and voussoir 7 on the right

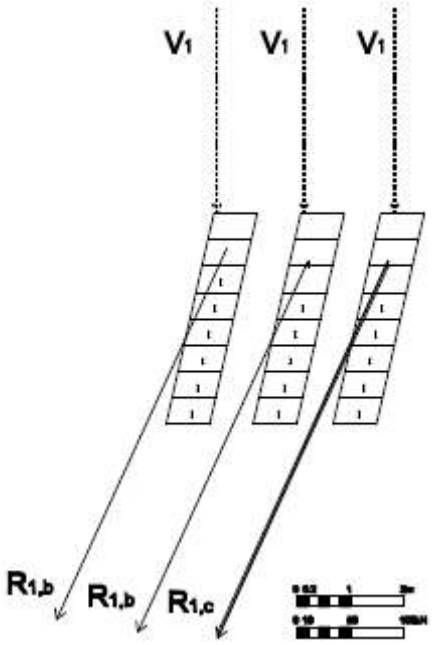

Figure 4.20 Sum of the vector of the resultant force of the thrust line and the force of voussoir 6

The sum of the resultant R1,c and the resultant force V1 is shown in the following Figure.

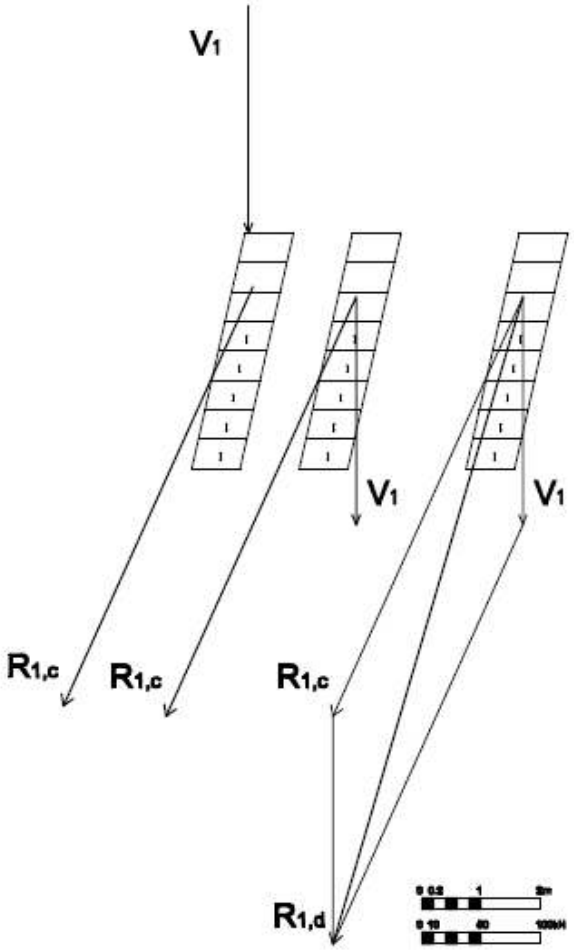

Figure 4.21 Sum of the vector of the resultant force of the thrust line R1,c and the resultant force V1

The sum of the resultant and the forces of the voussoirs 5 to 1 is shown in the following Figures.

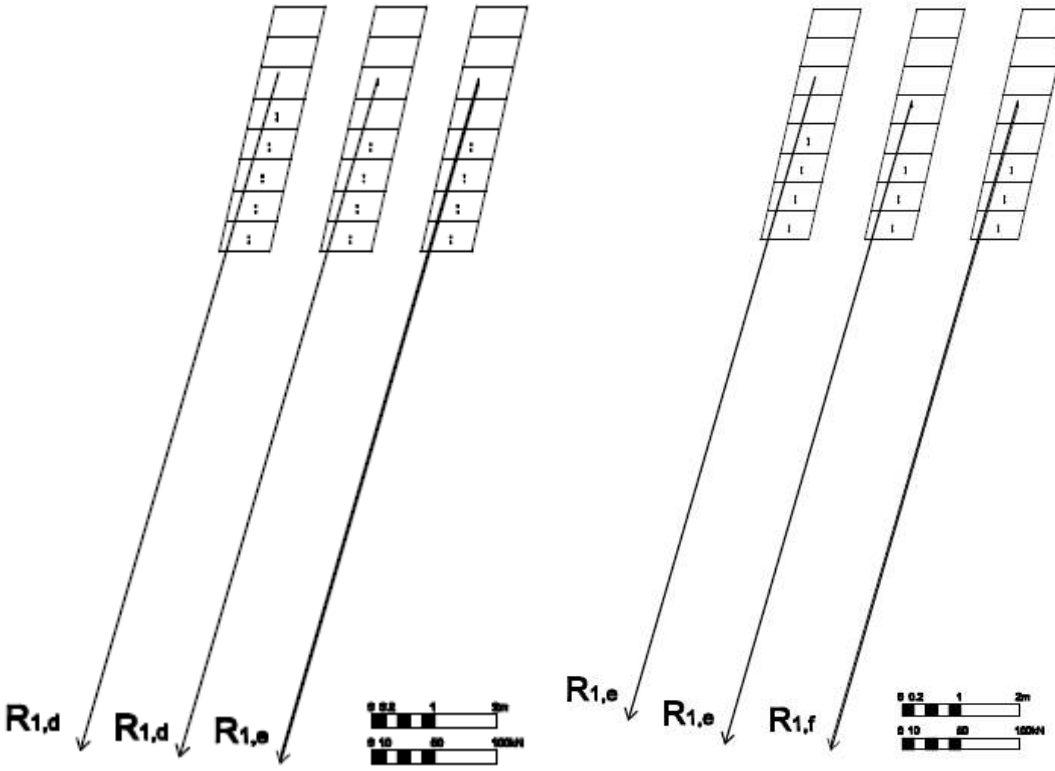

Figure 4.22 Sum of the vector of the resultant force of the thrust line and the force of voussoir 5 on the left and voussoir 4 on the right

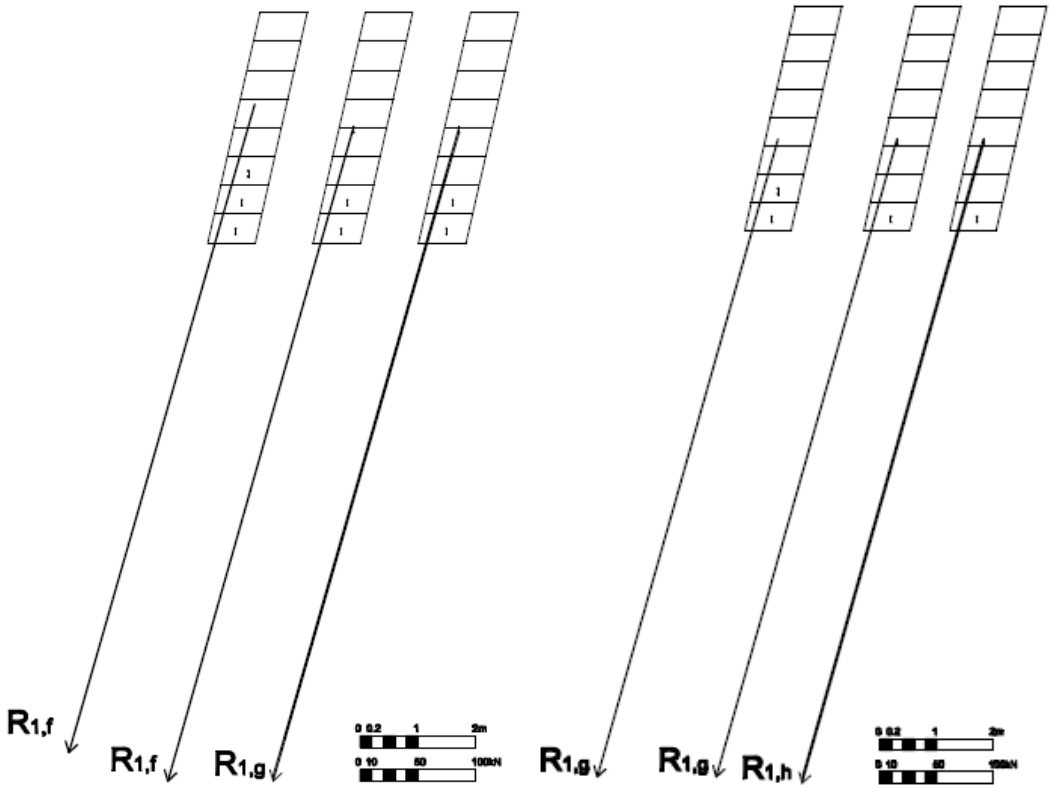

Figure 4.23 Sum of the vector of the resultant force of the thrust line and the force of voussoir 3 on the left and voussoir 2 on the right

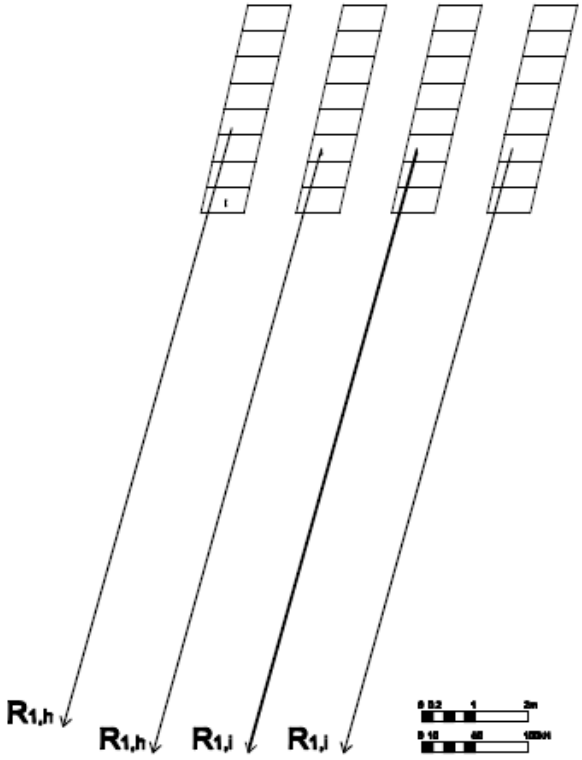

Figure 4.24 Sum of the vector of the resultant force of the thrust line and the force of voussoir 1.

According to the safe theorem the structure is stable since the resultant force is contained inside the limits of the column geometry as it can be seen in Figure 4.24.

The second part of the graphic statics analysis for the stability of the viaduct contains the application of the graphic statics method in the east part of the structure. The geometry of this part can be seen in Figure 4.25. This element of the south side of the structure is repeating through the structure.

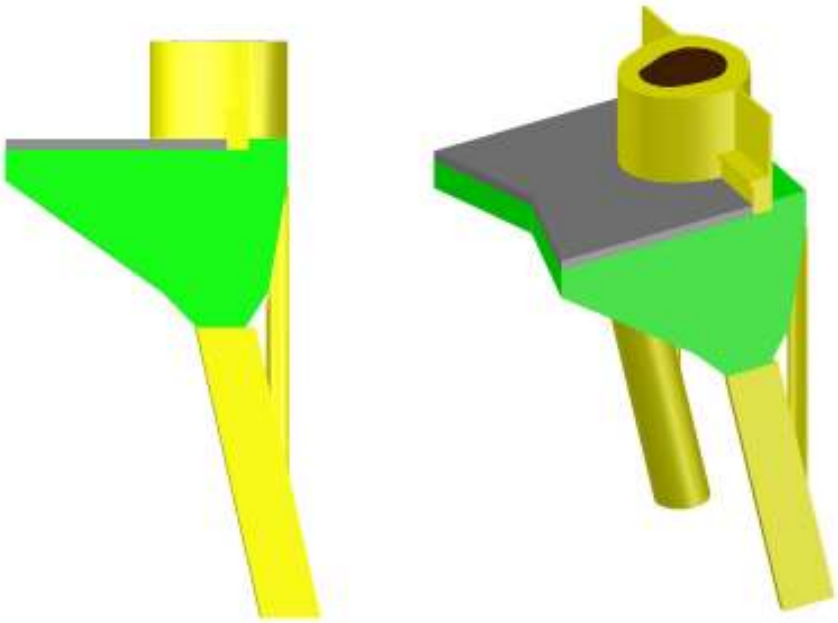

Figure 4.25 View of the characteristic part of the south side of the lower viaduct of Park Güell Right: 3D view of the model

In this part of the structure the railing on the deck of the bridge is substituted with the jardiniere and the benches. For the calculation of the thrust line the vault is divided in 15 voussoirs. The voussoirs of the part of the structure made of masonry are represented in Figure 4.26 in green and blue color while the voussoirs of the part of the vault made of concrete are represented in Figure 4.26 with grey and blue color. The soil voussoirs are represented with brown and magenta color. The column is also divided into 8 voussoirs as it can be seen in Figure 4.6. The numbering of the voussoirs of the vault and can be seen in Figure 4.27.

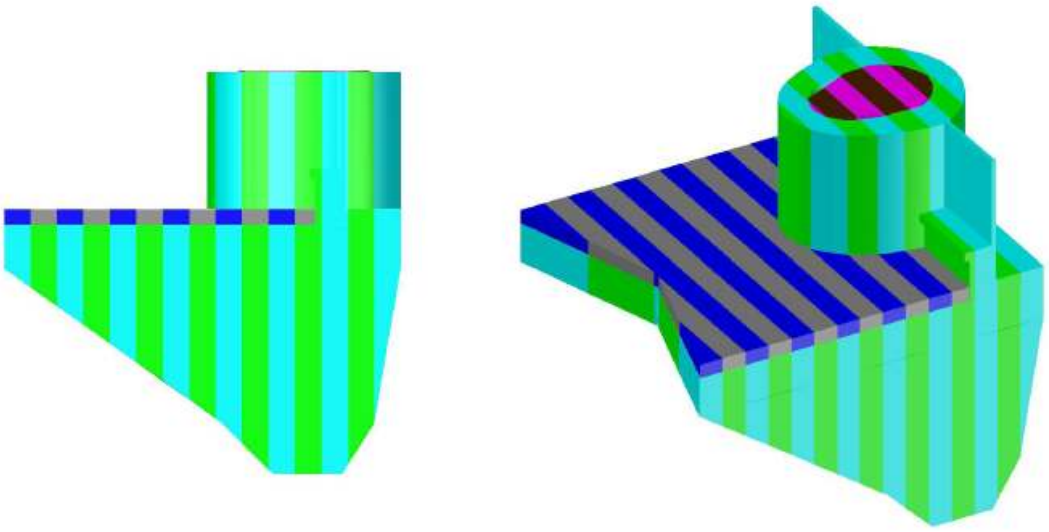

Figure 4.26 Discretization of the model into voussoirs for the mass calculation

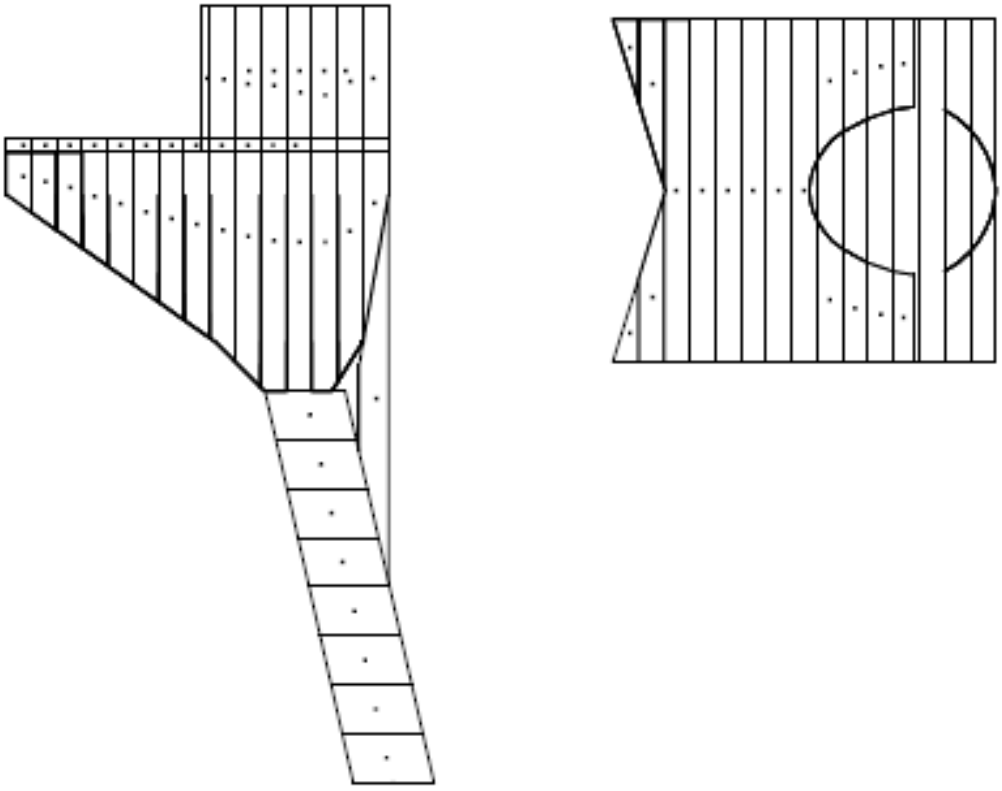

Figure 4.27 Left: Centers of mass of the different voussoirs. Right: Centers of mass of the deck surface

The position of the center of the mass for the voussoirs of the vault and the column is obtained with AutoCAD 3D and it can be can be seen at Figure 4.27. The center of the mass differs according to the material of the voussoir. The coordinates of the center of the mass are the points of application of the self weight of the masonry and concrete voussoirs. Also, the center of the upper surfaces of the voussoirs can be seen in figure 4.7. The center of the upper surfaces of the voussoirs has been calculated only for the part of the deck subject to traffic load because is the point of application of the traffic load of the structure.

The coordinates of the center of the mass of each voussoir made of masonry can be seen at Table 4.6 while the coordinates of the center of the mass for the voussoirs made of concrete can be seen in Table 4.7. The coordinates of the center of the upper surface are presented n Table 4.10.

The loads acting on the structure are divided in two categories. The first category is the dead load which is the self weight of the structure. There are three different type of materials in the structure for which the self weight is calculated; the masonry of the vault and the jardiniere, the concrete of the upper layer of the deck and the soil that is used as a filling in the jardiniere. Table 4.1 is presenting the price of the loads acting on the structure.

For the calculation of the self weight loads acting on the structure the volumes of the masonry and concrete voussoirs are given in the Table 4.6 and Table 4.7 accordingly. The self weight acting on the center of the mass of the masonry and concrete voussoirs is calculated with Excel and is presented also in Table 4.6 and Table 4.7. The load is scaled in order to be graphically represented and designed in AutoCAD. For this reason a scaling of 0.02 has been used for all the loads. The lengths of the AutoCAD lines representing the size of the vectors of the self weight forces are given in table 4.6 and Table 4.7.

Table 4.6 Self weight and center of the mass of the masonry voussoirs of the vault

Self Weight					
Masonry					
No unit vault	Volume m^3	Load kN	AutoCAD m	Centroid X m	Centroid Y m
1	0.11	2.40	0.05	-13.90	-39.46
2	0.38	8.37	0.17	-13.67	-39.51
3	0.63	13.89	0.28	-13.42	-39.57
4	0.78	17.22	0.34	-13.17	-39.66
5	0.92	20.19	0.40	-12.91	-39.74
6	1.04	22.79	0.46	-12.65	-39.82
7	1.14	25.01	0.50	-12.39	-39.89
8	1.22	26.87	0.54	-12.13	-39.95
9	1.29	28.41	0.57	-11.87	-40.01
10	1.36	30.03	0.60	-11.61	-40.07
11	1.42	31.21	0.62	-11.35	-40.12
12	1.42	31.33	0.63	-11.09	-40.13
13	1.42	31.30	0.63	-10.83	-40.13
14	1.44	31.74	0.63	-10.58	-40.02
15	1.03	22.58	0.45	-10.33	-39.73

In all the drawings that follow, the analogy between the lengths of the lines in meters that are representing the force vectors and the size of the force in kN is graphically represented with a scale graph in the lower part of the Figures.

Table 4.7 Self weight and center of the mass of the concrete voussoirs of the vault

Self Weight					
Concrete					
No unit vault	Volume m^3	Load kN	AutoCAD m	Centroid X m	Centroid Y m
1	0.03	0.76	0.02	-13.90	-39.14
2	0.10	2.29	0.05	-13.67	-39.14
3	0.14	3.13	0.06	-13.43	-39.14
4	0.14	3.13	0.06	-13.17	-39.14
5	0.14	3.13	0.06	-12.91	-39.14
6	0.14	3.13	0.06	-12.65	-39.14
7	0.14	3.13	0.06	-12.39	-39.14
8	0.13	3.02	0.06	-12.14	-39.14
9	0.10	2.27	0.05	-11.88	-39.14
10	0.08	1.93	0.04	-11.62	-39.14
11	0.07	1.72	0.03	-11.36	-39.14
12	0.05	1.23	0.02	-11.13	-39.14
13	-	-	-	-	-
14	-	-	-	-	-
15	-	-	-	-	-

The volumes of the masonry and soil voussoirs of the jardiniere are shown in Table 4.8 and Table 4.9 accordingly. Also the self weight of the masonry and soil voussoirs of the jardiniere is also shown in Table 4.8 and Table 4.9.

Table 4.8Self weight and center of the mass of the masonry voussoirs of the jardiniere

Self Weight					
Jardiniere' s masonry					
No unit vault	Volume m^3	Load kN	AutoCAD m	Centroid X m	Centroid Y m
1	-	-	-	-	-
2	-	-	-	-	-
3	-	-	-	-	-
4	-	-	-	-	-
5	-	-	-	-	-
6	-	-	-	-	-
7	-	-	-	-	-
8	0.05	1.11	0.02	-12.03	-38.46
9	0.36	8.01	0.16	-11.86	-38.47
10	0.30	6.71	0.13	-11.62	-38.52
11	0.32	6.95	0.14	-11.35	-38.53
12	0.41	8.94	0.18	-11.08	-38.60
13	0.68	14.87	0.30	-10.83	-38.63
14	0.42	9.19	0.18	-10.57	-38.49
15	0.32	7.10	0.14	-10.34	-38.46

The traffic load applied at the surface of the deck of the bridge is calculated for the upper surface of each of the voussoirs and is considered to be applied at the center of the upper surface. The prices of the surface of the upper areas of the voussoirs and the traffic load can be seen in Table 4.10.

Table 4.9 Self weight and center of the mass of the soil voussoirs of the jardiniere

Self Weight					
Jardiniere 's Soil					
No unit vault	Volume m^3	Load kN	AutoCAD m	Centroid X m	Centroid Y m
1	-	-	-	-	-
2	-	-	-	-	-
3	-	-	-	-	-
4	-	-	-	-	-
5	-	-	-	-	-
6	-	-	-	-	-
7	-	-	-	-	-
8	-	-	-	-	-
9	0.01	0.23	0.00	-11.76	-38.38
10	0.18	3.56	0.07	-11.60	-38.38
11	0.26	5.25	0.11	-11.35	-38.38
12	0.32	6.43	0.13	-11.09	-38.38
13	0.31	6.25	0.12	-10.84	-38.38
14	0.15	3.06	0.06	-10.62	-38.38
15	-	-	-	-	-

Table 4.10 Traffic load and center of the upper surface of the voussoirs of the vault

Traffic load					
Stone and concrete					
No unit vault	Surface m^2	Load kN	AutoCAD m	Centroid X m	Centroid Y m
1	0.22	2.20	0.04	-7.73	-38.14
2	0.66	6.60	0.13	-7.50	-40.69
3	0.91	9.07	0.18	-7.26	-39.60
4	0.91	9.08	0.18	-7.00	-39.60
5	0.91	9.08	0.18	-6.74	-39.60
6	0.91	9.08	0.18	-6.48	-39.60
7	0.91	9.08	0.18	-6.22	-39.60
8	0.87	8.74	0.17	-5.96	-39.60
9	0.66	6.60	0.13	-5.70	-40.72
10	0.46	4.60	0.09	-5.44	-40.81
11	0.50	5.00	0.10	-5.18	-40.87
12	0.36	3.57	0.07	-4.95	-40.90
13	-	-	-	-	-
14	-	-	-	-	-
15	-	-	-	-	-

The self weight of the stem like column of the south side of the viaduct is shown in Table 4.11 together with the center of the mass of the column.

Table 4.11 Self weight and center of the mass of the stem-like column

Self Weight					
Column					
No unit pillar	Volume m^3	Load kN	AutoCAD m	Centroid X m	Centroid Y m
1	0.17	3.74	0.07	-13.76	-86.38

The graphic representation of the loads is shown in Figure 4.28. A detail of all the different loads acting on the vault can be seen in Figure 4.29. The vectors acting on the same vertical direction are added as it can be seen on the right of the Figure 4.28.

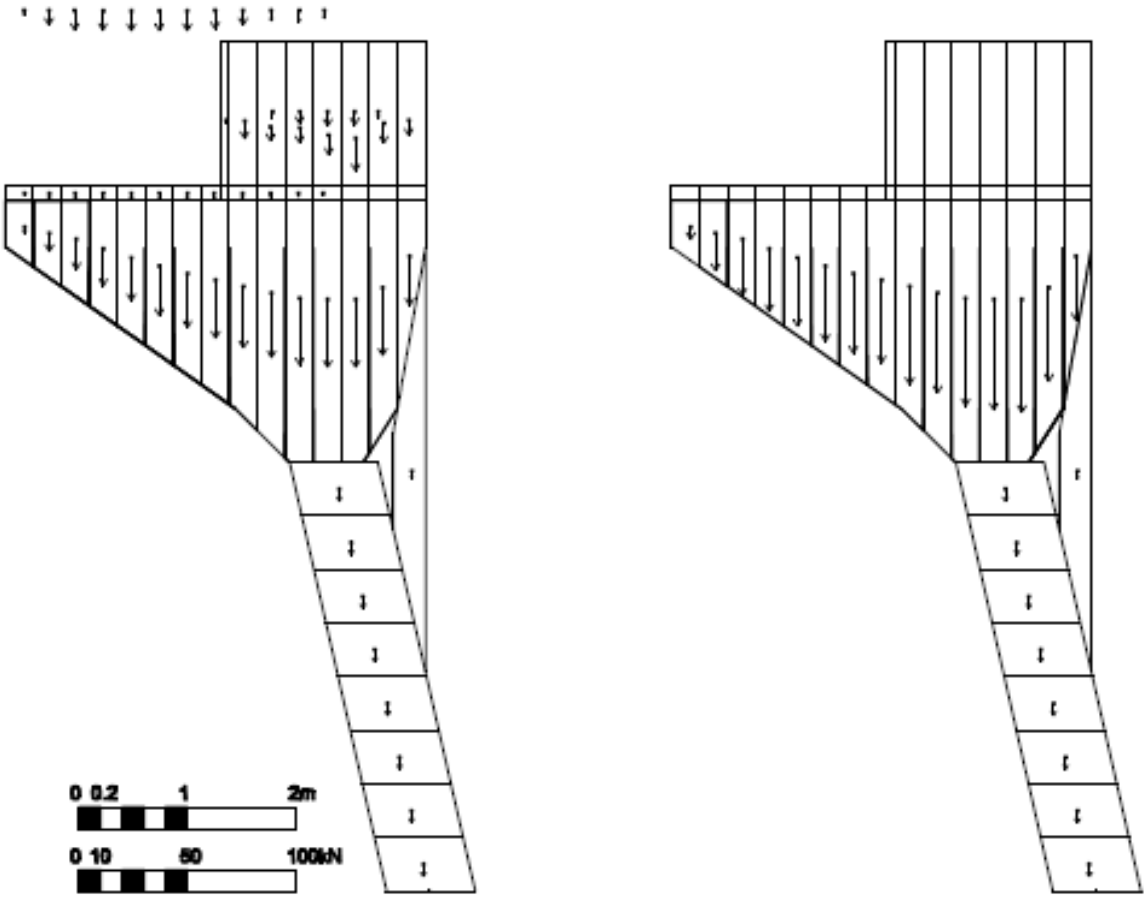

Figure 4.28 Left: Self weight and traffic loads applied to the voussoirs Right: Resultant loads acting at the voussoirs

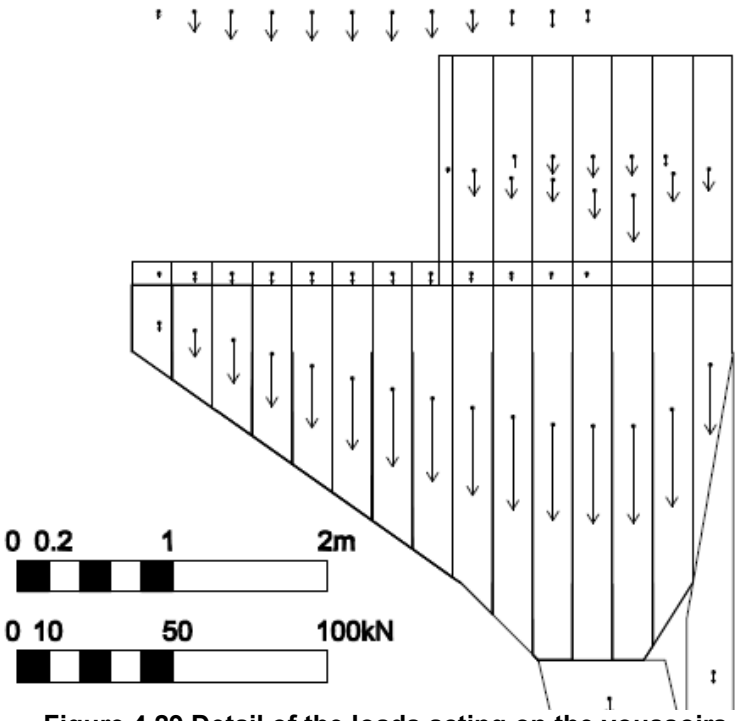

Figure 4.29 Detail of the loads acting on the voussoirs

The force polygon for the calculation of the resultant force of all the loads acting on the structure can be seen in Figure 4.30. The resultant force P2 is 539.5 KN. The position of the resultant force is very important for the estimation of the thrust line. The funicular polygon is created in order to be graphically calculated the position of the resultant force.

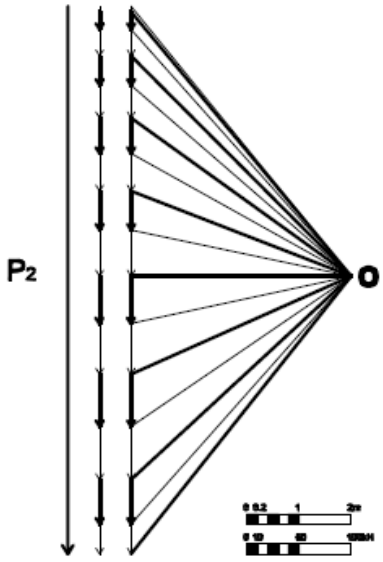

Figure 4.30 Force polygon for the calculation of the resultant force of the loads acting on the vault

The funicular polygon is shown in Figure 4.31.

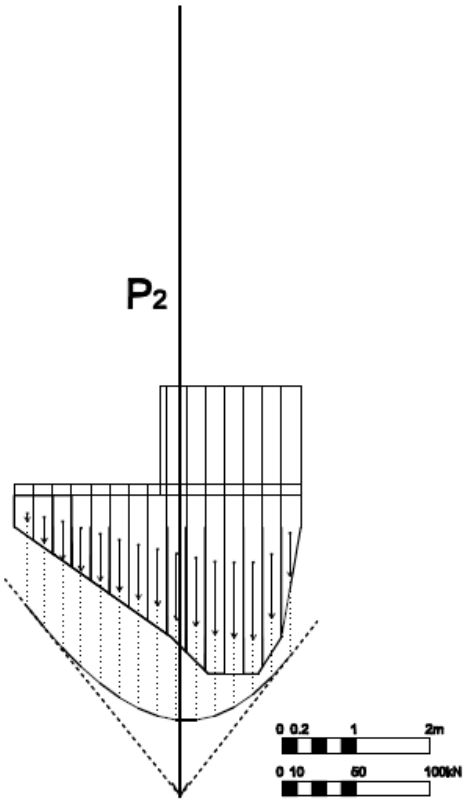

Figure 4.31 Funicular polygon for the calculation of the position of the resultant force

For the calculation of the thrust line the horizontal thrust used previously for the north side of the viaduct is used. The direction of the reaction at the pillar of the structure which is represented as R_2 is graphically calculated.

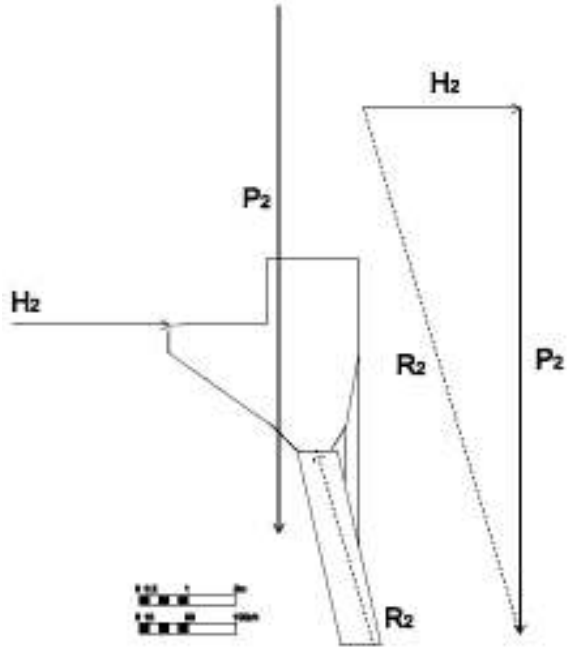

Figure 4.32 Left: Forces acting on the structure Right: Force polygon for the calculation of the size of the forces

The vector of the reaction must pass through the intersection of the vectors H_2 and P_2 representing the horizontal thrust and the resultant of the vertical loads on the vault as it can be seen in Figure 4.32. The inclination of the line of the vector is the same with the reaction R_1 of the north side as it can be seen in Figure 4.12. The force polygon on the right of Figure 4.32 has as a result the definition of the size of the vector of the reaction at the pillar R_2. The force polygon for the calculation of the thrust line of the vault can be seen in Figure 4.33.

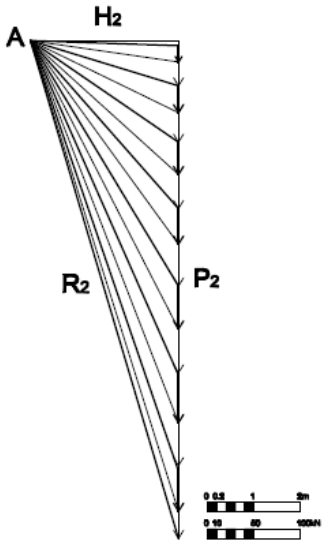

Figure 4.33 Force polygon for the calculation of the thrust line

The thrust line of the vault can be seen in Figure 4.34. The thrust line is in the limit of the structure so the vault is safe according to the safe theorem. However in order to conclude if the structure is stable or not the column must be taken into account too. Before the calculation of the thrust line in the column it is important to find the sum of the forces that were not included in the thrust line of the vault and these are the forces of voussoirs 12, 13, 14 and 15 as it is shown in Figure 4.35. The resultant force of the five forces as well as the force polygon for calculation of the position of the resultant force can be seen in Figure 4.36. The funicular polygon for finding the exact position of the resultant force V2 can be seen in Figure 4.37.

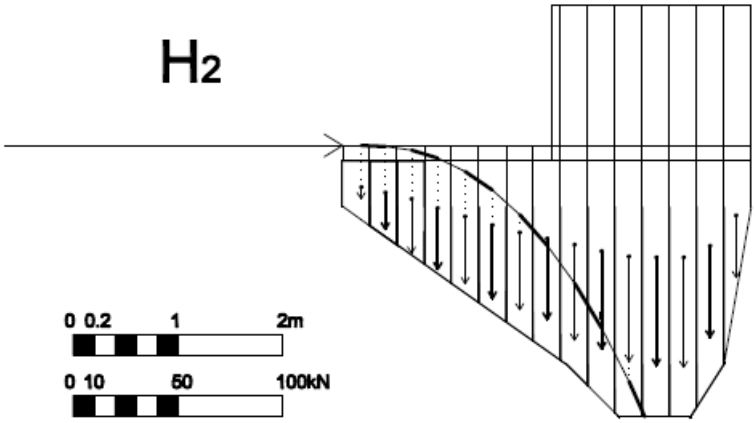

Figure 4.34 Thrust line of the vault. According to the safe theorem the vault is stable since the thrust line is contained within the limits of the vault geometry

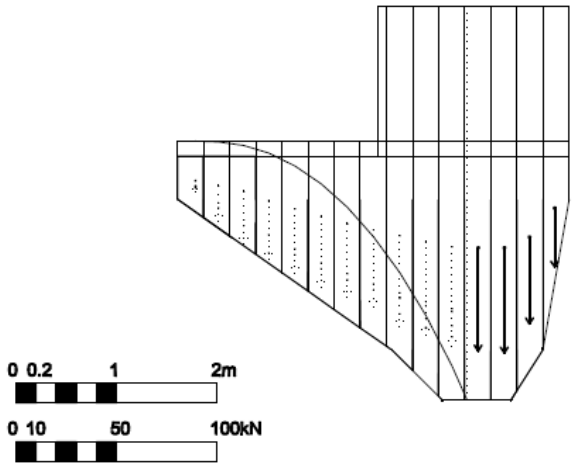

Figure 4.35 Forces which are not included in the thrust line

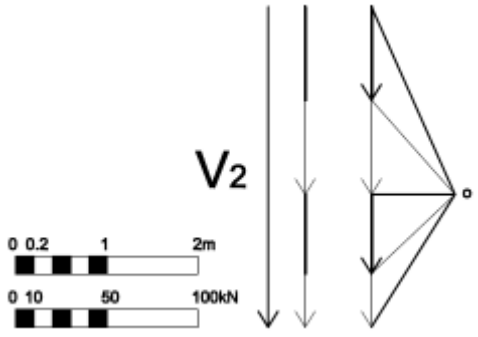

Figure 4.36 Force polygon for the calculation of the resultant force

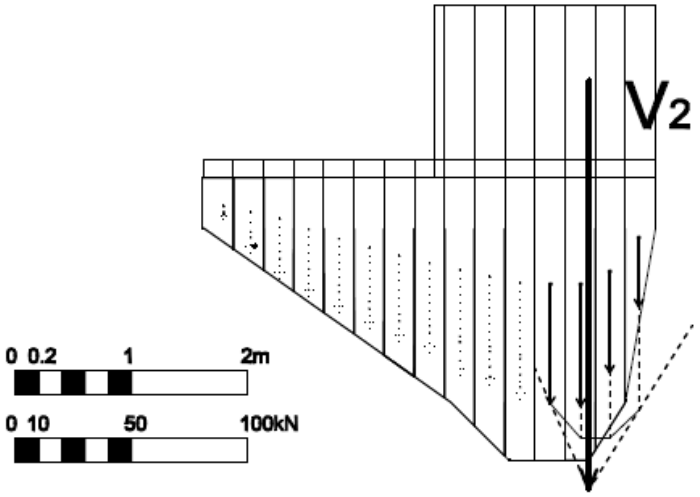

Figure 4.37 Funicular polygon for the calculation of the position of the resultant force

The forces applied at the structure can be seen on Figure 4.18. On the right of Figure 4.18 can be seen the forces applied at the column of the structure.

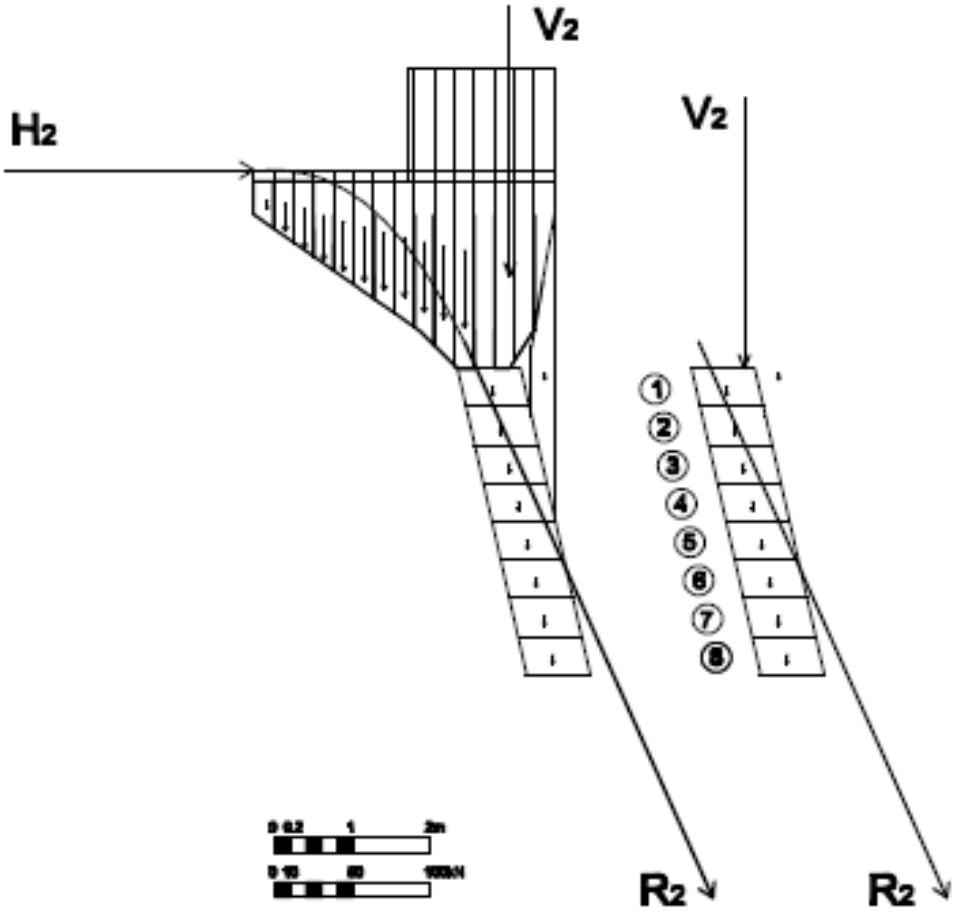

Figure 4.38 Left: Forces acting on the structure Right: Forces acting on the column of the structure and numbering of the voussoirs of the column

The synthesis of the vectors of the reaction R_2 and the forces of the voussoirs of the pillars is shown in the following Figures.

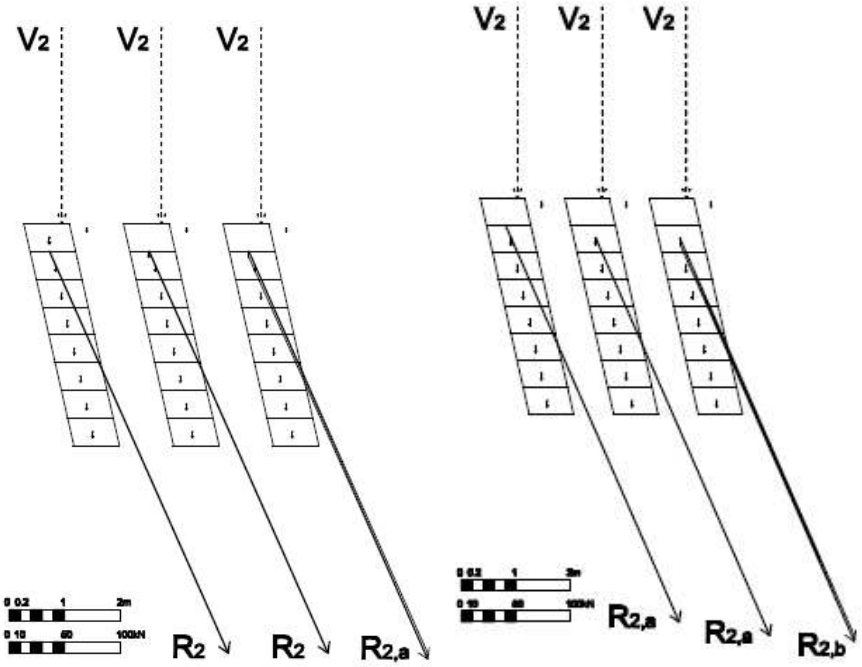

Figure 4.39 Sum of the vector of the resultant force of the thrust line and the force of voussoir 8 on the left and voussoir 7 on the right

The sum of the resultant $R_{2,b}$ and the resultant force V_2 is shown in the following Figure.

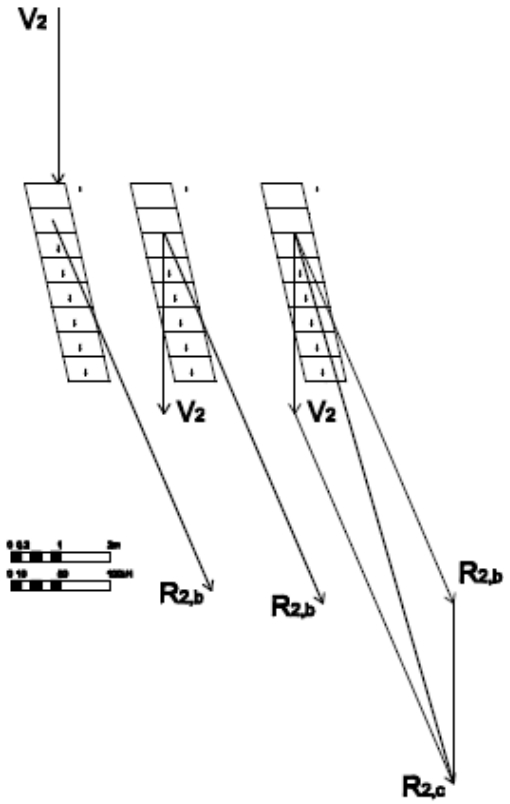

Figure 4.40 Sum of the vector of the resultant force of the thrust line $R_{2,b}$, the force of voussoir 6 and the resultant force V_2

The sum of the resultant force and the forces of the voussoirs 5 to 1 is shown in the following Figures.

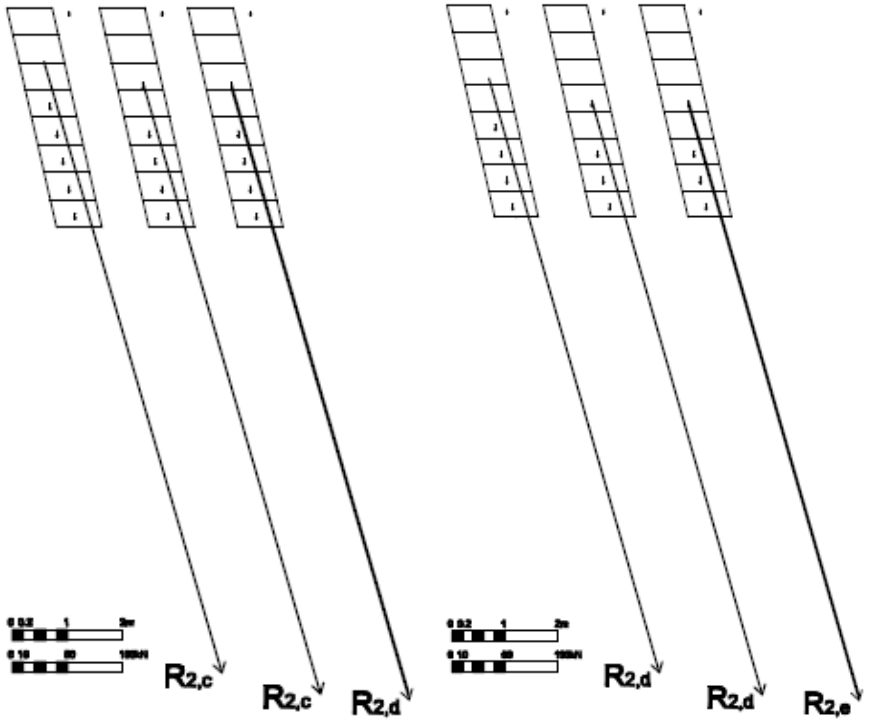

Figure 4.41 Sum of the vector of the resultant force of the thrust line and the force of voussoir 5 on the left and voussoir 4 on the right

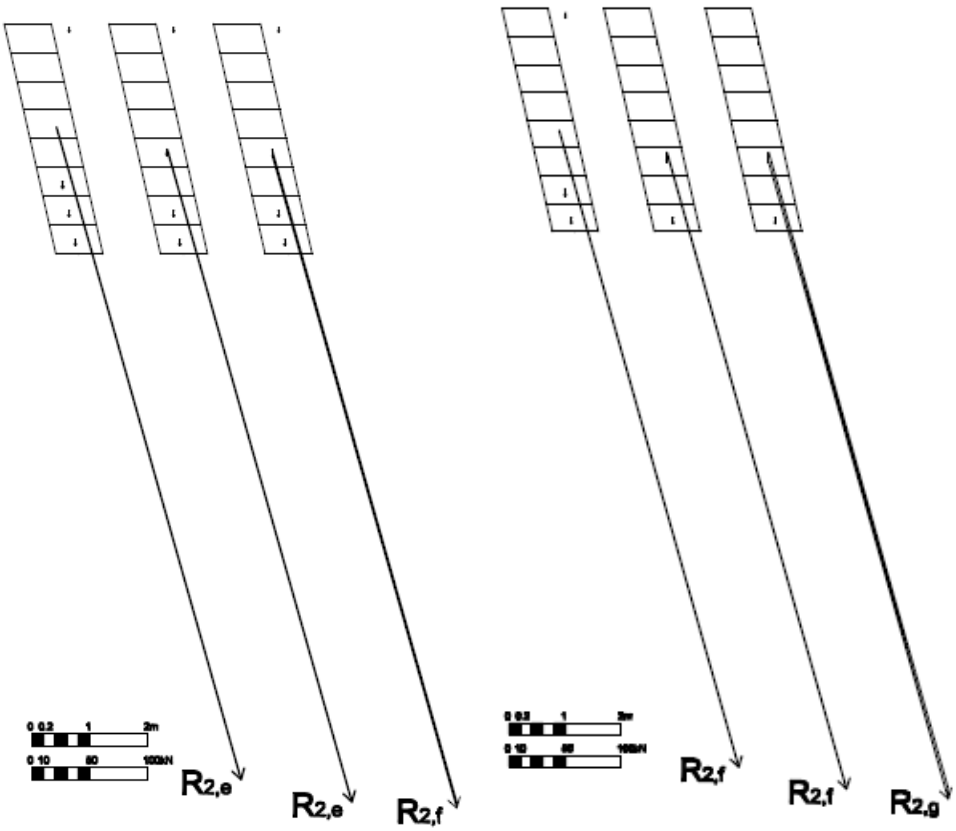

Figure 4.42 Left: Sum of the vector of the resultant force of the thrust line and the force of voussoir 3 Right: Sum of the vector of the resultant force of the thrust line, voussoir 2 and the force of the upper-column

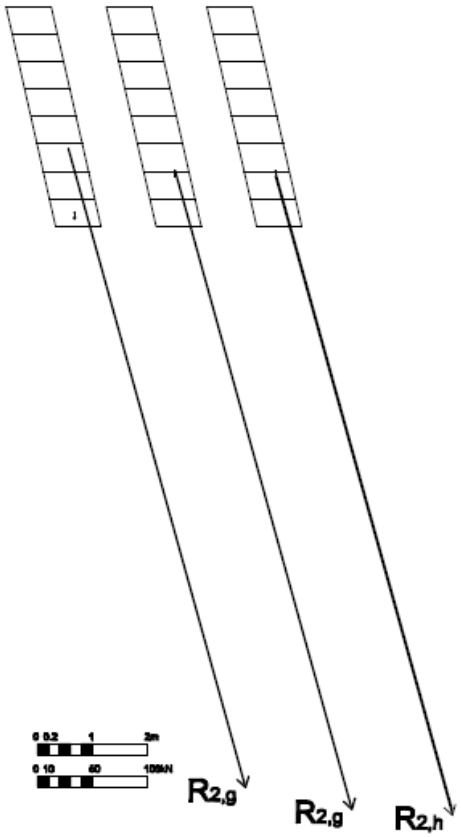

Figure 4.43 Sum of the vector of the resultant force of the thrust line and the force of voussoir 8

According to the safe theorem the structure is stable since the resultant force is contained inside the limits of the column geometry as it can be seen on the right Figure 4.43. Since both the north and the south parts are safe and due to symmetry conditions the structure is safe.

5. FUNICILAR ANALYSIS

5.1 Introduction

The application MASONRISK of GID has been used for the funicular modeling of the viaduct. The purpose is to create a cable network which deformed due to the loading must fit within the limits of the geometry of the structure. In this way according to the safe theorem the structure is stable. Before the modeling it has been necessary finding the appropriate element of the structure which would be used as a model for the program. This basic element must be symmetric and repeat through the structure. The basic element for modeling is shown in Figure 5.1. If this element is copied and rotated 180 degrees then another element is produced in continuity with the previous element so the element chosen is symmetric. Also it is necessary that the element chosen is having columns at all the corners so the catenary model can hang from all the columns. The red lines in Figure 5.1 represent the geometry of the catenary net.

The definition of the cables is based on the geometry of the structure. The meshing of the net has been designed manually. The criterion used for the discretization was a creation of a uniform mesh of the catenary that could take into account all the loads applied on the structure.

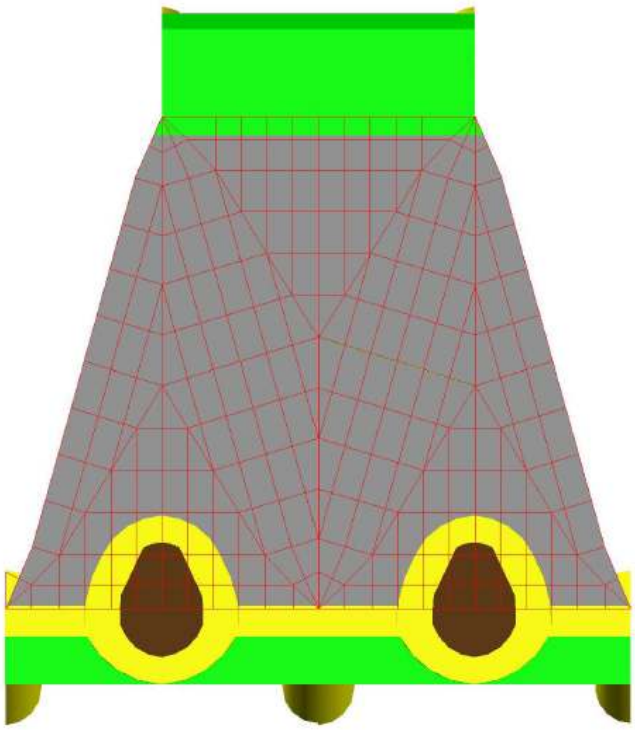

Figure 5.1 Basic element of the structure used for GID modeling

It is very important before the creation of the model with GID program to calculate the loads acting on all the elements. For this reason just two parts of the element are used as it can be seen in Figure 5.2.

Figure 5.2 The two parts of the characteristic element used for the calculation of the load

Both the north and the south part are sliced into pieces in order to calculate their volume and the concrete surface of each piece. After the calculation of the volume the self weight of the element can be calculated. Also the calculation of the concrete surface is necessary for the calculation of the traffic load.

5.2 Calculation of the loads

The south part of the structure is divided in two parts part 1 and part 2. The volumes and the concrete surfaces of the pieces of part 1 of the south element are shown in the following Figures.

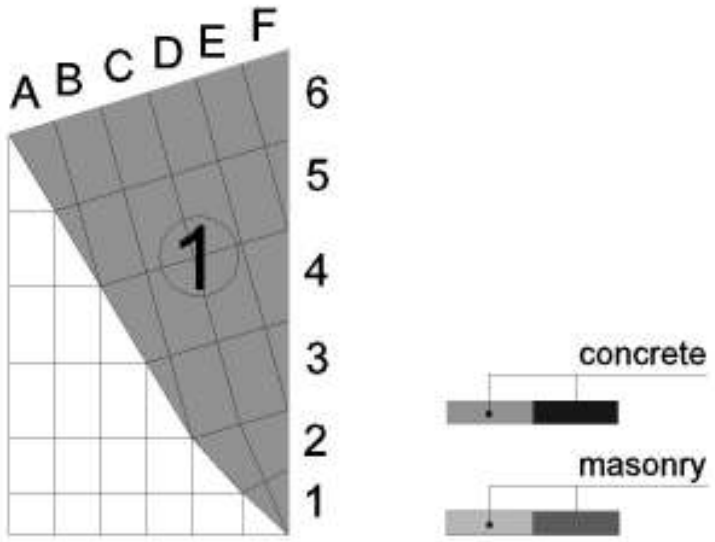

Figure 5.3 Geometry of part 1 of the south element

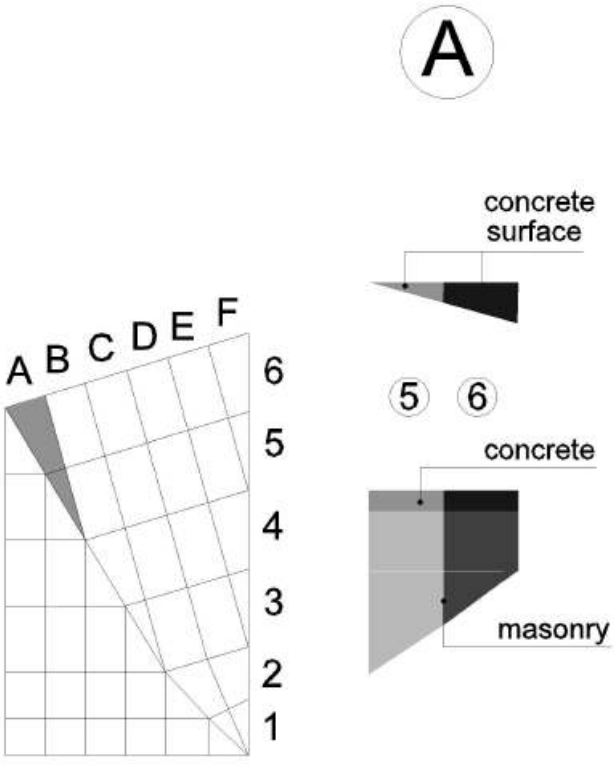

Figure 5.4 Volumes and concrete surfaces of piece A of part 1 of the south element

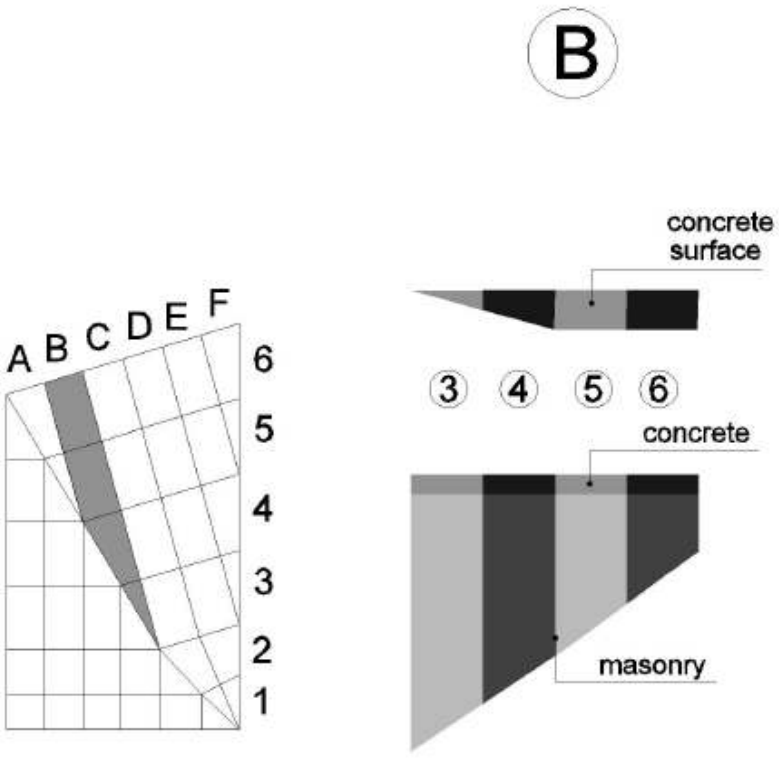

Figure 5.5 Volumes and concrete surfaces of piece B of part 1 of the south element

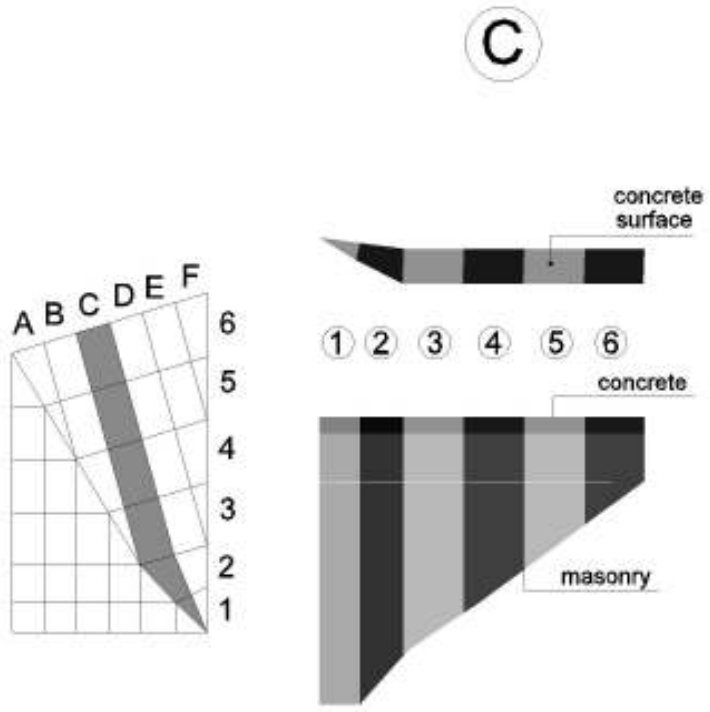

Figure 5.6 Volumes and concrete surfaces of piece C of part 1 of the south element

The volumes and concrete surfaces of pieces D, E and F are considered to be symmetric to pieces C, B and A accordingly.

The volumes and the concrete surfaces of the pieces of part 2 of the south element are shown in the following Figures.

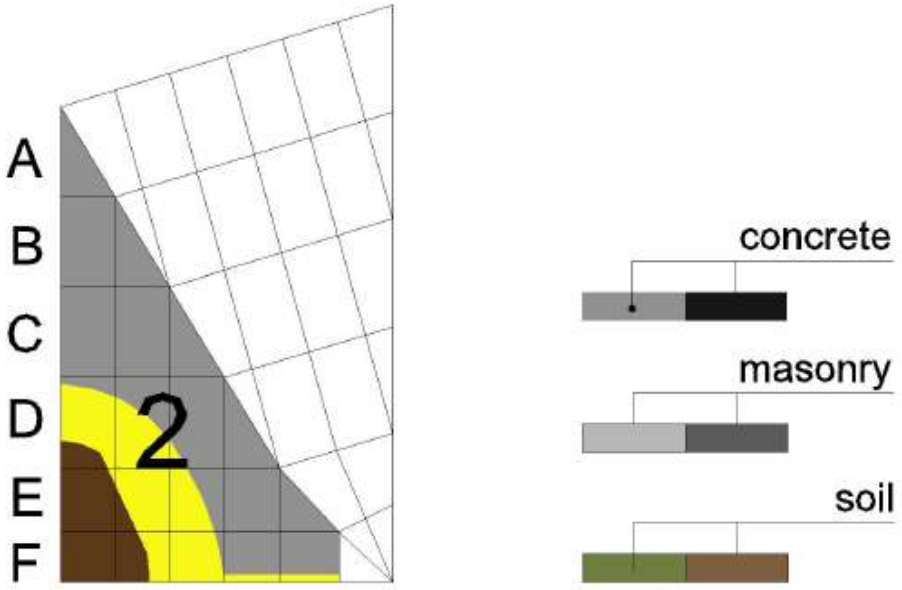

Figure 5.7 Geometry of part 2 of the south element

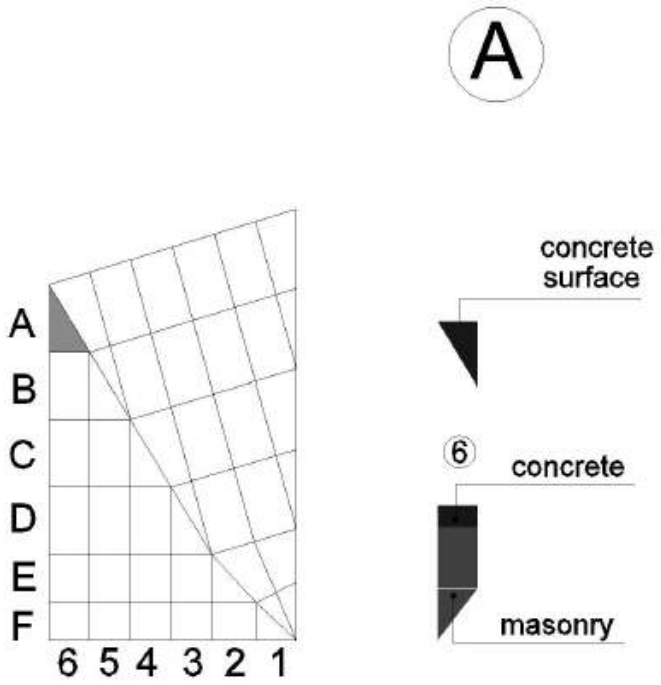

Figure 5.8 Volumes and concrete surfaces of piece A of part 2 of the south element

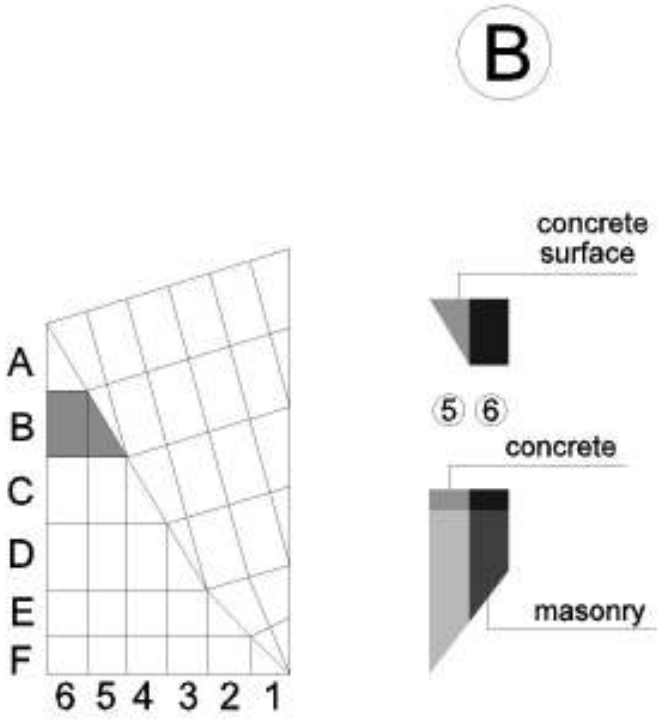

Figure 5.9 Volumes and concrete surfaces of piece B of part 2 of the south element

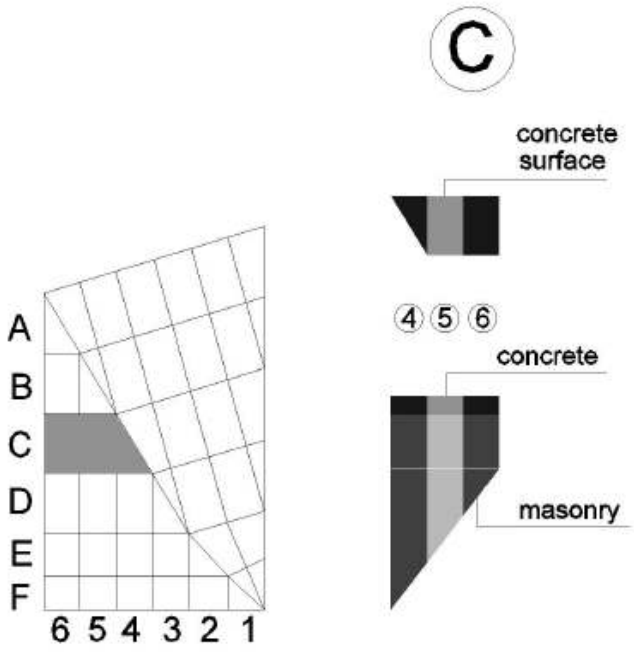

Figure 5.10 Volumes and concrete surfaces of piece C of part 2 of the south element

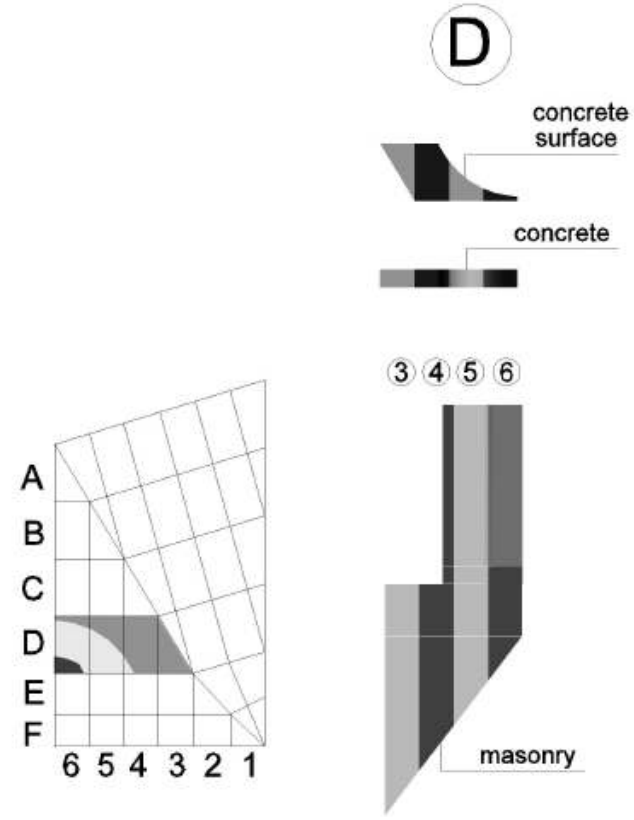

Figure 5.11 Volumes and concrete surfaces of piece D of part 2 of the south element

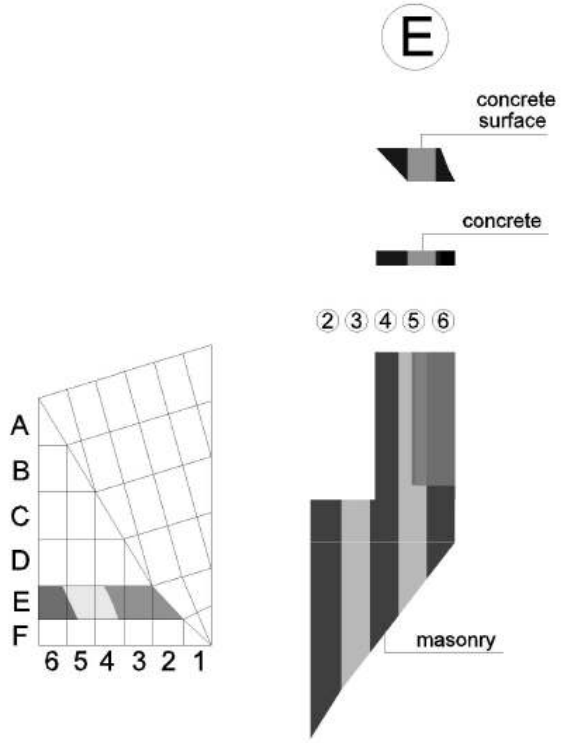

Figure 5.12 Volumes and concrete surfaces of piece E of part 2 of the south element

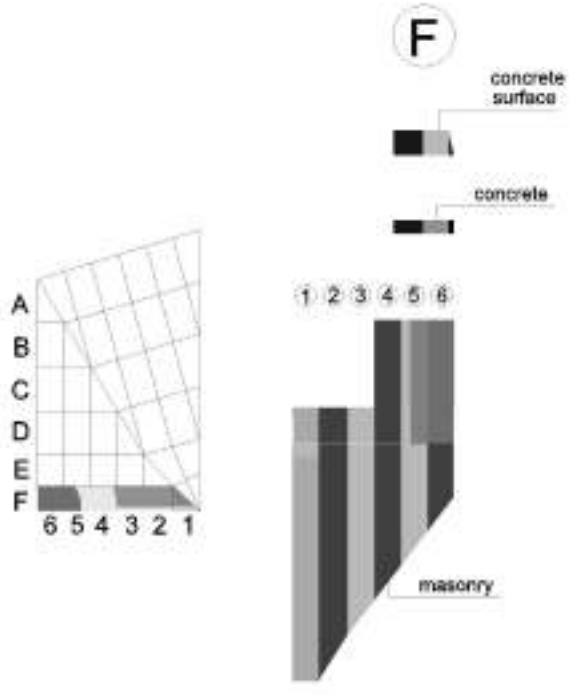

Figure 5.13 Volumes and concrete surfaces of piece F of part 2 of the south element

The volumes, concrete areas different loads and the total load applied to the different pieces of the south element are given at the following Tables.

Table 5.1 Volumes and concrete areas of the different pieces of part 1 of the south element

PART A					
No piece	No subdivision	Volume m^3			Area m^2
		concrete	stone	soil	concrete
A1	5	0.006	0.038	-	0.040
	6	0.018	0.072	-	0.120
B1	3	0.006	0.068	-	0.040
	4	0.018	0.166	-	0.122
	5	0.024	0.164	-	0.162
	6	0.024	0.100	-	0.161
C1	1	0.004	0.069	-	0.028
	2	0.014	0.208	-	0.096
	3	0.026	0.302	-	0.170
	4	0.026	0.241	-	0.170
	5	0.026	0.174	-	0.170
	6	0.026	0.105	-	0.170
D1	1	0.006	0.038	-	0.040
	2	0.018	0.072	-	0.120
	3	0.006	0.068	-	0.040
	4	0.018	0.166	-	0.122
	5	0.024	0.164	-	0.162
	6	0.024	0.100	-	0.161
E1	3	0.004	0.069	-	0.028
	4	0.014	0.208	-	0.096
	5	0.026	0.302	-	0.170
	6	0.026	0.241	-	0.170
F1	5	0.026	0.174	-	0.170
	6	0.026	0.105	-	0.170

Table 5.2 Self weight, traffic load and total load on the different pieces of part 1 of the south element

PART A						
No piece	No subdivision	Self weight kN			Traffic load kN	Total
		concrete	stone	soil	on concrete area	Force kN
A1	5	0.140	0.832	-	0.404	1.376
	6	0.414	1.588	-	1.202	3.204
B1	3	0.140	1.503	-	0.404	2.047
	4	0.419	3.641	-	1.215	5.275
	5	0.559	3.610	-	1.619	5.788
	6	0.554	2.209	-	1.607	4.370
C1	1	0.097	1.516	-	0.283	1.895
	2	0.331	4.585	-	0.957	5.873
	3	0.587	6.633	-	1.698	8.918
	4	0.589	5.295	-	1.698	7.582
	5	0.589	3.821	-	1.698	6.108
	6	0.589	2.319	-	1.698	4.606
D1	1	0.140	0.832	-	0.404	1.376
	2	0.414	1.588	-	1.202	3.204
	3	0.140	1.503	-	0.404	2.047
	4	0.419	3.641	-	1.215	5.275
	5	0.559	3.610	-	1.619	5.788
	6	0.554	2.209	-	1.607	4.370
E1	3	0.097	1.516	-	0.283	1.895
	4	0.331	4.585	-	0.957	5.873
	5	0.587	6.633	-	1.698	8.918
	6	0.589	5.295	-	1.698	7.582
F1	5	0.589	3.821	-	1.698	6.108
	6	0.589	2.319	-	1.698	4.606

Table 5.3 Volumes and concrete areas of the different pieces of part 2 of the south element

PART A					
No piece	No subdivision	Volume m^3			Area m^2
		concrete	stone	soil	concrete
A2	6	0.010	0.037	-	0.066
B2	5	0.010	0.020	-	0.069
	6	0.064	0.084	-	0.135
C2	4	0.010	0.089	-	0.069
	5	0.021	0.136	-	0.135
	6	0.021	0.084	-	0.135
D2	3	0.010	0.115	-	0.069
	4	0.020	0.198	-	0.130
	5	0.008	0.257	-	0.056
	6	0.002	0.224	0.036	0.016
E2	2	0.008	0.112	-	0.054
	3	0.015	0.170	-	0.098
	4	0.006	0.220	-	0.039
	5	-	0.194	0.020	-
	6	-	0.074	0.129	-
F2	1	-	0.111	-	-
	2	0.007	0.232	0.000	0.044
	3	0.006	0.176	0.000	0.039
	4	0.001	0.232	0.000	0.003
	5	-	0.139	0.065	0.000
	6	-	0.063	0.112	0.000

Table 5.4 Self weight, traffic load and total load on the different pieces of part 2 of the south element

PART A						
No piece	No subdivision	Self weight kN			Traffic load kN	Total
		concrete	stone	soil	concrete	force
A2	6	0.230	0.814	-	0.663	1.707
B2	5	0.237	0.444	-	0.686	1.367
	6	1.465	1.837	-	1.349	4.651
C2	4	0.237	1.967	-	0.686	2.890
	5	0.474	2.990	-	1.349	4.813
	6	0.474	1.837	-	1.349	3.660
D2	3	0.237	2.532	-	0.686	3.455
	4	0.449	4.358	-	1.298	6.105
	5	0.191	5.647	-	0.556	6.394
	6	0.055	4.928	0.726	0.160	5.869
E2	2	0.184	2.471	-	0.536	3.191
	3	0.336	3.738	-	0.976	5.050
	4	0.133	4.842	-	0.390	5.366
	5	-	4.272	0.394	-	4.666
	6	-	1.635	2.586	-	4.221
F2	1	-	2.437	-	-	2.437
	2	0.150	5.095	0.000	0.435	5.680
	3	0.133	3.874	0.000	0.388	4.396
	4	0.012	5.107	0.000	0.033	5.151
	5	-	3.068	1.295	0.000	4.363
	6	-	1.386	2.233	0.000	3.619

The numbering of the north element is shown in the following Figure.

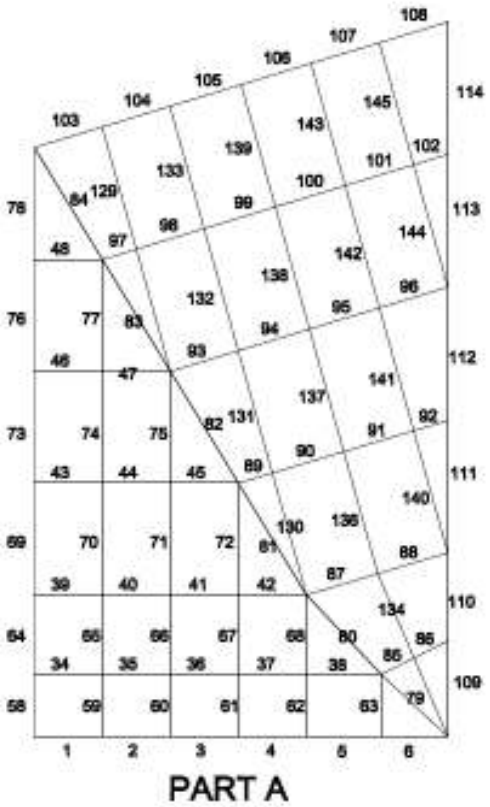

Figure 5.14 Numbering of the south element

A graphic representation of the total load (kN) acting on each piece of the south element is shown in the following Figure.

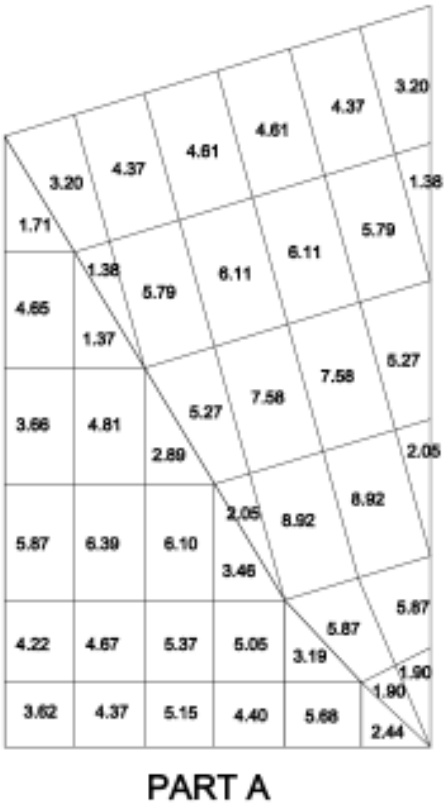

Figure 5.15 Total load acting on the different pieces of south element

For the distribution of the load from the solid pieces to the cables of the net it is necessary the subdivision of the mesh into sub surfaces. The division is done always dividing the angle into two equal angles using the bisector of the angle. The subdivision is shown in Figure 5.16.

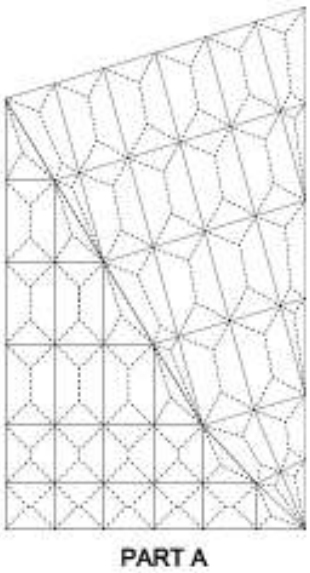

Figure 5.16 Division into sub surfaces for the distribution of the load to the cables

The area of each one of the sub surfaces is presented in the following Figure.

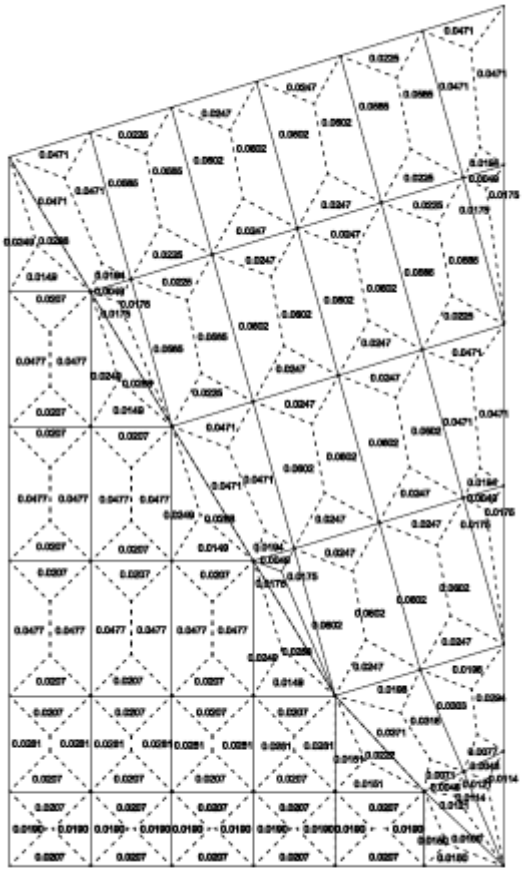

Figure 5.17 Area of the sub surfaces that the mesh is divided

The area of the different surfaces of the mesh is shown in the following Figure.

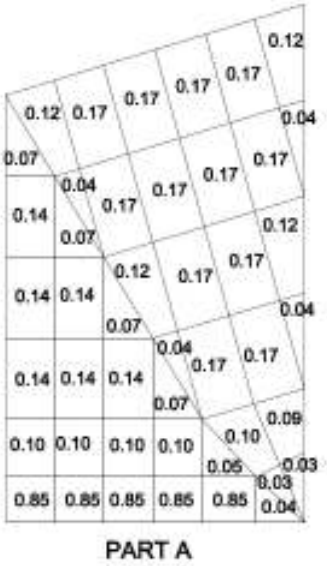

Figure 5.18 Areas of the different surfaces of the mesh

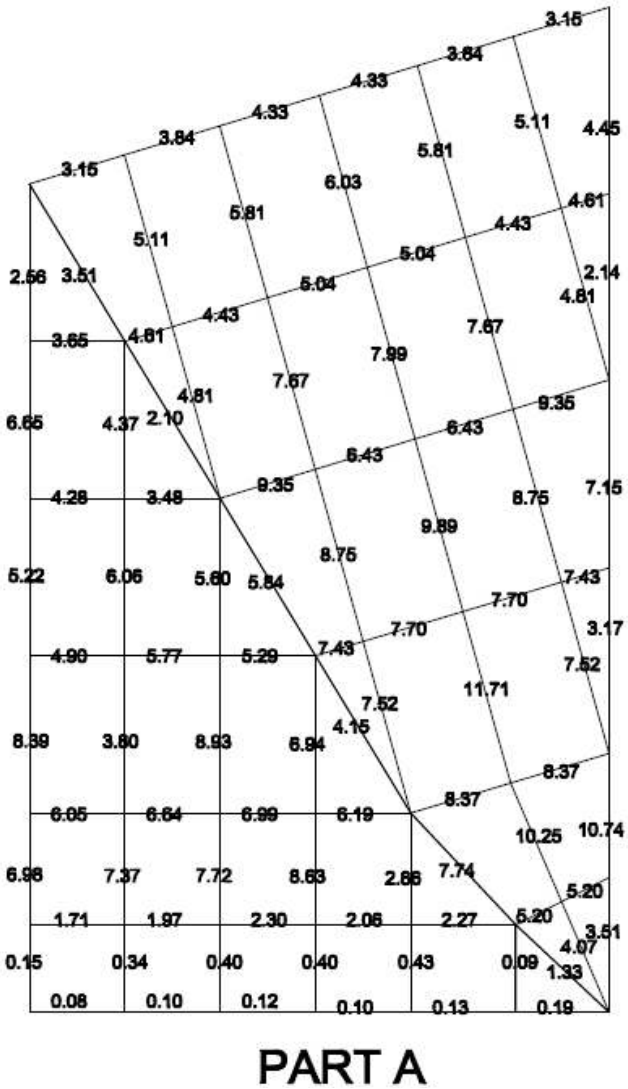

Figure 5.19 Loads acting on the cables of the net

The calculation of the total load is based on the rule below:

Load on the element = Sum[[(Area of the subsurface)/(Area of the surface)]·(Load on the piece)]

This means that all the pieces ending at a cable contribute with a load on the cable. This load is a percentage of the total load of the piece. This percentage is given by the term (Area of the subsurface)/(Area of the surface) where the subsurface is the subsurface of the piece facing the cable and the surface is the surface of the piece. By summing the load that the different pieces contribute to the cable the total load on the cable is calculated. The total loads applied on the cables are shown in Figure 5.19.

The same process is repeated for the calculation of the loads for the north element of the structure. The Figures that follow are showing the process of calculation of the loads. The volumes and the concrete surfaces of the pieces of part 1 of the north element are shown in the following Figures.

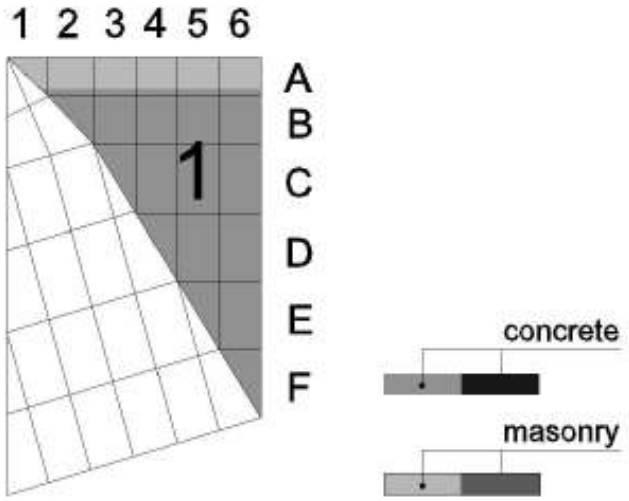

Figure 5.20 Geometry of part 1 of the north element

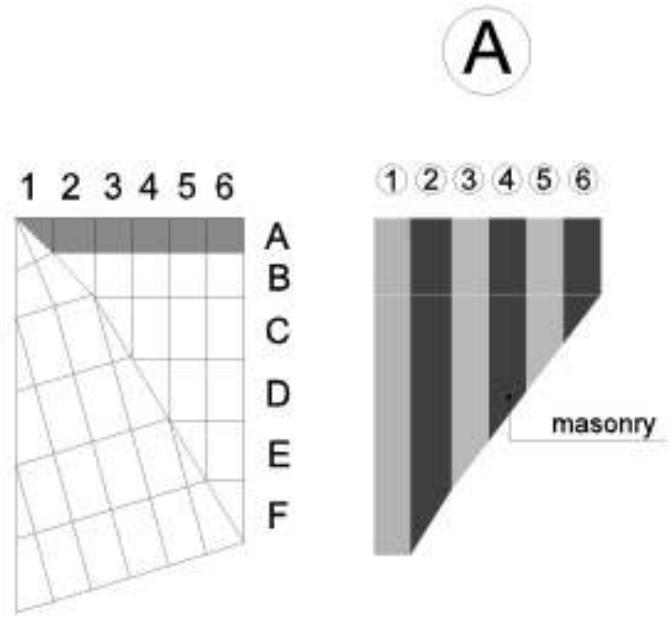

Figure 5.21 Volumes and concrete surfaces of piece A of part 1 of the north element

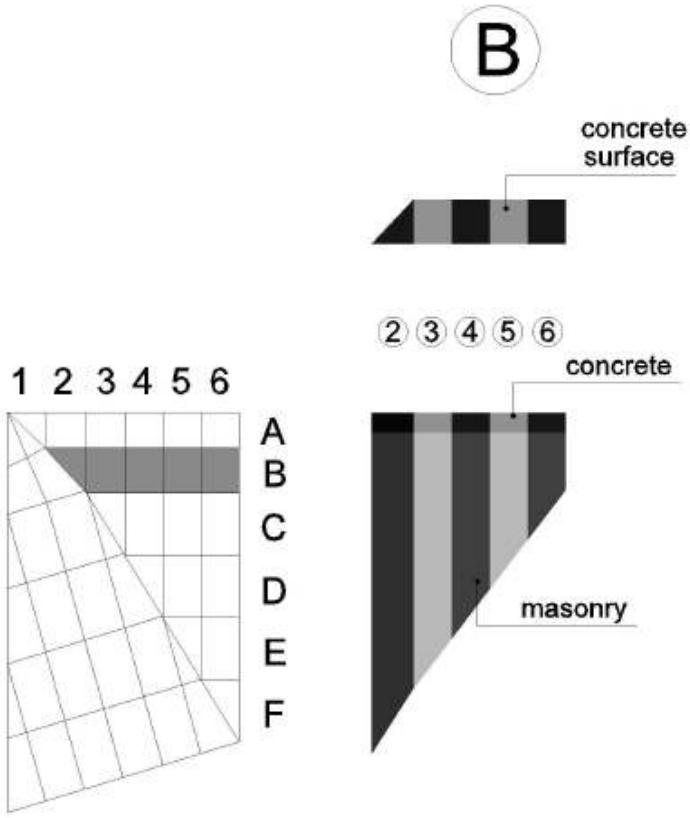

Figure 5.22 Volumes and concrete surfaces of piece B of part 1 of the north element

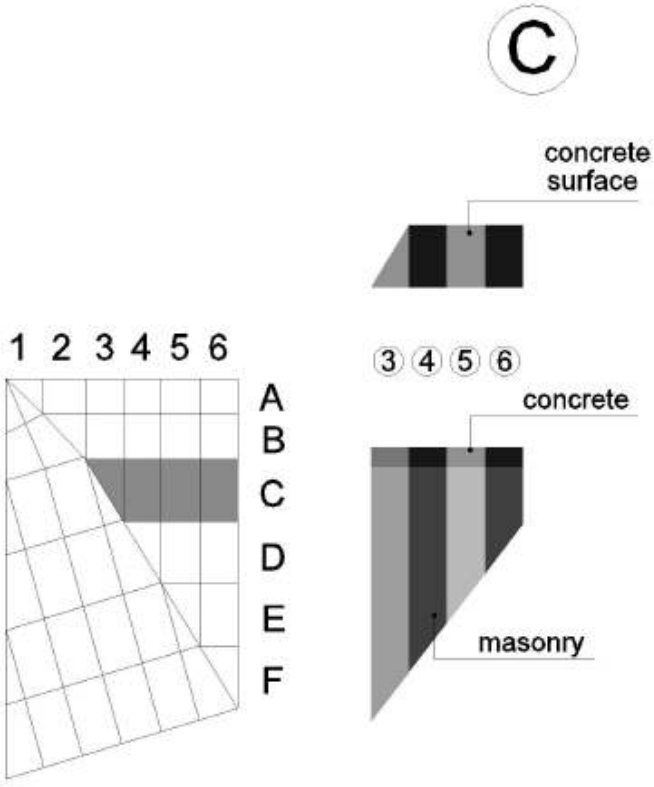

Figure 5.23 Volumes and concrete surfaces of piece C of part 1 of the north element

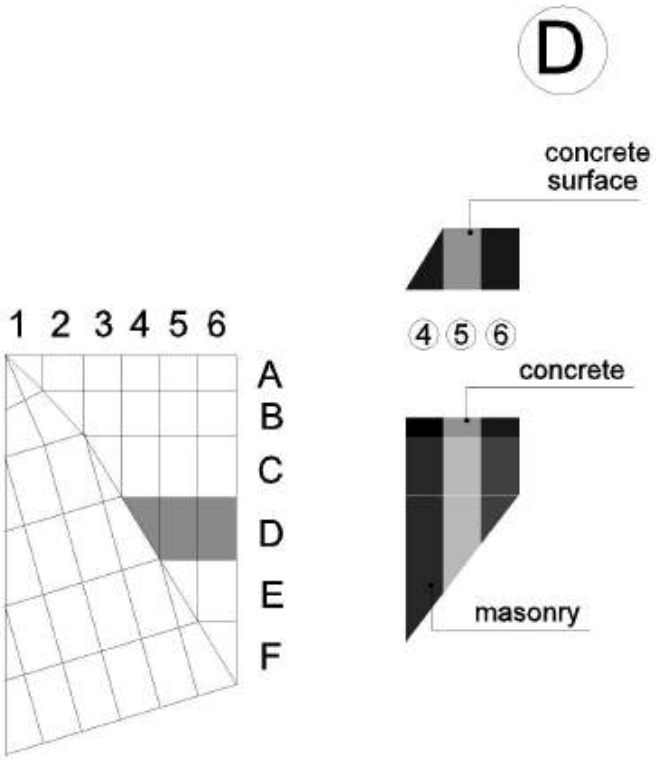

Figure 5.24 Volumes and concrete surfaces of piece D of part 1 of the north element

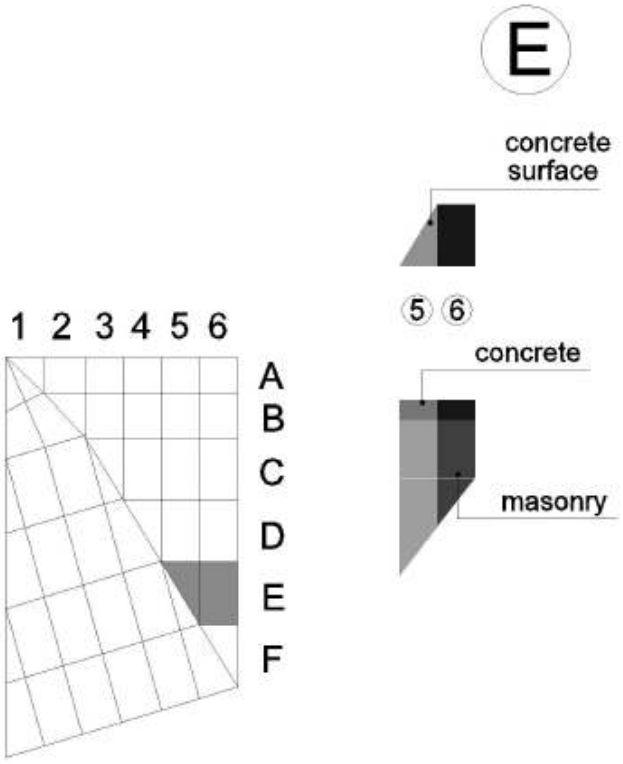

Figure 5.25 Volumes and concrete surfaces of piece E of part 1 of the north element

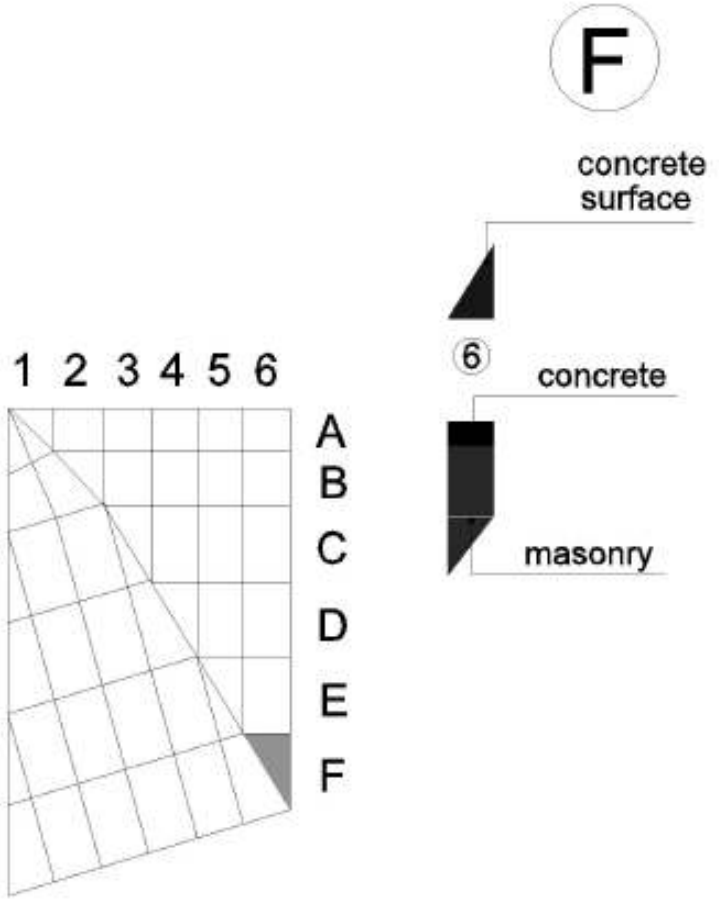

Figure 5.26 Volumes and concrete surfaces of piece F of part 1 of the north element

The volumes and the concrete surfaces of the pieces of part 1 of the north element are shown in the following Figures.

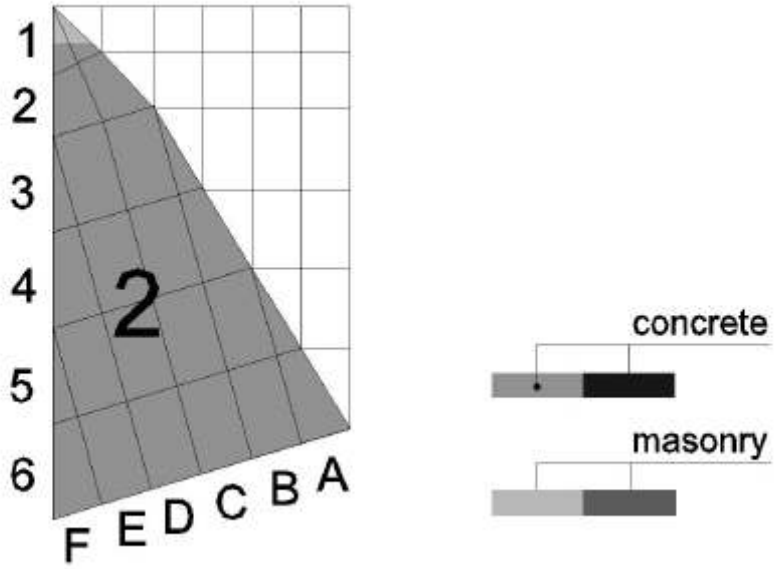

Figure 5.27 Geometry of part 2 of the north element

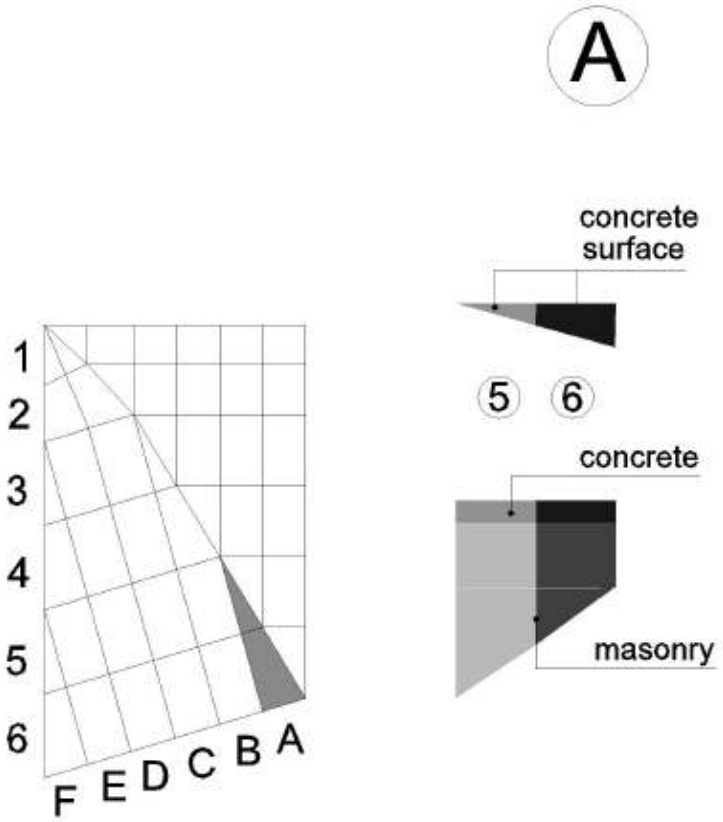

Figure 5.28 Volumes and concrete surfaces of piece A of part 2 of the north element

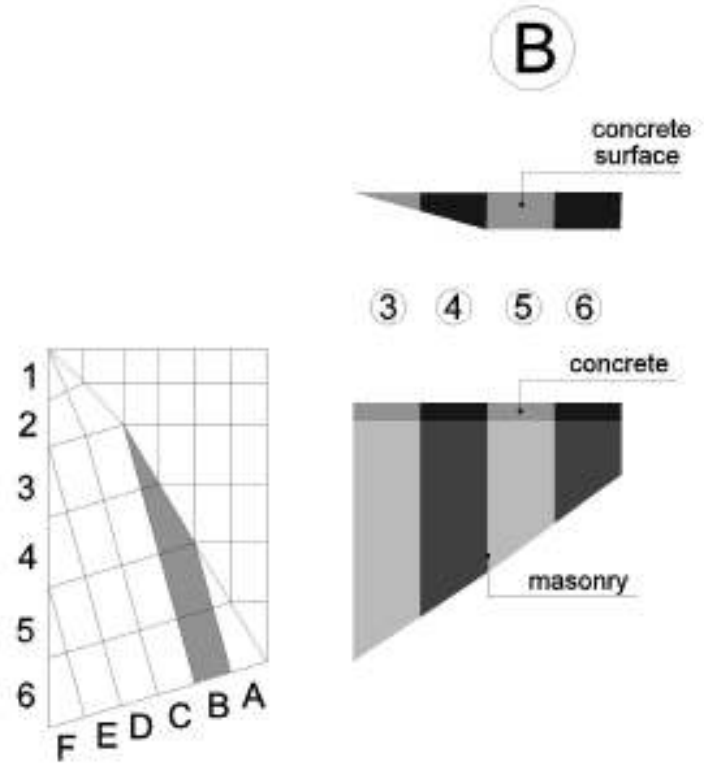

Figure 5.29 Volumes and concrete surfaces of piece B of part 2 of the north element

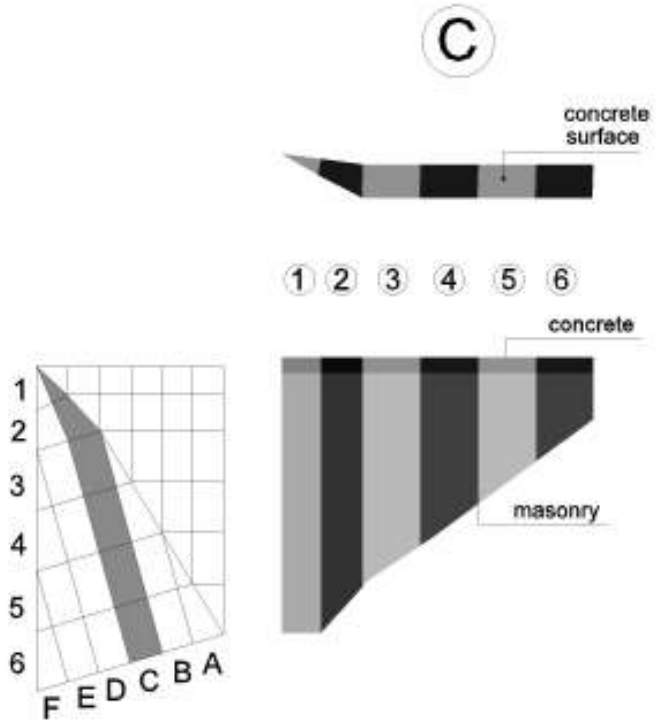

Figure 5.30 Volumes and concrete surfaces of piece C of part 2 of the north element

The volumes and concrete surfaces of pieces D, E and F are considered to be symmetric to pieces C, B and A accordingly. The volumes, areas different loads and the total load applied to the different pieces of the south element are given at the following Tables.

Table 5.5 Volumes and concrete areas of the different pieces of part 1 of the north element

PART B					
No piece	No subdivision	Volume m^3			Area m^2
		concrete	stone	soil	concrete
A1	1		0.097		
	2	-	0.199	-	-
	3	-	0.147	-	-
	4	-	0.118	-	-
	5	-	0.089	-	-
	6	-	0.060	-	-
B1	2	0.008	0.113	-	0.054
	3	0.015	0.171	-	0.098
	4	0.015	0.134	-	0.098
	5	0.015	0.097	-	0.098
	6	0.015	0.061	-	0.098
C1	3	0.010	0.114	-	0.068
	4	0.020	0.186	-	0.136
	5	0.020	0.135	-	0.136
	6	0.020	0.085	-	0.136
D1	4	0.010	0.089	-	0.068
	5	0.020	0.135	-	0.136
	6	0.020	0.085	-	0.136
E1	5	0.010	0.063	-	0.068
	6	0.020	0.085	-	0.136
F1	6	0.010	0.038	-	0.068

Table 5.6 Self weight, traffic load and total load on the different pieces of part 1 of the north element

PART B						
No piece	No subdivision	Self weight kN			Traffic load kN	Total
		concrete	stone	soil	on concrete area	Force kN
A1	1		2.125			2.125
	2	-	4.379	-	-	4.379
	3	-	3.238	-	-	3.238
	4	-	2.598	-	-	2.598
	5	-	1.958	-	-	1.958
	6	-	1.319	-	-	1.319
B1	2	0.184	2.479	-	0.536	3.199
	3	0.336	3.751	-	0.976	5.063
	4	0.336	2.946	-	0.976	4.258
	5	0.336	2.141	-	0.976	3.452
	6	0.336	1.335	-	0.976	2.647
C1	3	0.235	2.515	-	0.679	3.428
	4	0.469	4.099	-	1.357	5.925
	5	0.469	2.979	-	1.357	4.805
	6	0.469	1.859	-	1.357	3.685
D1	4	0.235	1.956	-	0.679	2.869
	5	0.469	2.979	-	1.357	4.805
	6	0.469	1.859	-	1.357	3.685
E1	5	0.235	1.395	-	0.679	2.308
	6	0.469	1.859	-	1.357	3.685
F1	6	0.235	0.836	-	0.679	1.750

Table 5.7 Volumes and concrete areas of the different pieces of part 2 of the north element

PART B					
No piece	No subdivision	Volume m^3			Area m^2
		concrete	stone	soil	concrete
A2	5	0.006	0.038		0.040
	6	0.018	0.072		0.120
B2	3	0.006	0.068		0.040
	4	0.018	0.166		0.122
	5	0.024	0.164		0.162
	6	0.024	0.100		0.161
C2	1	0.004	0.069		0.028
	2	0.014	0.208		0.096
	3	0.026	0.302		0.170
	4	0.026	0.241		0.170
	5	0.026	0.174		0.170
	6	0.026	0.105		0.170
D2	1	0.006	0.038		0.040
	2	0.018	0.072		0.120
	3	0.006	0.068		0.040
	4	0.018	0.166		0.122
	5	0.024	0.164		0.162
	6	0.024	0.100		0.161
E2	3	0.004	0.069		0.028
	4	0.014	0.208		0.096
	5	0.026	0.302		0.170
	6	0.026	0.241		0.170
F2	5	0.026	0.174		0.170
	6	0.026	0.105		0.170

Table 5.8 Self weight, traffic load and total load on the different pieces of part 2 of the south element

PART B						
No piece	No subdivision	Self weight kN			Traffic load kN	Total
		concrete	stone	soil	on concrete area	Force kN
A2	5	0.140	0.832		0.404	1.376
	6	0.414	1.588		1.202	3.204
B2	3	0.140	1.503		0.404	2.047
	4	0.419	3.641		1.215	5.275
	5	0.559	3.610		1.619	5.788
	6	0.554	2.209		1.607	4.370
C2	1	0.097	1.516		0.283	1.895
	2	0.331	4.585		0.957	5.873
	3	0.587	6.633		1.698	8.918
	4	0.589	5.295		1.698	7.582
	5	0.589	3.821		1.698	6.108
	6	0.5888	2.3188		1.698	4.6056
D2	1	0.1403	0.8316		0.404	1.3759
	2	0.414	1.5884		1.202	3.2044
	3	0.1403	1.5026		0.404	2.0469
	4	0.4186	3.641		1.215	5.2746
	5	0.5589	3.6102		1.619	5.7881
	6	0.5543	2.2088		1.607	4.3701
E2	3	0.0966	1.5158		0.283	1.8954
	4	0.3312	4.5848		0.957	5.873
	5	0.5865	6.633		1.698	8.9175
	6	0.5888	5.2954		1.698	7.5822
F2	5	0.5888	3.8214		1.698	6.1082
	6	0.5888	2.3188		1.698	4.6056

The numbering of the north element is shown in the following Figure.

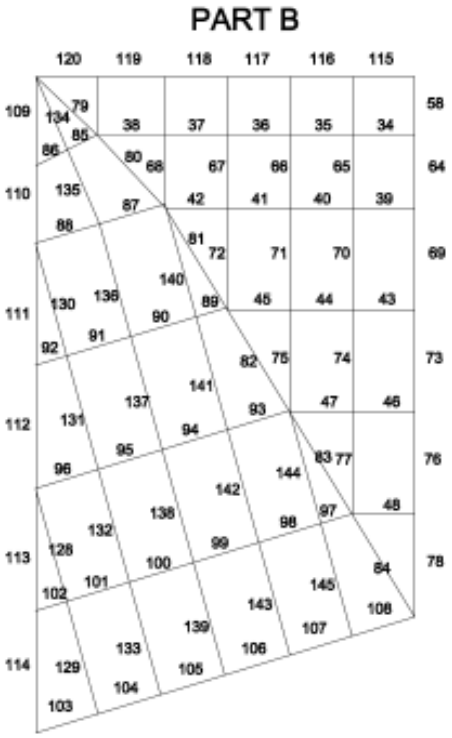

Figure 5.31 Numbering of the cables of the south element

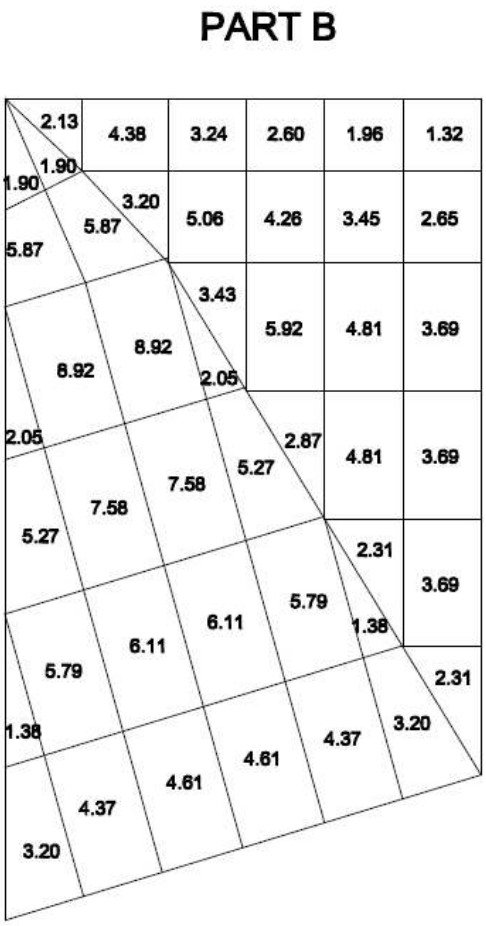

Figure 5.32 Total load acting on the different pieces of south element

For the distribution of the load from the solid pieces to the cables of the net it is necessary the subdivision of the mesh into sub surfaces. The division is done always dividing the angle into two equal angles using the bisector of the angle. The subdivision is shown in Figure 5.33.

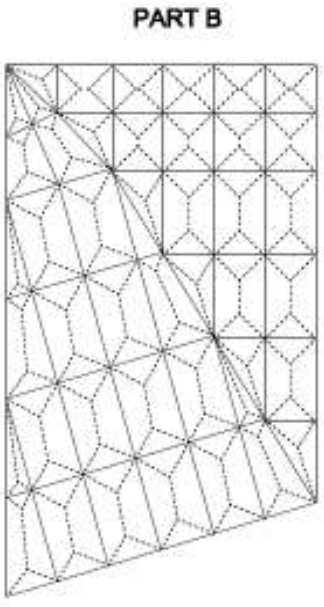

Figure 5.33 Division of the mesh into sub surfaces for the distribution of the load to the cables

The area of each one of the sub surfaces is presented in the following Figure.

PART B

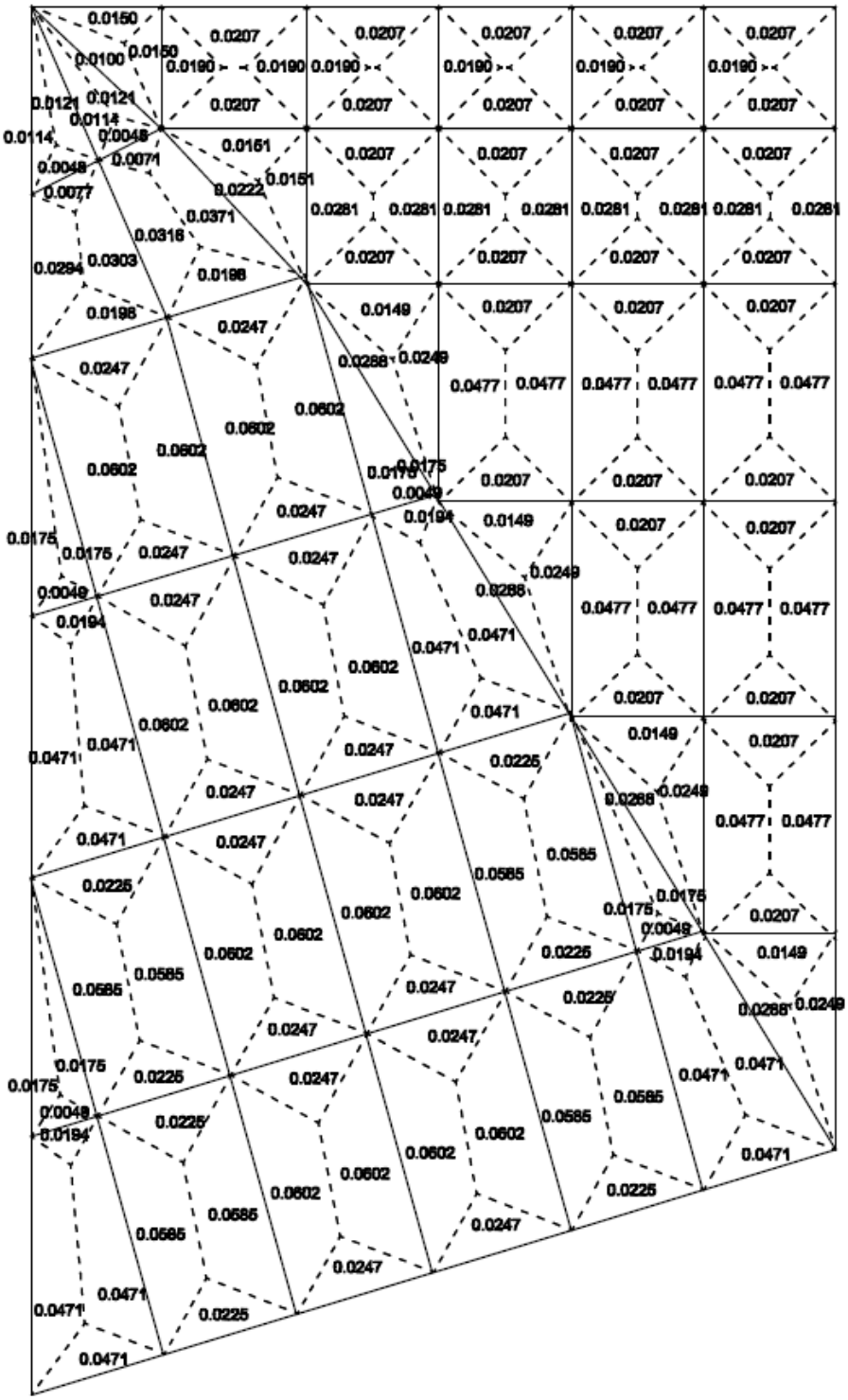

Figure 5.34 Area of the sub surfaces that the mesh is divided

The area of the different surfaces of the mesh is shown in the following Figure.

PART B

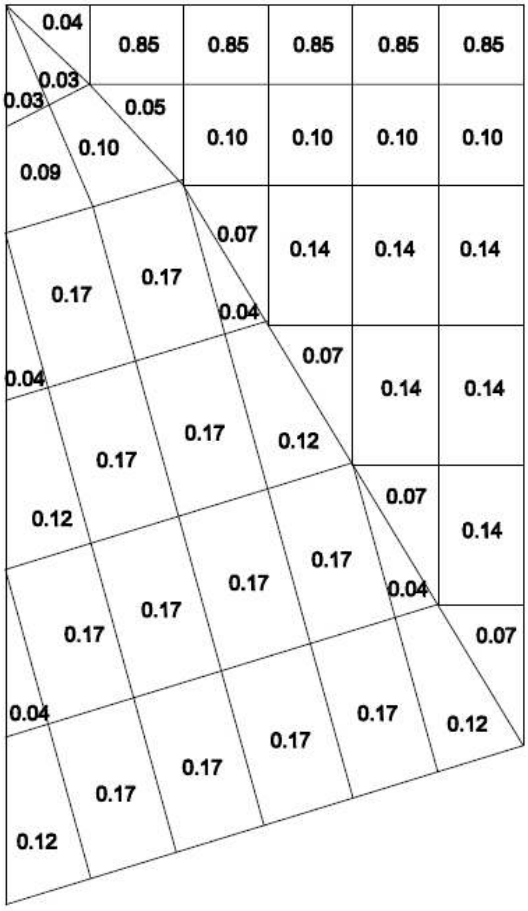

Figure 5.35 Areas of the different surfaces of the mesh

The calculation of the total load is based on the rule below:

Load on the element = Sum [[(Area of the subsurface)/(Area of the surface)]·(Load on the piece)]

This means that all the pieces ending at a cable contribute with loading the cable with a percentage of the total load of the piece. This percentage is given by the term (Area of the subsurface)/(Area of the surface) where the subsurface is the subsurface of the piece facing the cable and the surface is the surface of the piece. By summing the load that the different pieces contribute the load of the cable is calculated. The total loads applied on the cables are shown in Figure 5.36.

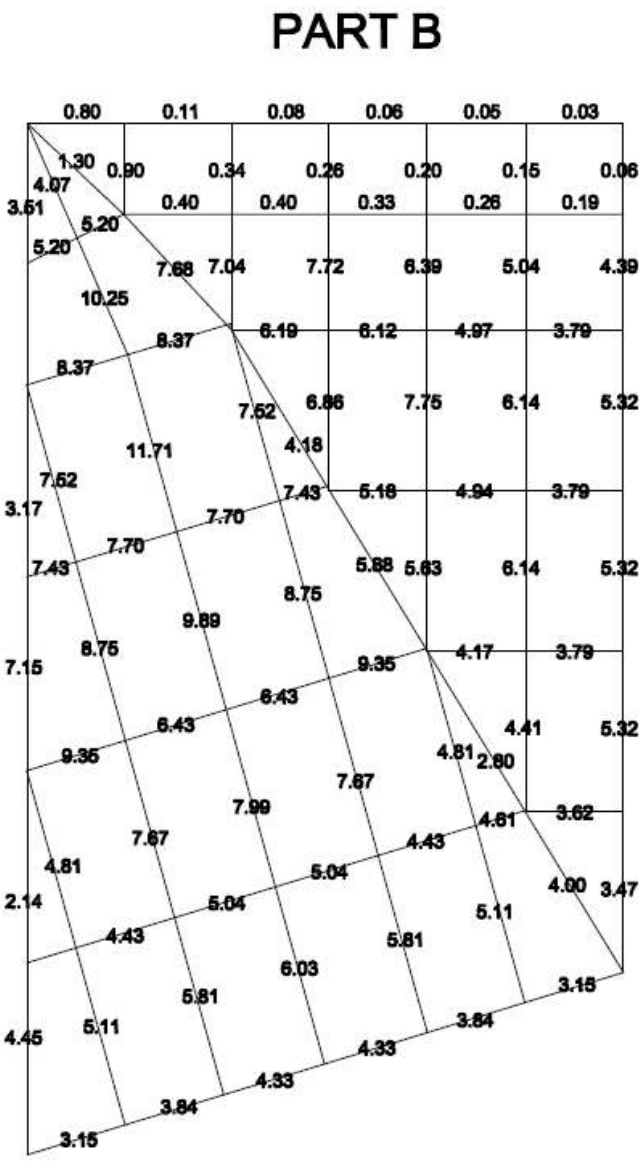

Figure 5.36 Loads acting on the cables of the net

5.3 Modeling and analysis of the cable network

After the calculation of the loads the model geometry is introduced in MASONRISK application of GID program. A plan view of the geometry of the net is shown in Figure 5.37 while a 3D view of the model is shown in Figure 5.38. The cable net has 100 points and 100 lines representing the different cables.

All the cable nets are created horizontally apart from the cables represented the columns that are three-dimensional.

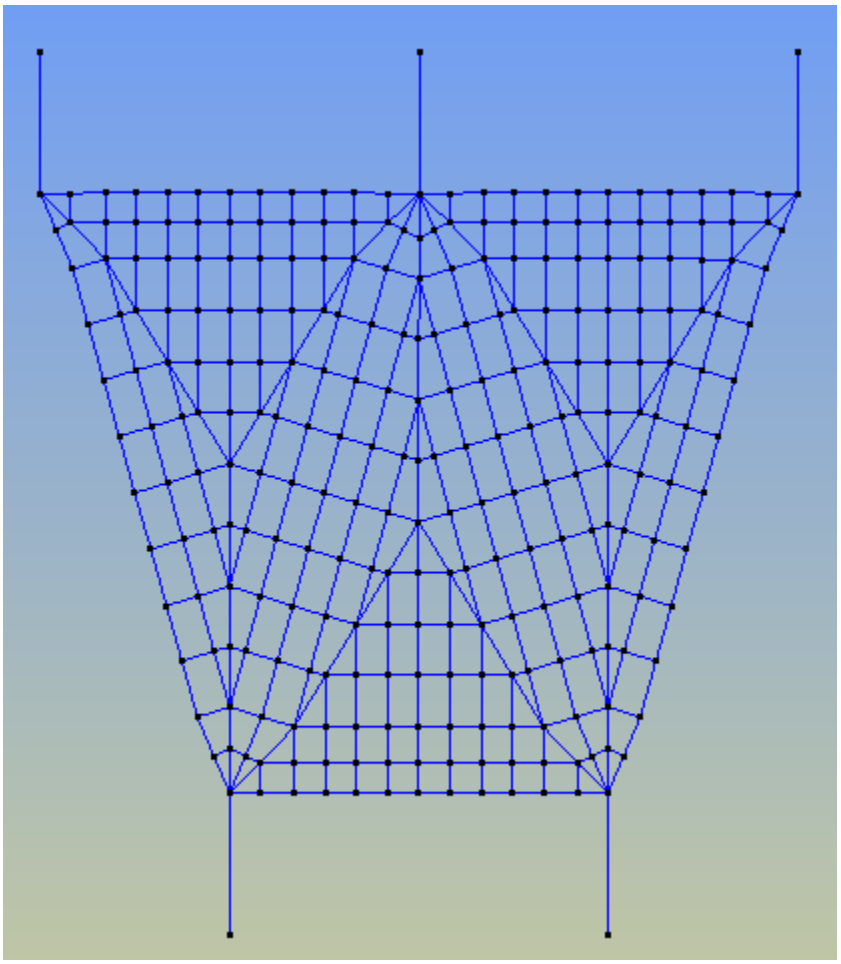

Figure 5.37 Plan view of the cable net generated with MASONRISK application of GID

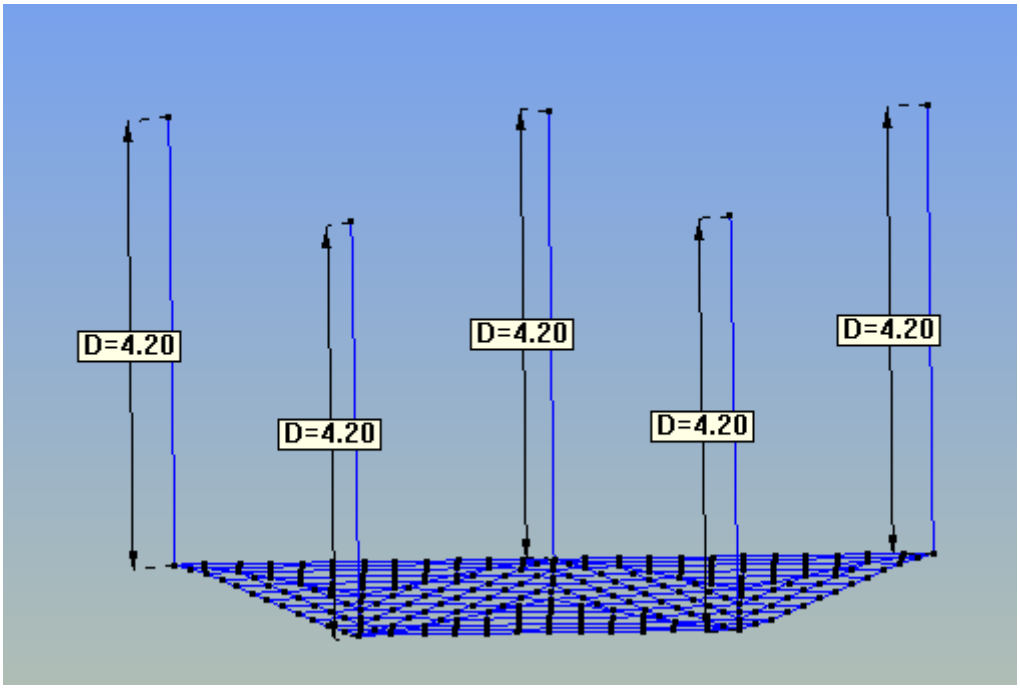

Figure 5.38 3D view of the cable net generated with MASONRISK application of GID

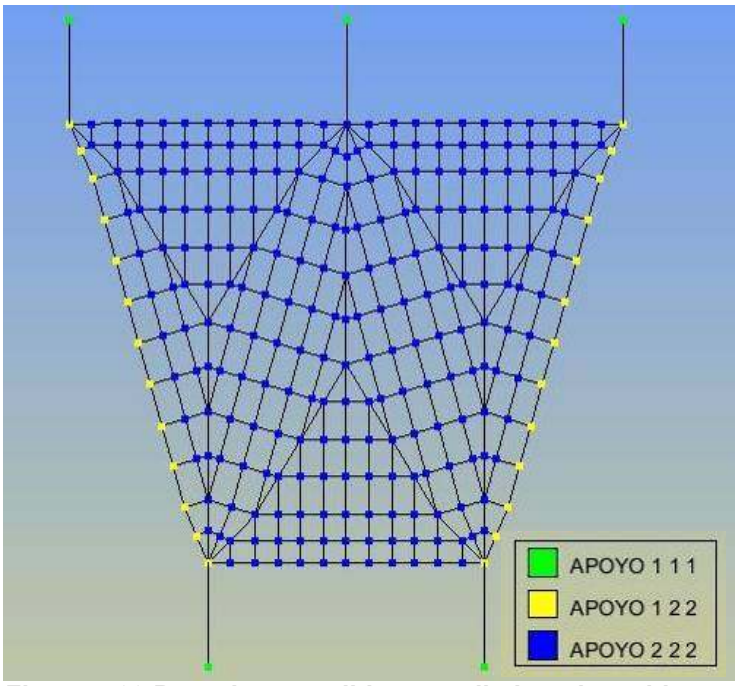

Figure 5.39 Boundary conditions applied on the cable net

The boundary conditions applied on the cable net can be seen in Figure 5.39. The only fixed points are the end points of the cable of the elements of the columns from where the all structure is going to hang in order to deform and give the deformed catenary model. The fixed points can be seen in Figure 5.39 and are represented with the reference “APOYO 1 1 1”. The cables of the net where the geometry of the structure is cut in order to model the structure are characterized by boundary conditions “APOYO 1 2 2”. This means that the horizontal movement of these elements is restricted. This is because the whole structure does not move horizontally so also these elements due to symmetry reasons should not move horizontally. The boundary condition for all the other elements is “APOYO 2 2 2” which means that they are free to move in all the degrees of freedom.

The material characteristic assigned on the horizontal cables can be seen in the following Figure.

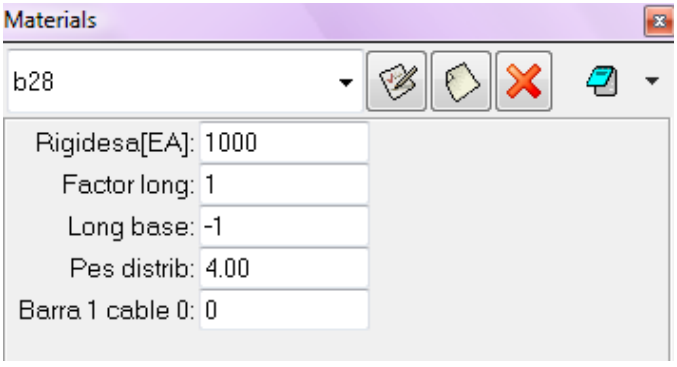

Figure 5.40 Material characteristics assigned on the cables

The Rigidesa is the rigidness of the structure and is given a price of 1000kN.

The factor long is a coefficient that multiplies the length bases defined by the Long_base variable to obtain the length of the element. It is practical to use when the Long_base variable takes the value of the distance

between the extreme knots of the element. The factor long has been chosen equal to 1.1 for the horizontal cables of the edge of the network where the structure is cut to due to symmetry reasons and 1 for all the other horizontal cables.

The long base defines the length bases of the element at issue. If a negative value in this variable is placed the program takes directly the length between the nodes of the element. In this case the long base is equal to the actual length of the element because the long base is equal to 1.

The Pes distrib expresses the load by units of length of the element (measured in the development of the element). The Pes didtrib is the price of the loads calculated on the element given in Figures 5.19 and 5.36 divided by the length of the element.

The material properties assigned at the cables stimulating the columns can be seen in the following Figures.

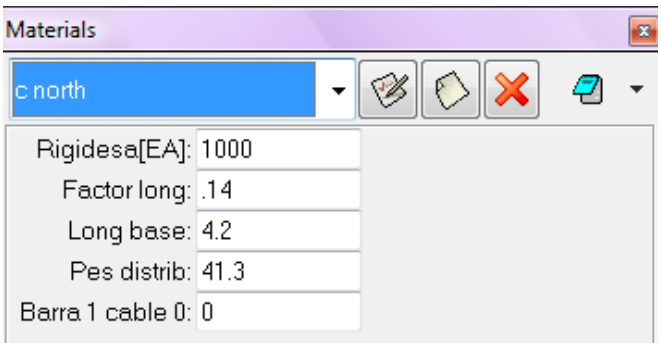

Figure 5.41 Material properties assigned on the cable stimulating the column of the north side

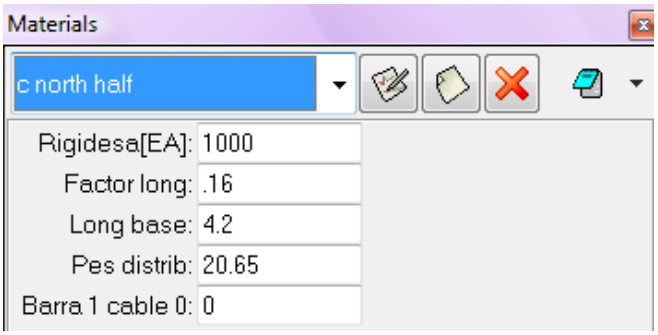

Figure 5.42 Material properties assigned on the cable stimulating the half column of the north side

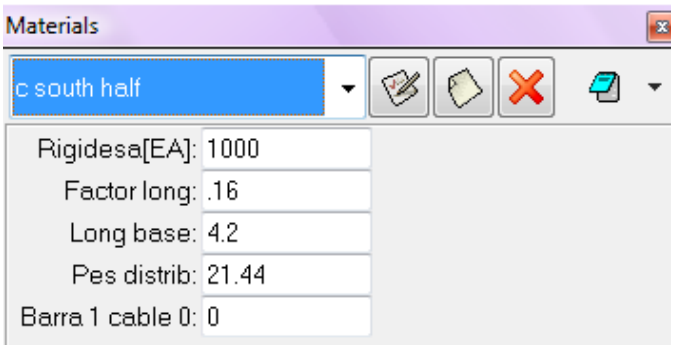

Figure 5.43 Material properties assigned on the cable stimulating the half column of the north side

The load of the columns is a sum of the self weight of the columns and the rest of the load of the structure not applied on the cable net because as it can be seen in Figure 5.1 only one part of the structure is stimulated with cable elements. The exact calculation of the load of the columns is presented in the following Figure.

Volume m^3	2.06
Length m	4.20
Self-weight kN	45.34
Dead and live load NORTH column kN	128.11
Dead and live load SOUTH column kN	134.72
Total load NORTH column kN/m	41.30
Total load HALF NORTH column kN/m	20.65
Total load HALF SOUTH column kN/m	21.44

Figure 5.44 Loads acting on the cables stimulating the columns

The different material properties represented by the different colors are shown in Figure 5.45. From this Figure is visible the symmetric application of the loads on the structure

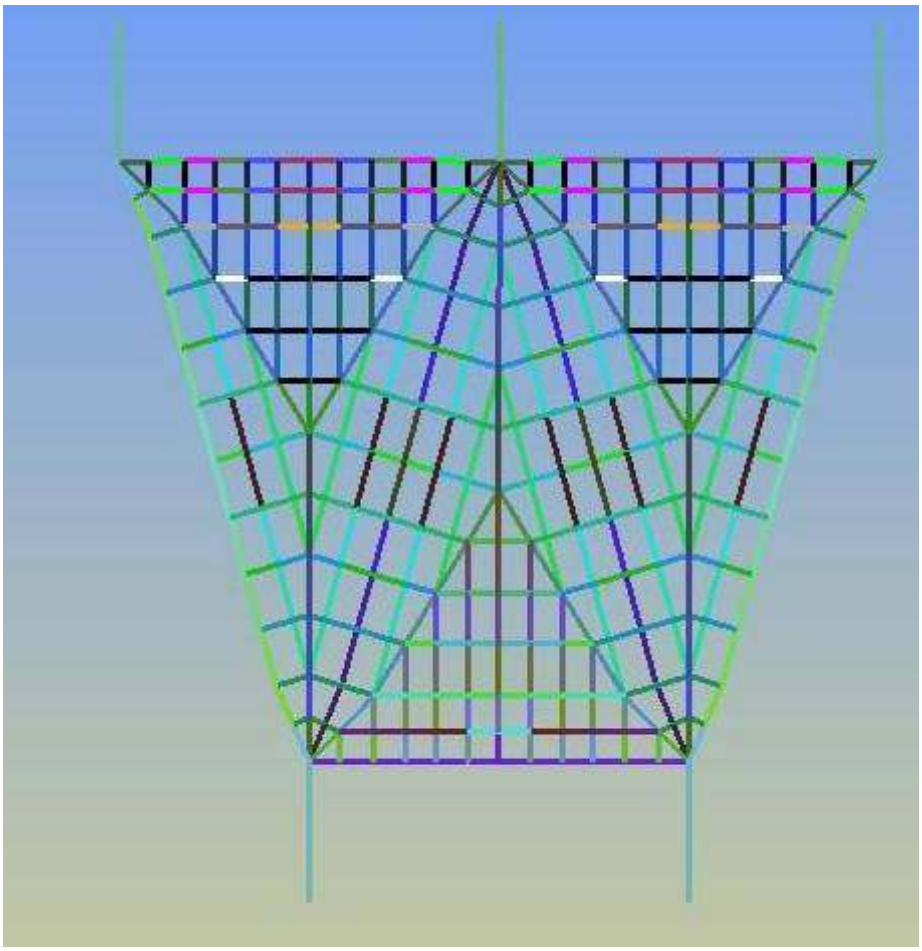

Figure 5.45 Different colors representing the different material loads on the cable net

Before the calculation of the mesh is important the definition of the problem Data which can be seen in the following Figure.

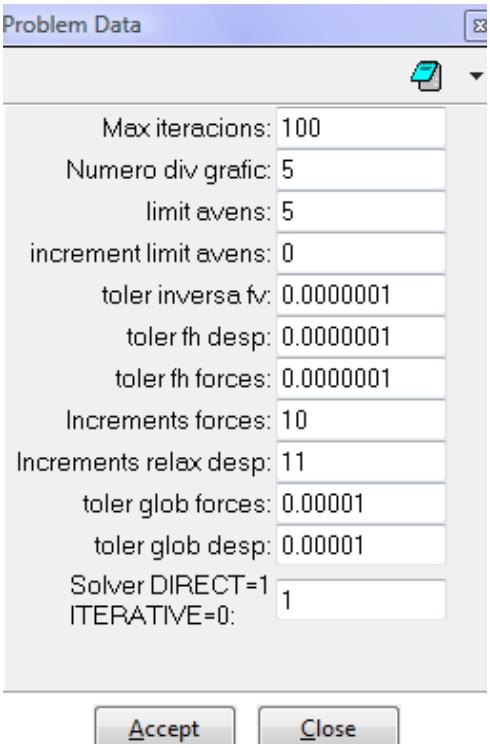

Figure 5.46 Problem Data of the catenary model

The Numero_div_grafic is the most important parameter that is defined as follows: The resulting catenaries are visualized by means of polygonal and this parameter defines the number of parts of these.

The meshing of the cable net is shown in the following Figure 5.47. The size of the elements to be calculated is one. After the meshing the model has a number of 559 linear elements and 290 nodes because at the problem data the number of graphic division (Numero div graphic) is defined as 5.

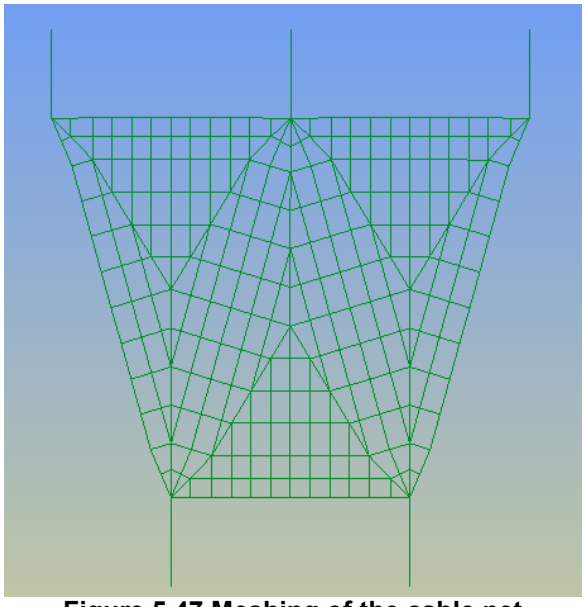

Figure 5.47 Meshing of the cable net

The two following Figures are presenting 2 details of the cable net. The north part is represented in Figure 5.48 and the south part in Figure 5.49.

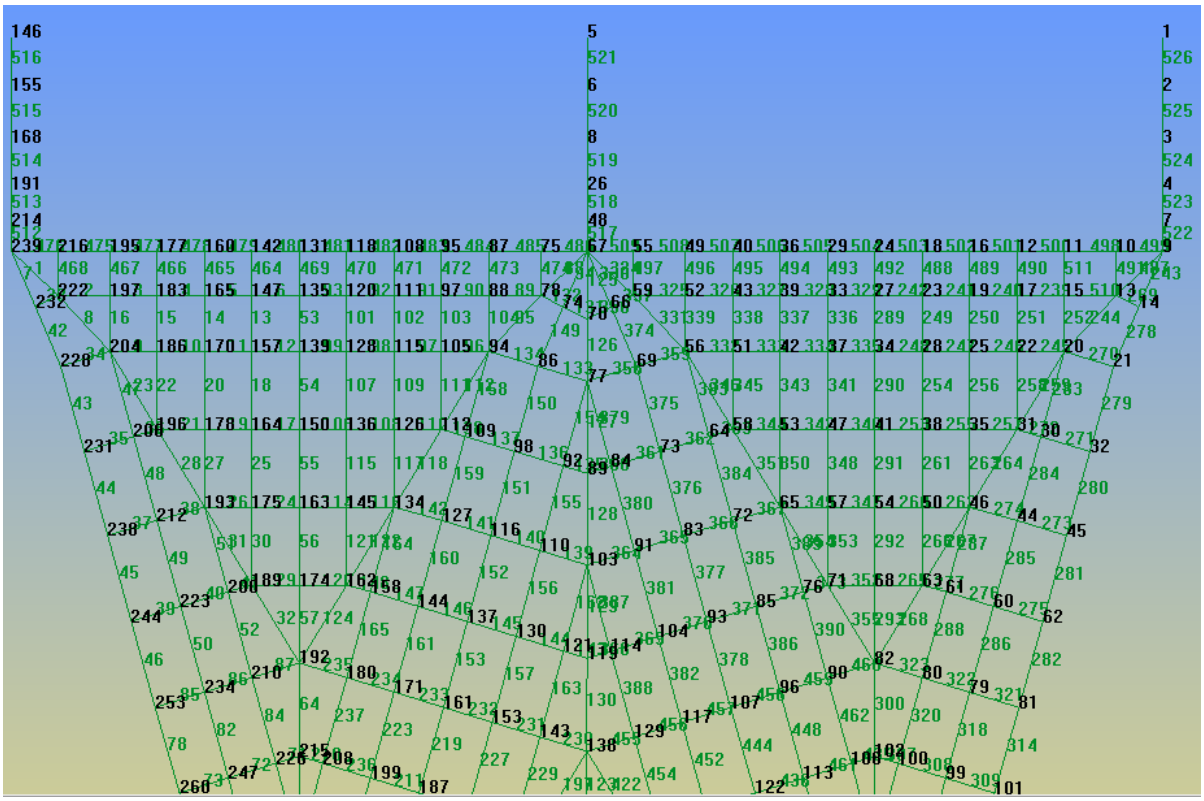

Figure 5.48 Detail of the mesh of the north side of the cable net

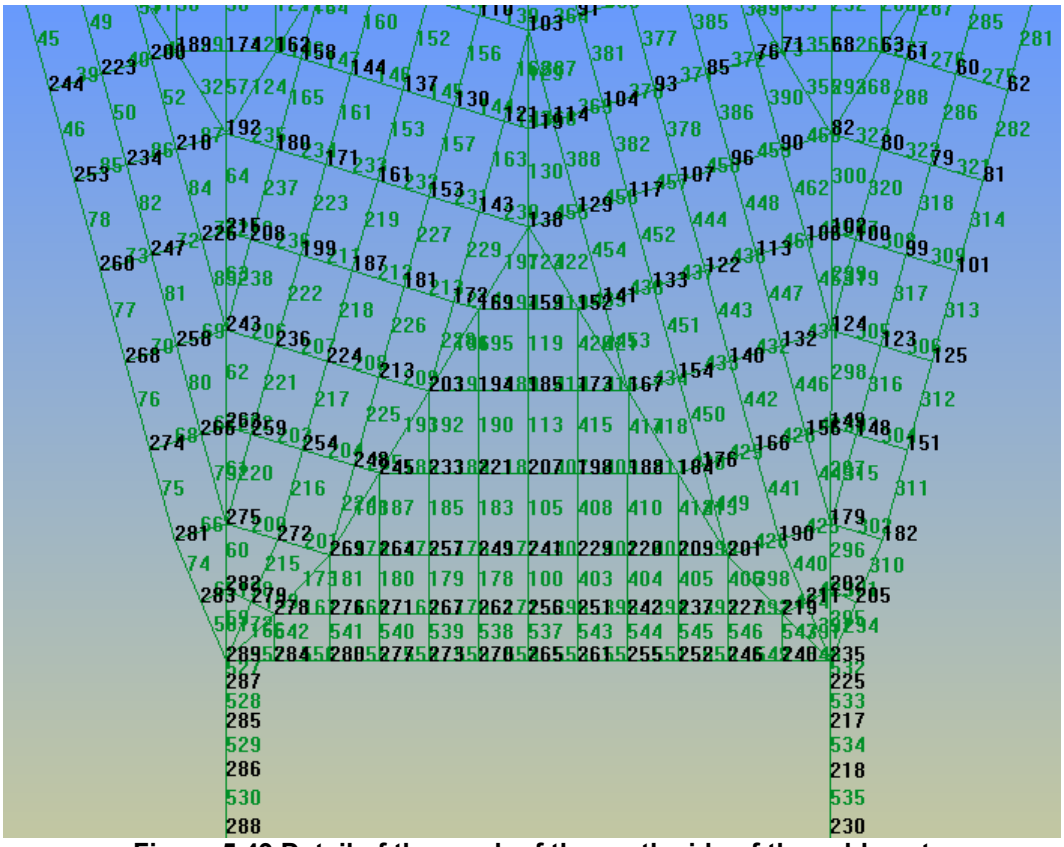

Figure 5.49 Detail of the mesh of the north side of the cable net

5.4 Presentation of the results

After the calculation of the structure GID produces the deformed catenary model as shown in the following Figure.

Figure 5.50 Deformed catenary net produced by MASONRISK application of GID

In order to compare the catenary model with the geometry of the structure the catenary model is inverted. A three-dimensional presentation of the inverted model is shown in Figure 5.51.

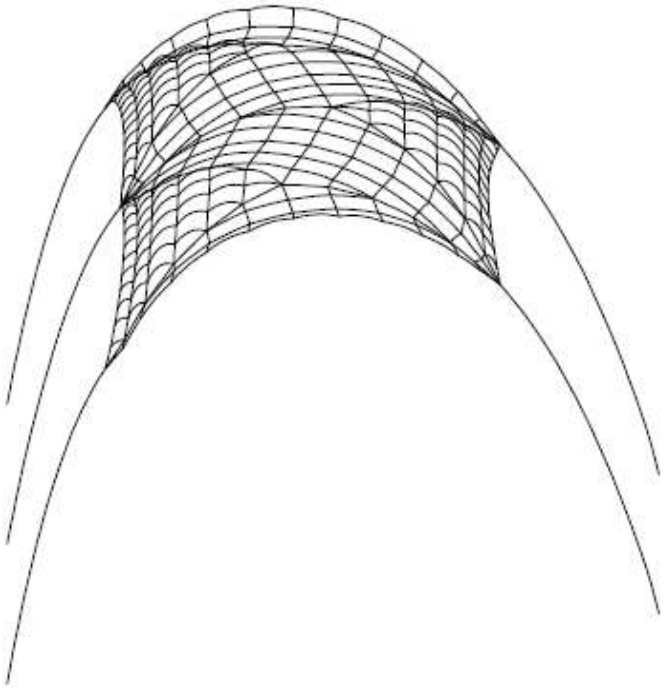

Figure 5.51 3D view of the inverted catenary model

This inverted model must fit in the limits of the geometry of the viaduct in order to conclude that the structure is stable according to the safe theorem.

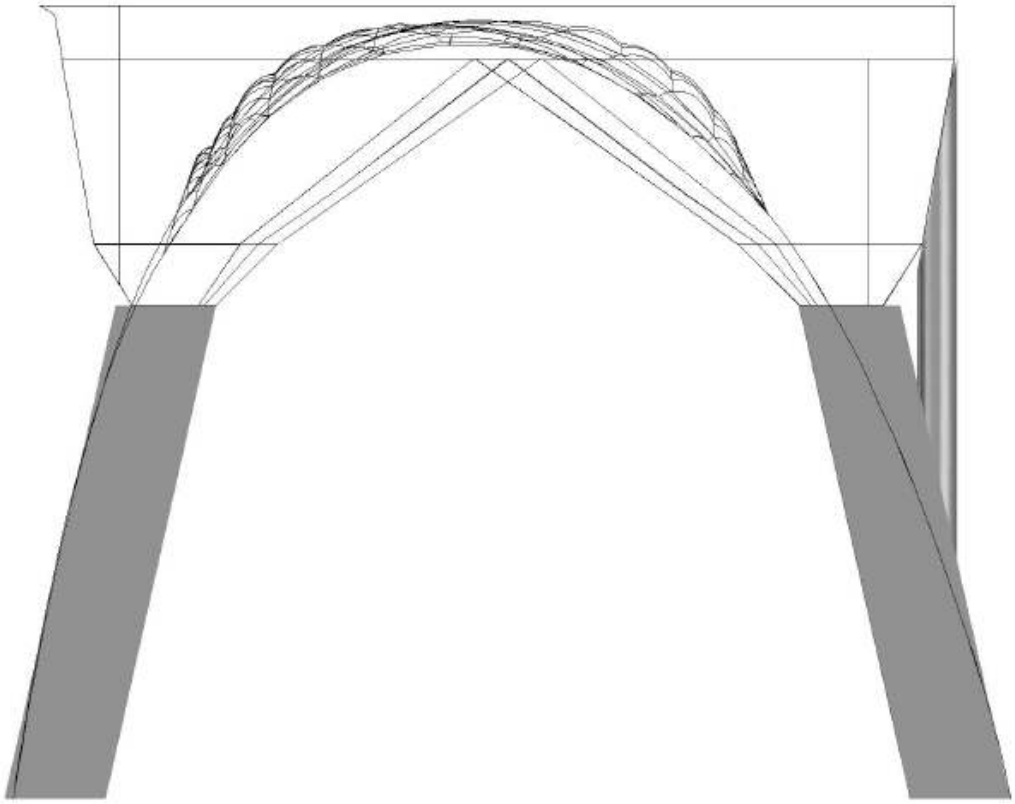

Figure 5.52 View of the final solution of the catenary model fitting within the limits of the structure

Figure 5.52 and Figure 5.53 and Figure 5.54 confirm that the catenary model fits within the limits of the structure so the structure is stable.

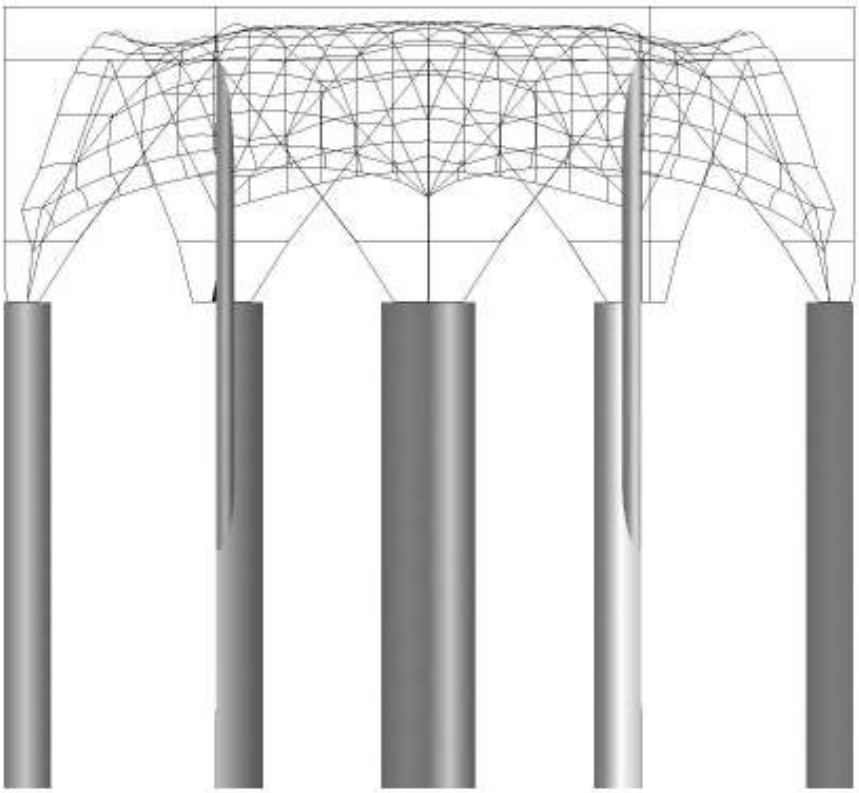

Figure 5.53 Front view of final solution of the catenary model fitting within the limits of the structure

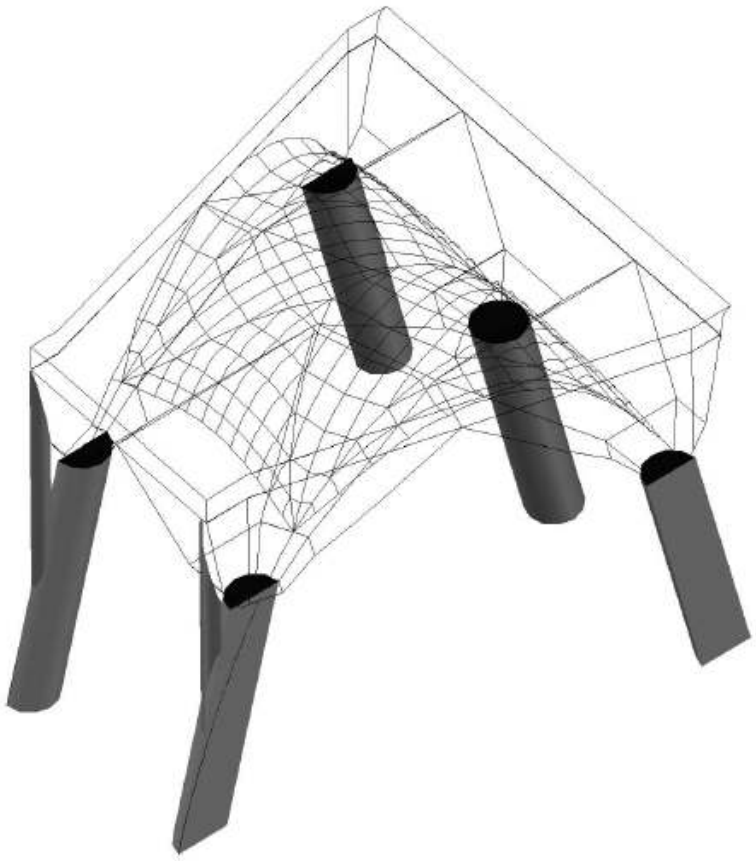

Figure 5.54 3D view of the final solution of the catenary model fitting within the limits of the structure

According to the results of both studies the graphic statics method and the funicular analysis method the lower viaduct of park Güell is stable.

6. CONCLUSIONS AND RECOMMENDATIONS

6.1 Conclusions and recommendations on Graphic statics method

The graphic statics method for the calculation of the thrust line is always a very useful tool for the engineers that want to study the stability of historic structures. The main advantage of the method is that is simple to understand and can be applied to many different types of historic structures. Even for a complex geometry like this of the lower viaduct the application of the method has been easy. However the main disadvantage of the graphic statics method is that many trials are necessary until a final solution is found. The fact that the graphic statics application at lower viaduct has been manual with the help of AutoCAD 3D increased even more the time of the calculation. A good recommendation for the use of graphic statics with the help of CAD tools when the loading conditions are complex would be the first trial to include only the self weight of the structure. After a solution is obtained only for the self weight, this solution can be used as an input for the final calculation of the thrust line regarding all the loads. The graphic statics method for the calculation of the thrust line is accurate however is applied only in two-dimensions and is not taking account the three-dimensional geometry of the structure.

6.2 Conclusions and recommendations on the funicular analysis method

The fundamental idea of the funicular analysis method, the creation of a catenary model is an old process that found an application in Gaudi‘s designing process of Colonia Güell and many other structures. The use of the catenary model was to produce compression only geometries appropriate for the masonry structures. However the funicular analysis method applied on the MASONRISK application of GID is a new method aiming at finding a cable net that deformed due to the loads applied on it and inverted can fit within the limits of the structure in order to prove that the structure is stable.

The generation of the geometry of the cable net, the application of the properties on the net and the calculation of the deformed model is a simple process. However the assignment of different material properties for 100 different lines manually is a time consuming process. Also the calculation of the loads applied on the cables is very time consuming for structures with varying loading condition along the geometry like the lower viaduct of Parc Güell. The fact that the load calculation has been manual with the help of AutoCAD 3D increased the time of the pre process of the cable net. The main difficulty for finding the final solution has been the repeat of the trial and error process many times. Every time that the deformed catenary model did not fit within the limits of the geometry of the structure a change in the cable net was necessary. The parameter that was mainly changed was the factor long on the material properties box which influences the length of the cable. This parameter had to be changed many times in order to find the final solution. However even the smallest change at the length of the cable had many times as a result bigger change at the deformed catenary model so it was not always easy to predict how the structure will deform after the change of the length of one or more cables.

In general this method is very useful for the study of the historic structures because of its accuracy. It is very important that it provides a three dimensional solution which is closer to the real three-dimensional geometry

of the structure. In contrast the graphic statics method is applied only in two dimensions neglecting the three-dimensional geometry of the structure.

7. REFERENCES

Kent and Prindle, PARK GUELL, Princeton architectural press, 1993

Martinez Lapena and Torres, Park Güell, Gustavo Gili, Barcelona 2002

BIS architects, Diagnosi estructural viaductes parc Güell, Barcelona 2011

Block P. Equilibrium systems: studies in masonry structure, M.S. thesis, Cambridge: Massachusetts Institute of Technology, 2005.

P Block, T. Ciblac, J. Ochsendorf, Real-time limit analysis of vaulted masonry buildings, Computers & Structures, 2006

Boothby TE. Analysis of masonry arches and vaults. Progr Struct Eng Mater 2001, 3:246–56.

Wolfe WS. Graphical analysis: a handbook on graphic statics. New York: McGraw-Hill, 1921.

Andreu, A., Gil, L. & Roca, P. Computational Analysis of Masonry Structures with a Funicular Model. Journal of Engineering Mechanics 133(4): 473-480, 2007

Andreu, A., Gil, L. & Roca, P. PhD, Analysis of masonry structures by funicular networks, Engineering and Computational Mechanics 163, 147–154, 2010